UNIVERSITY OF CALIFORNIA, SAN DIEGO

Response of Strongly Nonlinear Dissipative Metamaterials to Quasiharmonic And Pulses Excitation

A dissertation submitted in partial satisfaction of the
requirements for the degree
Doctor of Philosophy

in

Material Science and Engineering

by

Si Yin Wang

Committee in charge:

Vitali F. Nesterenko, Chair
Shengqiang Cai
Renkun Chen
Hyonny Kim
Vlado Lubarda

2016

The dissertation of Si Yin Wang is approved, and it is acceptable in quality and form for publication on microfilm and electronically:

_____

_____

_____

_____

_____

Chair

University of California, San Diego

2016

DEDICATION

To my loving parents and husband.

TABLE OF CONTENTS

LIST OF FIGURES

LIST OF TABLES

ACKNOWLEDGEMENTS

I would like to express my special appreciation and thanks to my advisor Professor Vitali Nesterenko, he been a tremendous mentor for me. I would like to thank him for encouraging my research and for guidance throughout my doctoral years of study and research. His advice on research have been priceless. I would especially like to thank Professor Vlado Lubarda, Professor Ann Conn and Professor Hidenori Murakami for selecting me as their teaching assistant during the past few years and being financially supportive so I can get through and finish my PhD studies. I would also like to give thanks to Tom Chalfant, Nick Busan, for providing me help with using the machineries to prepare my samples for experiments and always keen to help me out when I needed. Without them I could not possibly finish my researches.

During my years at the material science and engineering graduate program, where most of my work was accomplished, there are many people I have worked with and/or got assistance. I would like especially mention Eric Herbold, Chiu Po, and Yichao Xu. I would like to thank them all and wish them the best luck in their career and future. Assistance and support from these colleagues also very important in my work, and I feel fortunate to have them facilitating all my achievements.

A special thanks to my family. I am so grateful to my parents for all of the sacrifices that they've made on my behalf. Their supportive attitude has been my solid foundation to sustain me thus far. I would also like to thank all of my friends who supported me in writing, and incented me to strive towards my goal. At the end I would like express appreciation to my beloved husband Han who spent sleepless nights helping me with my research. He was always available to support me in the moments when there was no one to answer my queries.

The text of Chapter II is, in part, based on the material in the following publications: S. Y. Wang, E. B. Herbold, and V. F. Nesterenko, in "Wave Propagation In Strongly

Non- linear Two-Mass Chains", in IUTAM Proceedings on granular materials, J.D. Goddard, J.T. Jenkins, P. Giovine (eds.), AIP Conference Proceedings, IUTAM-ISIMM Symposium on Mathematical Modeling and Physical Instances of Granular Flow, Reggio Calabria, September 14-18, 2009. American Institute of Physics, vol. 1227, Melville, New York, pp. 425-434, (2010). The dissertation author was a primary researcher and an author of the cited material.

I also would like to thank NSF (Grant No. DCMS03013220) for my funding during the initial period of my research.

VITA

2008	B. E. in Material Science Engineering, B. Com. in Finance, University of Auckland, New Zealand
2010-2016	Graduate Teaching Assistant, University of California, San Diego
2016	Ph. D. in Material Science and Engineering, University of California, San Diego, USA

PUBLICATIONS

I.F Collins, Qu Bai, and S. Y. Wang, "Modeling the Granular Nature of Soils", *Inter. Confer. IACMAG* Oct, 2008.

P. Chiu, S.Y. Wang, E. Vitali, E. B. Herbold, D. J. Benson, and V. F. Nesterenko, "Particle Size Effect in Granular Composite Aluminum/Tungsten", *AIP Conference Proceedings 1195*, American Institute of Physics, Melville, New York, part 2, pp.1345-1348, (2009).

E. B. Herbold, J. Kim, V. F. Nesterenko, S. Y. Wang, and C.Daraio, "Pulse Propagation in a Linear and Nonlinear Diatomic Periodic Chain: Effects of Acoustic Frequency Band-gap", *Acta. Mech.* 205, 85, 2009.

Si Yin Wang, Eric B. Herbold, Vitali F. Nesterenko, "Wave Propagation In Strongly Nonlinear Two-Mass Chains", in IUTAM Proceedings on granular materials, J.D. Goddard, J.T. Jenkins, P. Giovine (eds.), *AIP Conference Proceedings*, IUTAM-ISIMM Symposium on Mathematical Modeling and Physical Instances of Granular Flow, Reggio Calabria, September 14-18, 2009. American Institute of Physics, vol. 1227, Melville, New York, pp. 425-434, (2010)

S. Y. Wang, and V. F. Nesterenko, "Attenuation of short strongly nonlinear stress pulses in dissipative granular chains", *Physical Review E*, 91, 062211 2015.

S. Y. Wang, and V. F. Nesterenko, "Solitary waves in sonic vacuum generated by the striker impact", *Physical Review E*, (paper in preparation)

S. Y. Wang, and V. F. Nesterenko, "Role of dissipation on the striker behavior and shape of propagating pulses", *Physical Review E*, (paper in preparation)

ABSTRACT OF THE DISSERTATION

Response of Strongly Nonlinear Dissipative Metamaterials to Quasiharmonic And Pulses Excitation

by

Si Yin Wang

Doctor of Philosophy in Material Science and Engineering

University of California, San Diego, 2016

Vitali F. Nesterenko, Chair

Strongly nonlinear waves were investigated experimentally, numerically and analytically in two-mass and one mass systems. Experimental setups consist of one dimensional assembly of elastic stainless steel spheres or cylinders with different masses layered alternatively. When such assembly is not compressed, the sound speed is zero therefore creating a new state called “sonic vacuum”. Such systems does not supports sound waves but strongly nonlinear solitary waves can propagate in it. Band-gap phenomenon was observed and discussed for strongly nonlinear and nonlinear quasi-harmonic excitations in two-mass systems.

Formation and transformation of short, strongly nonlinear stress pulses were investigated in granular systems with different mass ratios, but with the same contact. Dissipation in the system with mass ratio close to 1 was faster than in the system with mass ratio 0.55. This is contrary to the expected behavior of corresponding non dissipative systems.

Striker impact generates a single solitary wave or a train of solitary waves depending on the mass ratio between the striker and the particle mass inside the chain. Imaginary scenarios of striker interacting with a single mass, that's called "effective mass", will be discussed to model the striker interaction with a collective of particles. This approach is based on two conservation laws. It satisfactorily predicts the upper estimate for the linear momenta, energies and amplitudes in the train of solitary wave in far field depending on the relative mass of the striker and particles in the chain.

Chapter 1

Introduction

1.1 Strongly nonlinear dimer system, linear elastic limit, unsolved problems

The research in strongly nonlinear wave dynamics of discrete systems, particularly of one-dimensional granular chains has become a growing area of interest [1-4]. The study of low dimensional granular chains is a logical step forward in wave dynamics with possible "translation" of results to totally different areas, particularly for design of new metamaterials with tunable properties. Discrete granular chains with a strongly nonlinear interaction law (i.e. the linear part is absent or small in comparison with the nonlinear interaction law) are more general systems than traditional linear and weakly nonlinear systems. Strong nonlinearity results in highly tunable systems where relatively small external forces can dramatically change their behavior. It was demonstrated experimentally, numerically and analytically that strongly nonlinear granular chains support a new type of waves -strongly nonlinear solitary waves - Nesterenko wave [5] with qualitatively different properties than well-known solitary waves of the Kortweg-de Vries equation [1,2].

A relatively new area is the investigation of nonlinear and strongly nonlinear waves in two mass granular chains [6,7]. These systems represent a unique opportunity to create tunable band gap materials where the band gap frequencies may be adjusted by external forces [6]. Most of the previous research of wave propagation in two mass chains was related to linear and weakly nonlinear discrete systems [8-15]. Chapter 2 investigates the propagation of quasiharmonic signals and the influence of band-gaps in nonlinear and strongly nonlinear diatomic periodic chains composed of stainless steel cylinders and stainless steel spheres.

A band gap is a well-known phenomenon for systems with linear interaction law between particles [16]. In the one dimensional elastic granular chain, the force

between the contact particles interacting by Hertz law [17] is represented by the following equation:

$$F = A(\delta_0 + \delta_d)^{3/2}. \tag{1.1}$$

The constant A depends on the material properties and the geometry of the contact area [17]:

$$A = \frac{4E_C E_S (1/R_S + 1/R_C)^{-1/2}}{[E_S(1-\nu_C^2)] + E_C(1-\nu_S^2)]}, \tag{1.2}$$

where in this case, $E_C = E_S = 193G$Pa and $\nu_C = \nu_S = 0.3$ are the elastic modulus and Poisson's ratio for the stainless steel cylinder and stainless steel sphere. The radii of contact particles are $R_S = 1$ mm and $R_C = 5$ mm with $1/R_C = 0$ because the cylinder has a planar contact surface.

The application of the Hertz law for dynamic contact behavior is valid for the following conditions: (1) The maximum shear stress close to the contact is smaller than the elastic limit; (2) the contact surface has a much smaller radius than the radius of the contacting particles; and (3) the characteristic time of the problem is much larger than the oscillation period of the basic harmonics for the elastic sphere particle. These conditions constraint the velocity of the particles.

The strongly nonlinear contact force can be linearized by assuming that the dynamic relative displacement in the wave between neighboring particles is much smaller than their initial displacement caused by static compressive force ($\delta_0 \gg \delta_d$):

$$F \approx A\delta_0^{3/2} + \frac{3}{2}A\delta_0^{1/2}\delta_d. \tag{1.3}$$

The two force components are the static force $F_0 = A\delta_0^{3/2}$ and dynamic force

$F_d = \frac{3}{2} A \delta_0^{1/2} \delta_d = \beta \delta_d$, where

$$\beta = \frac{3}{2} A \delta_0^{1/2} = \frac{3}{2} A^{2/3} F_0^{1/3}. \tag{1.4}$$

The upper and lower bound of the band gap for this system can be calculated following the classical approach presented, for example, in [15]:

$$f_1 = \frac{1}{2\pi} \left(\frac{2\beta}{M} \right)^{1/2}, f_2 = \frac{1}{2\pi} \left(\frac{2\beta}{m} \right)^{1/2}. \tag{1.5}$$

where M is the mass of the stainless steel cylinder and m is the mass of the stainless steel sphere. This band-gap can be tuned by changing the value of β, which depends on elastic properties and geometry of the contacting particles. In our experiments a static load equal 7.8 N results in cutoff frequencies of $f_1 = 9.2k$Hz and $f_2 = 88.4k$Hz and for a static load 0.8 N the cutoff frequencies are $f_1 = 6.3k$Hz and $f_2 = 60.6k$Hz.

Numerical calculations in the paper [5] are related to propagation of harmonic signals which are difficult to realize in experiments. Also system composed from PTFE balls and steel cylinders demonstrated a large attenuation masking band gap effects [6]. The response of nonlinear and especially strongly nonlinear discrete diatomic system to periodic boundary excitations was investigated in Chapter 2. Chapter 2 attempted to address the following questions. Whether the granular diatomic chains can support strongly nonlinear periodic waves in experiments? Can we develop a mechanical system with a band gap in the audible range of frequencies based on granular chains with a low level of dissipation where the major influence on signal propagation is caused by dispersive properties? Is the band gap introduced for a linear elastic interaction relevant to the transmission of nonlinear and strongly nonlinear quasiharmonic waves? What is the length of a discrete chain where some harmonics can be suppressed by the chain structure due to the band gap influence? Can we transform oscillatory shock waves on

short distances from the entrance? These questions are related to a basic science and also are important for practical applications where tuning of strong amplitude signals is desirable.

1.2 Strongly nonlinear wave in "Sonic Vacuum" state of dimer chain, role of dissipation

Granular chain with strongly nonlinear interaction between elastic spherical particles [17] of the same mass presents an example of the discrete systems with qualitatively new wave dynamics different than behavior of chains with elastically linear or weakly nonlinear interactions between elements [1-4,18-24]. One dimensional granular chains not precompressed by a static force represent an example of "sonic vacuum" [3]. This name emphasizes that sound speed in its classical sense is zero. "Sonic vacuum" or weakly precompressed granular chains (dynamic strains being much larger than initial strains) supports strongly nonlinear waves which are qualitatively different than weakly nonlinear solitary waves [1-4,18-24]. For example, strongly nonlinear solitary wave named Nesterenko solitary wave [5] has a width which does not depend on its amplitude, unlike width of weakly nonlinear solitary wave. The number of particles in this solitary wave depends on the details of interaction force, for example on the exponent in power law for interaction force [3]. Width of solitary wave, composed mostly from five particles in chains of spherical beads, comes from force exponent 3/2 in Hertzian interaction force. Ratio of solitary wave speed in sonic vacuum to initial sound speed is infinity, while for weakly nonlinear solitary wave this ratio is close to one. Strongly nonlinear solitary wave can be considered as "quasiparticle" with effective mass ~ 1.4 mass of the elements in Hertzian chain. A strongly nonlinear Nesterenko solitary wave converged into weakly nonlinear KdV solitary wace when strain amplitude is close to the initial

value, the opposite transition is not valid [3].

The behavior of these waves was investigated by different groups of researchers numerically, for example [2, 4,19], and experimentally using gauges embedded in the particles made from different materials [2, 3,18,20-23]. High speed photography allowing to measure particles displacements with a micrometer-scale resolution was used in [24]. Theoretical studies include exact analytical solution of strongly nonlinear wave equation [1, 3], stability of periodic solution in "sonic vacuum" [3, 25], proofs of existence of solitary wave in discreet systems [26, 27] and single pulse character with double exponential decay in [28-31].

Two mass, strongly nonlinear chains (dimer systems consisting of alternatively arranged particles with two different masses) demonstrate a new very interesting behavior which was first presented in [3] for relatively short chain composed from 40 particles. In the long wave approximation the system supports solitary waves with a characteristic space scale $L \approx 10a$, being twice that in the case of particles with the same masses, when the mass of one particle (m_1) is much larger than the mass of another (m_2) ($k = m_1/m_2 \gg 1$), and both have the same diameter a.

Behavior of two mass chains with different mass ratios (2, 4, 16, 24, 64) have been studied numerically keeping the chain's macroproperties (linear density and elastic properties) the same, and equal to the properties of the chain with equal mass m. It was ensured by redistribution of masses between neighboring particles under the condition $2m = m_1 + m_2$ and choosing the same distances between particle centers and interaction constants for both types of chains. The force acting on the contact of the chain with a supporting wall was used for the comparison of pulse attenuation in different systems [3].

Numerical simulations demonstrated that initial disturbance (created by impact of particle with mass equal to 2.5 mass of the cell ($5m$)) in the chain with large mass ratio (64) was quickly transformed into three solitary-like waves, unlike in the chain with

equal mass particles where six clearly detectable solitons were created. This behavior is in agreement with the discussed analytical prediction for $k \gg 1$. The phase speeds of leading pulses in both systems are practically identical. The time history of the light particle was similar to the velocity profile for the neighboring heavy particle only with amplitudes much smaller than amplitude of the leading pulse for the former particle. Additionally the motion of light particles exhibits a qualitatively new feature: high-frequency small-amplitude modulation of the velocity profile, more pronounced with the decrease of wave amplitude.

A new type of behavior was observed for a chain with smaller mass ratio despite keeping the same global properties of the system and impact by the same striker with the same velocity. When the mass ratio for the particles in the chain become equal to 2 or 4, there are no solitary waves formed based on the observation of the velocity history of light and heavy particles and force acting on the supporting wall. In this case the light and heavy particles behave significantly differently (see Fig. 1.18(b) and (c) in [3]). The velocity of the light particles in leading pulse has two maximums following by oscillatory tail with amplitude about two times smaller than amplitude of the leading pulse, even negative velocities were present in this oscillatory tail. These stress waves with complex shape mostly preserve their shape and amplitudes as they propagate along the investigated chain with 80 particles. Therefore, on this space scale they may be characterized as quasitationary waves.

The velocity of the heavy particles in leading pulse is represented by an asymmetric single peak followed by another peak with a wider duration and smaller amplitude. These two peaks mostly preserve their shape and amplitudes as they propagate with different speeds along the investigated chain with 80 particles, with an increase of space between them. These results were later confirmed in experiments [3].

It is important that at the same macroproperties and at the same striker impact,

the systems with different mass ratios demonstrate better mitigation properties (charged by force acting on the supported wall) in comparison with the system with equal masses of particle. The difference is more than twice at optimal mass ratio demonstrating the possibility of optimization of the granular chains as nondissipative impact protectors keeping their global properties the same [3].

Very important new type of behavior of stress pulses in strongly nonlinear dimer chains excited by δ-force applied to the first particle (global properties of these chains were not kept constant) was observed numerically in [5]. At certain discrete mass ratios of light to heavy spherical particles ($\varepsilon_n = 0.3428, 0.1548, 0.0901$ and also at other smaller values of ε_n) a true solitary wave was observed in numerical calculations. This solitary wave propagated without any detectable attenuation over long distances in system with a total number of 251 beads. Its behavior is explained by the antiresonances in the dimer chain satisfied only for certain values of ε_n. These specific quantum values of mass ratios ensure unique behavior of particles in the wave - the synchronization of the motion of light and heavy beads, providing transferring of the entire energy of the pulse through the chain. The conditions of propagating of unattenuated compression pulse were also formulated using the asymptotic analysis based on slow-fast time scale separation of the system dynamics in a reasonable agreement with numerical simulation of discrete system [5].

At general values of ε in nondissipative chains localized soliton-like propagating stress pulses were also observed, but their amplitude slowly decayed with distance and they were accompanied by oscillating tails. At values of ε different from specific quantum values ε_n the light bead loses contact with its left heavy neighbor at the end of the compression pulse, generating oscillations. They left behind the main compression pulse taking away its energy and resulting in its decay. In numerical calculations the maximum attenuation of compression stress pulse was observed at value $\varepsilon = 0.59$ [5].

The maximum attenuation was confirmed in recent experiments with a chain of 21 spheres suspended on the rods to minimize the dissipation effects [32]. Three chains were investigated with values of $\varepsilon = 1$ (homogeneous chain), and two dimer chains with $\varepsilon = 0.5$, and 0.125. The homogeneous chain and dimer chain ($\varepsilon = 0.125$) supported solitary wave. The dimer chain with $\varepsilon = 0.5$ demonstrated stronger attenuated behavior of the main pulse followed by oscillating tail. Three different levels of impacting forces were used to excite single pulses at the impacted end of the chain. The experimental results agree with numerical calculations (using damping coefficient in the range 32-35.4 Ns/m) demonstrating an expected deep minimum in transmitted force nearby $\varepsilon = 0.5$, characteristic for nondissipative chain.

Dissipation is present in all experiments with granular chains. This dissipation can be due to viscoelastoplastic deformation of contacts [33, 34], which in general has nonlinear dependence on strains [35-37]. Another strongly nonlinear discrete metamaterial composed from steel cylinders and rubber o-rings (with better tunability than system with Hertzian contacts [38-41]), demonstrated nonlinear dependence on strains and strain rates being sensitive to loading path [42, 43].

Simpler models were also used to account for the dissipative properties of contact interaction using approach based on coefficients of restitution [44], viscous friction [45] or using standard viscous dissipation model depending only on strain rate [32, 46, 47]. These approaches allowed analysis of the unique role of dissipation on the pulse nature. For example, at certain dissipation level excitation by δ-force resulted in two wave structure [46, 47]. This dissipation model allowed to establish analytical conditions for the transition from oscillatory to monotonous shock wave profiles [48, 49]. In this case the damping coefficient is a new effective parameter which may account for the complex nature of the dissipative processes during contact interaction. Of course its validity needs to be checked experimentally and may depend on conditions of experiments and material

properties.

In Chapter 3 we conducted experiments and numerical calculations to check if two mass chains with mass ratio (0.55), being close to optimal mass ratio for attenuation in nondissipative chain, is still the preferable attenuating system also in the presence of dissipation. To keep mechanism of dissipation identical for both systems we used steel cylinders in contact with spheres. The mass ratio was changed only by the changing the height of cylinders keeping spheres the same thus preserving the type of contact interaction between neighboring particles unlike in case where diameters of spheres were changed [31, 32]. This allowed to clarify the role of nonlinear dispersion caused by periodic arrangement of particles on pulse attenuation. The comparison of the attenuating properties of these two systems were made at the same number of particles from impacted end and also at the same mass of the system above particles where impulse was detected.

In the investigated range of pulse amplitudes, the linear viscous model with damping coefficient 6 kg/s satisfactorily described not only the attenuation of pulse amplitudes, but also the transformation of their shapes in both systems. The value of damping coefficient was significantly smaller than 32-35 kg/s in [32] probably due to the different nature of contacts. Two mass chain with mass ratio 0.55 demonstrated better performance in experiments and in numerical calculations only when the damping coefficient was below critical value. In numerical calculations with damping coefficient above this value, the one mass chain outperfoms the two mass system in attenuating pulse amplitudes.

1.3 Wave generated in “Sonic Vacuum” by impactor

Chains of elastic particles (e.g., steel beads) interacting by Hertz law exhibit nonclassical strongly nonlinear wave propagation behavior supporting new type of

solitary waves, shock waves and periodic waves [1-3, 50]. In case of zero precompression these chains can be characterized as “sonic vacuum”. This term was coined in [51, 52] emphasizing that classical sound waves can’t propagate and the basic excitations are solitary waves and not phonons.

Important feature of this system is fast transformation of incoming pulse excited by striker (or external dynamic force) into the train of solitary waves in weakly dissipative chains. This behavior is due to the strong nonlinearity of Hertzian contact interaction and dispersive behavior caused by the chain periodicity. Impact of striker results in the fast generation of solitary waves with their numbers (n) depending on the ratio of striker mass and mass of particles in the chain (if striker mass is larger than mass of particles) observed in numerical calculations and in experiments [1-3, 18, 22, 50, 53]. If mass of striker is equal or less than a mass of particles then a single solitary wave is generated [1-3, 19-23, 28, 53].

The train of solitary waves can be generated also by the time dependent force applied to the end of the chain. For example, triangular pulse with duration 10^{-4}s applied to the chain of steel particles with radius 3 mm resulted in 7 solitary waves and reduction of pulse duration to 10^{-5} s resulted in a single solitary wave [1] as well as application of delta function pulse to the end of the chain [54]. Influence of loading pulse duration on dynamic load transfer in a simulated granular medium was investigated in [18] for short (90 microseconds), intermediate (200 microseconds) and long (650 microseconds) input time dynamic load. Single solitary wave was generated in the first case, train of a few solitary waves was developed at 60th disk from the entrance while in third case initial smooth pulse was transformed into oscillating profile. The scaling of the number of solitary waves with ratio of the duration of incoming pulse and duration of solitary wave corresponding to the characteristic velocity at the boundary (e.g., striker velocity or velocity caused by external force) was introduced in [3] (see Eq. 1.79 in [3]). It was

suggested that single solitary wave is generated when characteristic time of the collision of striker is shorter or equal the duration of the transmitted solitary wave [22]. Universal relation for the solitary waves generated by the external force with finite rise and decay times was introduced in [55].

Single solitary wave or train of solitary waves can be generated by the incident solitary wave at the interface of two granular chains depending on the mass ratio of particles in these chains [50, 56-58].

Incident solitary wave approaching the interface from the "light" particles (PTFE beads) results in transmitted and reflected solitary waves which parameters can be found based on linear momentum and energy conservation laws considering a solitary wave as quasiparticles [3, 50]. Consideration of solitary wave in "sonic vacuum" as quasiparticle with effective mass is possible because the linear momentum and kinetic energy are a linear and quadratic functions of maximum particle velocity, and ratio of its kinetic and potential energies is a constant. It allows to write down the total energy (kinetic plus potential) of particles in a solitary wave as effective kinetic energy of quasiparticle with effective mass and linear momentum of all particles [50]. The effective mass of solitary wave in Hertzian chain is about $1.4m$, where m is mass of particles [23,53]. It should be mentioned that this effective mass depends on the interaction law between particles in the chain [3].

Very different behavior is observed when incident solitary wave approached the interface from the "heavy" particles chain (stainless steel beads). In this case the interfacial stainless steel particle quickly absorbed the main part of the energy of the incident wave. It acts as a striker on later stages generating oscillating wave profile and transmitting the linear momentum and energy into the chain with the "light" particles (PTFE beads). This wave is transformed later into train of solitary waves. This process can be characterized as practically the unidirectional energy transfer from the incident

pulse propagating in “heavy” stainless steel chain to the “light” PTFE chain without sending any tensile wave back to the former chain due to the zero tensile strength of the system [57]. Parameters of generated multiple solitary waves ($n \geq 3$) can’t be predicted based only on two conservation laws.

When train of solitary waves was excited by striker the maximum forces in the specific solitary wave in the train were approximated by exponential function depending on the solitary wave number (the first, second etc.,) with coefficient α being some function of the mass ratio of striker and particles in chain [53]. The authors were unable to find a specific function and to establish that exponential decrease of amplitude of solitary wave with its number [53].

Job et al [22] demonstrated that force amplitudes of the solitary wave in the train excited by striker decrease exponentially with solitary wave number. They demonstrated that the interaction between the striker and the chain is better characterized as collision with effective mass equal to effective mass of solitary wave and presented the equation for the relation between linear momentum of the striker and linear momentum of the leading solitary wave in the chain. Considering that linear momentum and energy of solitary waves in the chain are equal to the linear momentum and energy of striker authors found the dependence of coefficient α on mass ratio of striker and particles.

There is no direct way to find the parameters of separated solitary waves in the train far away from the interface of two sonic vacuum generated by interfacial particles or striker. Tichler *etal* [58] applied conservation of energy and linear momentum assuming the imaginary “collision” process between the end bead in the heavy chain (acting as a striker) and “in rest” solitary wave in the light chain treated as a quasiparticle with corresponding effective mass. This approach supplements two conservation laws by the imaginary process of linear momentum and energy transfer from the heavy interfacial particle to the train of solitary waves in the “light” chain far away from the interface. It

ignores the transient oscillatory wave in the "light" chain at the vicinity of the interface. But it allows calculation the linear momentum and energy of solitary waves in the train depending on the solitary wave number and mass ratio of heavy particle and effective mass of solitary wave in the chain of light particles in a satisfactory agreement with results of numerical calculations. It should be emphasized that proposed imaginary process to calculate properties of solitary waves far away from the interface is not unique and other approaches may be also possible.

In Chapter 4 we extended the analytical approach to calculate the parameters of solitary wave train generated at the interface of two sonic vacua (granular chains) proposed in [58] to the case of striker impact with different masses. It should be mentioned that though the "heavy" interfacial particle acted as a striker it also was supported by the rest of the "heavy" chain. It is not clear that approach proposed in [58] would be also applicable to find the parameters of solitary waves in the train generated by striker. In numerical calculations we found the scaling between the linear momentum of solitary wave and its maximum particle velocity. Using this scaling we demonstrated that approach similar to [58] allows to find parameters of solitary waves excited by striker with different masses in nondissipative chains with reasonable accuracy. The transition from generation of single solitary wave to the train of solitary waves is better described by ratio of striker mass and effective mass of solitary wave, and not by ratio of striker mass to particle mass.

We also addressed in more details the behavior of striker impacting "sonic vacuum". It was found that the transition between different striker's behavior: rebound of the striker from sonic vacuum or gradual decrease of its velocity with time to the value close to zero, is happening with its mass close to $1.4m$, where m is the mass of particles in the Hertzian chain. This value is close to the effective mass of solitary wave. Thus transition from complete transfer of striker energy into the chain to its recoil is better

modeled by ratio of striker mass and effective mass of solitary wave, and not by ratio of striker mass to particle mass. It reflects the striker intreraction with collective of particles near impacted end.

1.4 References

1 V.F. Nesterenko, "Propagation of nonlinear compression pulses in granular media",in *Prikl. Mekh. Tekh. Fiz.* **24**, 136 (1983) [*J. Appl. Mech. Tech. Phys*. **24**, 733 (1984)].

2 A.N. Lazaridi and V.F. Nesterenko, "Observation of a new type of solitary waves in a one-dimensional granular medium", in *Prikl. Mekh. Tekh. Fiz.* **26**, 115 (1985) [*J. Appl. Mech. Tech. Phys.* **26**, 405 (1985)].

3 V. F. Nesterenko, *Dynamics of Heterogeneous Materials*. New York: Springer, 2001.

4 S. Sen, J. Hong, J. Bang, E. Avalos, and R. Doney, "Solitary waves in the granular chain", in *Physics Reports*, **462**, 21 (2008).

5 K.R. Jayaprakash, Y. Starosvetsky, A. F. Vakakis,"New family of solitary waves in granular dimer chains with no precompression", in *Phys. Rev. E* **83**, 036606 (2011).

6 E. B. Herbold, J. Kim, V. F. Nesterenko, S. Y. Wang, and C.Daraio, "Pulse Propagation in a Linear and Nonlinear Diatomic Periodic Chain: Effects of Acoustic Frequency Band-gap", in *Acta. Mech.* **205**, 85 (2009).

7 M. A. Porter, C. Daraio, I. Szelengowicz, E. B. Herbold, and P. G. Kevrekidis, "Highly Nonlinear Solitary Waves in Heterogeneous Periodic Granular Media", in *Physica D* **238**, 6 (2009).

8 J. Tasi, "Initial-value problems for nonlinear diatomic chains", in *Physical Review B*, **14**, 2358 (1976).

9 St. Pnevmatikos, N. Flytzanis, and M. Remoissenet, "Soliton dynamics of nonlinear diatomic lattices", in *Phys. Rev. B*, **33**, 2308 (1986).

10 O.A. Chubykalo, A.S. Kovalev, and O.V. Usatenko, "Dynamical solitons in a one-dimensional nonlinear diatomic chain", in *Phys. Rev. B*, **47**, 3153 (1993).

11 S. Parmley, T. Zobrist, T. Clough, A. Perez-Miller, M. Makela, and R. Yu, "Phononic band structure in a mass chain", in *Appl. Phys. Lett.* **67**, 777 (1995).

12 A. Franchini, V. Bortolani and R.F. Wallis, "Intrinsic localized modes in the bulk and at the surface of anharmonic diatomic chains", in *Phys. Rev. B*, **53**, 5420 (1996).

13 A.V. Gorbach and M. Johansson, "Discrete gap breathers in a diatomic Klein-Gordon chain: Stability and mobility", in *Phys. Rev. E*, **67**, 066608 (2003).

14 P. Maniadis, A.V. Zolotaryuk, and G.P. Tsironis, "Existence and stability of discrete gap breathers in a diatomic Fermi-Pasta-Ulam chain", in *Phys. Rev. E*, **67**, 046612 (2003).

15 A.C. Hladky-Hennion, G. Allan and M. de Billy, "Localized modes in a one-dimensional diatomic chain of coupled spheres", in *J. Applied. Phys*, **98**, 054909 (2005).

16 C.Kittel, *Introduction to Solid State Physics* (Wiley, 2005), Chap. 4.

17 H. Hertz, "On the contact of elastic solids", in *J. Reine Angew. Math.* **92**, 156 (1881).

18 A. Shukla, M. H. Sadd, Y. Xu, and Q.M. Tai, "Influence of loading pulse duration on dynamic load transfer in a simulated granular medium", in *J. Mech. Phys. Solids* **41**, 1795 (1993).

19 E.J. Hinch and S. Saint-Jean, "The Fragmentation of a Line of Balls by an Impact", in *Proc. R. Soc. London A* **455**, 3201 (1999).

20 C. Coste, E. Falcon, and S. Fauve, "Solitary waves in a chain of beads under Hertz contact", in *Phys. Rev. E* **56**, 6104 (1997).

21 S. Job, F. Melo, A. Sokolow, and S. Sen, "How Hertzian solitary waves interact with boundaries in a 1D granular medium", in *Phys. Rev. Lett.* **94**, 178002 (2005).

22 F. Santibanez, R. Munoz, A. Caussarieu, S. Job, and F. Melo, "Experimental evidence of solitary wave interaction in Hertzian chains", in *Phys. Rev. E* **84**, 026604 (2011).

23 S. Job, F. Melo, A. Sokolow, S. Sen, "Solitary wave trains in granular chains: experiments, theory and simulations", in *Granular Matter* **10**,13 (2007).

24 J. Yang, M. Gonzalez, E. Kim, C. Agbasi, M. Sutton, "Attenuation and localization of solitary waves in 1D granular crystals visualized via high speed photography",

in *Experimental Mechanics* **54**, 1043 (2014).

25 S.L.Gavrilyuk and V.F.Nesterenko, "stability of periodic Excitations for one model of 'sonic vacuum' ", in *Prikl. Mekh. Tekh. Fiz.* **34**, 45 (1993) [*J. Appl. Mech. Tech. Phys.* **34**, 784 (1993)].

26 G. Friesecke and J. A. D. Wattis, "Existence theorem for solitary waves on lattices", in *Commun. Math. Phys.* **161**, 391-418 (1994);

27 R. S. MacKay, "Solitary waves in a chain of beads under Hertz contact", in *Phys. Lett. A* **251**, 191-192 (1999).

28 A. Chatterjee, "An Asymptotic Solution for Solitary Waves in a Chain of Elastic Spheres", *Phys. Rev. E* **59**, 5912-5919 (1998).

29 J.M. English and R.L.Pego, "On the solitary wave pulse in a chain of beads", in *Proc. AMS* **133**, 1763-1768 (2005).

30 K. Ahnert and A. Pikovsky, "Compactons and chaos in strongly nonlinear lattices", in *Phys. Rev. E* **79**, 026209 (2009).

31 A. Stefanov and P.G. Kevrekidis, "On the existence of solitary traveling waves for generalized Hertzian chains", in *J. Nonlin. Sci.* **22**, 327-349 (2012).

32 R.Potekin, K.R. Jayaprakash, D.M. McFarland, K. Remick, L.A. Bergman, A.F. Vakakis, "Experimental Study of Strongly Nonlinear Resonances and Anti- Resonances in Granular Dimer Chains", in *Exper. Mech.* **53**, 861 (2013).

33 E. Wang, T. On, and J. Lambros, "An experimental study of the dynamic elasto-plastic contact behavior of dimer metallic granules", in *Exper. Mechanics* **53**, 883 (2013).

34 R.K. Pal, A.P. Awasthi, and P.H. Geubelle, "Characterization of wave propagation in elastic and elastoplastic granular chains", in *Phys. Rev. E* **89**, 012204, (2014).

35 G. Kuwabara and K. Kono, "Restitution coefficient in a collision between two spheres", in *Jpn. J. Appl. Phys.* **26**, 1230 (1987).

36 N. V. Brilliantov, F. Spahn, J.-M. Hertzsch and T. Poschel, "Model for collisions in granular gases", in *Phys. Rev. E* **53**, 5382 (1996).

37 W. Morgado, and I. Oppenheim, "Energy dissipation for quasielastic granular particle collisions", in *Phys. Rev. E* **55**, 1940 (1997).

38 E.B. Herbold, and V. F. Nesterenko, "Solitary and shock waves in discrete strongly

nonlinear double power-law materials", in *Appl. Phys. Lett.* **90**, 261902 (2007).

39 P.I. Dias, A. Rosas, A.H. Romero, and K. Lindenberg, "Pulse propagation in a chain of o-rings with and without precompression", in *Phys. Rev. E* **82**, 031308 (2010).

40 A. Spadoni, C. Daraio, W. Hurst, and M. Brown, "Nonlinear phononic crystals based on chains of disks alternating with toroidal structures", in *Appl. Phys. Lett.* **98**, 161901 (2011).

41 Y. Xu and V. F. Nesterenko, "Propagation of short stress pulses in discrete strongly nonlinear tunable metamaterials", in *Phil Trans R. Soc. A* **372**, 20130186 (2014).

42 C. Lee, and V. F. Nesterenko, "Dynamic deformation of strongly nonlinear toroidal rubber elements", in *J. Appl. Phys.* **114**, 083509 (2013).

43 C. Lee, and V. F. Nesterenko, "Path Dependent High Strain, Strain-rate Deformation of Polymer Toroidal Elements", in *J. Appl. Phys.* **116**, 083512 (2013).

44 M. Manciu, S. Sen, A.J. Hurd, "Impulse propagation in dissipative and disordered chains with power-law repulsive potentials", in *Physica D* **157**, 226 (2001).

45 A. Rosas and K. Lindenberg, "Pulse dynamics in a chain of granules with friction", in*Phys. Rev. E* **68**, 041304 (2003).

46 A. Rosas, A. H. Romero, V. F. Nesterenko, and K. Lindenberg, "Observation of Two-Wave Structure in Strongly Nonlinear Dissipative Granular Chains", in *Phys. Rev. Lett.* **98**, 164301 (2007).

47 A. Rosas, A. H. Romero, V. F. Nesterenko, and K. Lindenberg, "Short-pulse dynamics in strongly nonlinear dissipative granular chains", in *Phys. Rev. E* **78**, 051303 (2008).

48 E. B. Herbold and V. F. Nesterenko, "Shock wave structure in a strongly nonlinear lattice with viscous dissipation", in *Phys. Rev E* **75**, 021304 (2007).

49 E.B. Herbold, V.F. Nesterenko, "Periodic waves in a Hertzian chain", in *Physics Procedia 3*, 465(2010).

50 V. F. Nesterenko, "Solitary waves in discrete media with anomalous compressibility and similar to 'sonic vacuum' ", *Journal De Physique IV*, Colloque **C8**, supplement au Journal de Physique III, 1994, **4**, C8-729 - C8-734 (1994).

51 V.F. Nesterenko, "Nonlinear waves in 'sonic vacuum' ", *Fizika gorenia i vzryva*, **28**, 3, 121-123 (1992) (in Russian).

52 V.F. Nesterenko, “Examples of ’sonic vacuum’ ”, *Fizika gorenia i vzryva*, 1993, **29**, 2, 132-134 (1993) (in Russian).

53 A. Sokolow, E.G. Bittle, S. Sen, “Solitary wave train formation in Hertzian chains”, in*Europhys. Let.* **77**, 24002 (2007).

54 S. Sen, M. Manciu, “Solitary wave dynamics in generalized Hertz chains: An improved solution of the equation of motion”, in *Phys. Rev., E*, **64**, 056605 (2001).

55 X. M. Arif Hasa, and S. Nemat-Nasser, “Universal relations for solity waves in granular crystals under shocks with finite rise and decay times”, in *Phys. Rev E*, **93**, 042905, (2016).

56 V.F. Nesterenko, A.N. Lazaridi, and E.B. Sibiryakov, “The decay of soliton at the contact of two ’acoustic vacuums’ ”, in *Prikl. Mekh. Tekh. Fiz.*, **36**, 2, 19-22 (1995). [*Journal of Applied Mechanics and Technical Physics* (JAM), **36**, 2, 166-168 (1995)].

57 V.F. Nesterenko, C. Daraio, E. Herbold, and S. Jin, “Anomalous wave reflection at the interface of two strongly nonlinear granular media”, *Physical Review Letters*, **95**, 158702 (2005).

58 A. M. Tichler, L. R. Gomez, N. Upadhyaya, X. Campman, V. F. Nesterenko, and V. Vitelli, “Transmission and reflection of strongly nonlinear solitary waves at granular interfaces”, *Physical Review Letters*, **111**, 048001 (2013).

Chapter 2

Quasiharmonic Wave Propagation In Strongly Nonlinear Two-Mass Chains

Experimental set up was developed to allow the generation of quasi-harmonic signals at the end of nonlinear and strongly nonlinear two-mass granular chains composed of steel cylinders and steel spheres. This chapter presents the first experimental data related to the propagation of quasi-harmonic signals in nonlinear and strongly nonlinear chains. The signals were detected using gauges imbedded inside particles at the entrance of the system and at depths equal to 4 cells and 8 cells. At this relatively short distances we were able to detect practically perfect transparency at low frequencies and cut off effects at band gap frequencies for nonlinear and strongly nonlinear signals. It was also observed that oscillatory shocks were transformed into monotonous shocks at these short propagating distances. Systems which are able to transform nonlinear and strongly nonlinear signals at small sizes of the system are important for practical applications such as attenuation of high amplitude pulses. Numerical calculations of signal transformation by non-dissipative granular chains were also performed which demonstrated transparency of the system at low frequencies and cut off phenomenon at high frequencies in reasonable

agreement with experiments.

2.1 Experimental procedures

The one-dimensional granular chains are assembled using a PTFE cylinder with an inner diameter of 10 mm. The stainless steel cylinders and stainless steel spheres were arranged in alternative order with each other (Fig. 2.1a). This chain consisted of one magnetic particle, 55 stainless steel cylinders with height 5mm, diameter 10 mm and mass $3.21g$ and 57 stainless steel spheres with diameter 2 mm and mass $0.35g$. An additional magnetic particle was placed on the top of the chain to induce a compression force due to a magnetic interaction with the outside magnet. The static force applied was tunable by changing the weight of the magnet. We use magnets with different weights ($80g$ and $800g$) on the top of the chain. A magnet with a relatively small weight was used for creating conditions for a strongly nonlinear system (dynamic force being similar to static force) and magnet with a larger weight was used for nonlinear systems (dynamic force significantly smaller than static force).

Three calibrated piezoelectric sensors ($RC \sim 10^3 \mu s$) were embedded in three stainless steel cylinders and were connected to an oscilloscope Tektronix TDS 2014 to detect the force-time curve. The piezoelectric sensors were placed in the 1st, 5th and 9th cell, so there were 4 cells between them.

A B&K vibration generator with a stainless steel rod having length of 20 cm and diameter of 5 mm attached to it was used to the generate a quasiharmonic excitation at the entrance of the diatomic chain. Agilent 33220A $20M$Hz function/arbitrary waveform generator was used in our experiments.

The contact force between the rod and last particle represented boundary conditions for our system which were controlled by the first gauge close to the corresponding

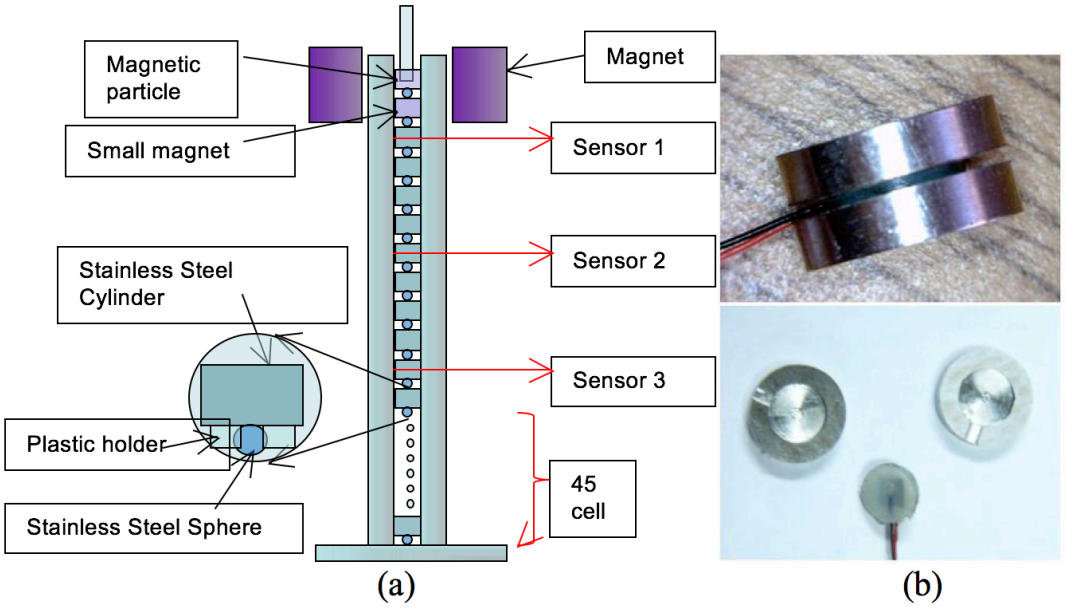

Figure 2.1: Schematic drawing of the experiment setup for two mass chains. (a) The general experimental setting. (b) The pictures of sensor assembly.

end of a system. The generator created an incoming signal with different frequencies and amplitudes that can tune the amplitude of vibrations of the rod and parameters of waves in the chains. A soft spring supported the vibrator to control the additional static force which may come from the weight of vibrator.

2.2 Results and Discussions

2.2.1 Nonlinear Case

To create a nonlinear system we used a relatively large (in comparison with dynamic force in the wave) static compression of 8 N. In this system a quasiperiodic signal with amplitude about 2N was created at the top of the chain. The strength of the signal was smaller than initial precompression, but of the same order of magnitude with the static force. This kept the system in the nonlinear regime. A quasiharmonic

signal with 5kHz was first generated. The signal had a frequency lower than the lower bound of band gap corresponding to this static force, which is $f_1 = 9.2k$Hz, upper band frequency $f_2 = 88.4k$Hz. It was observed that the signal was transmitted without change of fundamental frequency, but with some attenuation. The high transparency of the system can be explained given that the 5kHz was outside the band gap. The attenuation of the amplitude is connected to the unavoidable dissipation in experiments.

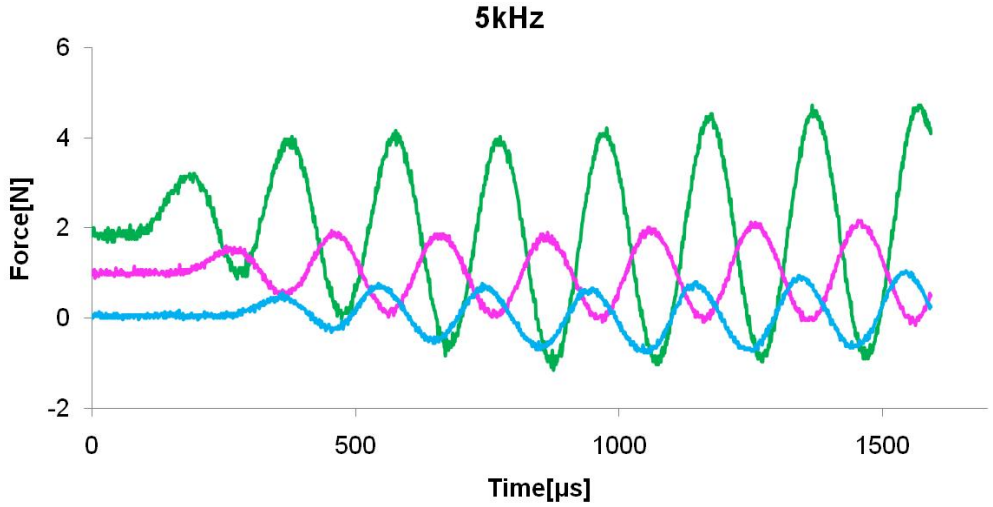

Figure 2.2: Experimental results , the propagation of quasiharmonic nonlinear pulse with main initial frequency of 5kHz at the entrance of the system, static force $F_0 = 7.8$N. The lower range of the forbidden frequency is 9.2kHz which is higher than the major harmonic in the input signal.

The experimental results were compared with numerical calculation of the chain without dissipation. We tried to create an input signals at the system in numerical calculations similar to input signals in experiments. We were able to match relatively closely the amplitudes of main harmonics though these signals are not identical. It should be mentioned that only elastic properties of particles were used to calculate forces between particles (Eqs. 1.1-1.4), no adjustable parameters were used in calculations. From Fig. 2.3, we can observe that time intervals corresponding to traveling of pulses from gauges placed in 1st and 5th, and 5th and 9th cells are similar in experiments and numerical

calculations demonstrating that the speeds of the pulses in calculations were in agreement with experiments. The main frequency of 5 kHz was carried on during transmission without attenuation. In numerical calculation where there is no dissipation, that is why the signal is able to propagate with no attenuation. In the experiments, however, the initial amplitude of the signal was reduced at the 5th cell due to inevitable dissipation (Fig. 2.2, 2.3(b), top figure). The shape of transmitted signal remains practically the same with only reduced amplitude. The Fourier coefficients derived from a fast-Fourier-transform similar to [5] are presented for numerical and experimental signals correspondingly at the left and right bottom parts of Fig. 2.3.

From the comparison of numerical and experimental data we can observe that quasiperiodic nonlinear signal with main frequency 5 kHz below lower band gap corresponding to elastically linear system ($f_1 = 9.2k$Hz, Eq. 1.5) propagates almost without attenuation in calculations and with significant attenuation in experiments.

The example of quasiharmonic signal with a frequency $15k$Hz, which is inside the band gap is shown in Fig. 2.4, comparison between experimental and numerical data is presented in Fig. 2.5. In experiments the signals with main frequency $15k$Hz propagated with strong attenuation and shape of signal changed dramatically. Still the fundamental frequency can be clearly picked out after its propagation through 9 cells at sensor 3. Numerical calculations of nonlinear granular chains were used to clarify a mechanism of attenuation. The bottom waves in Fig. 2.5 (a) show that $15k$Hz component was completely wiped out at the second and third gauges, the cut off frequency in numerical calculations is about $11k$Hz. This behavior is in contradiction with some transparency at the fundamental frequency $15k$Hz in experiments. We can provide a preliminary explanation that this may be due to the nonlinearity of the system where low frequency harmonics present in experiments (input signal in numerical calculations did not have this low frequency components) cause some transparency inside band gap in experiments. We

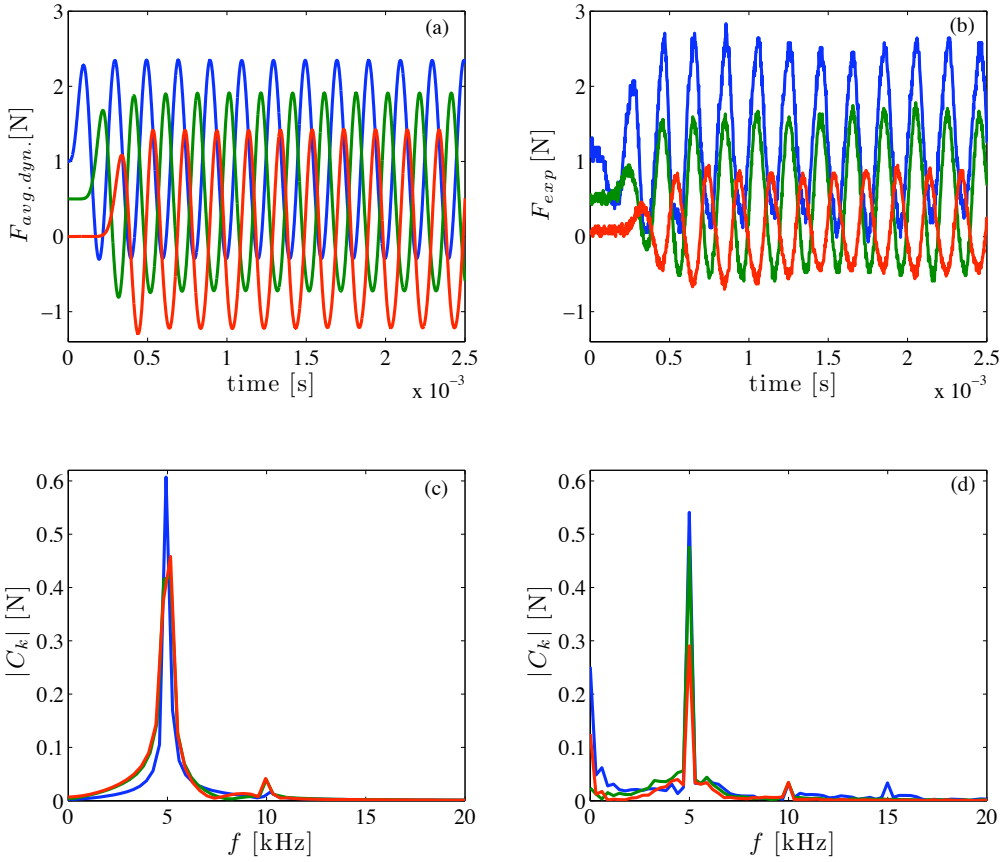

Figure 2.3: The comparison between the numerical calculation of the 5 kHz signal propagating through the system and the experimental results. (a) Numerical calculations: dynamic force inside corresponding particles (c) their Fourier-transforms. (b) Experimental results: dynamic force inside corresponding particles and (d) their Fourier-transforms.

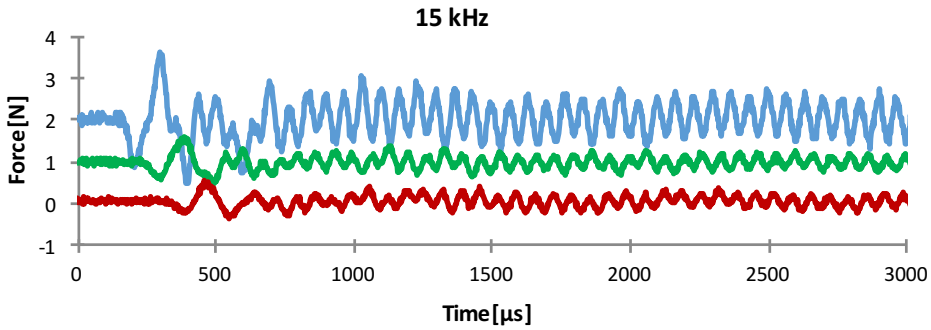

Figure 2.4: Experimental results , the propagation of quasiharmonic nonlinear pulse with main initial frequency of 15kHz at the entrance of the system. Nonlinear system, static force $F_0 = 7.8$N. The lower range of the forbidden frequency is 9.2kHz which is lower than the input signal frequency.

plan to investigate this interesting discrepancy between numerical data and experimental results in our future research. We also observe a cut off frequency equal about 11kHz in numerical calculations which is different than 9.2kHz calculated for the lower band gap frequency in linear approximation corresponding to the static force 7.8N. This cut off frequency is not reflected in experimental data.

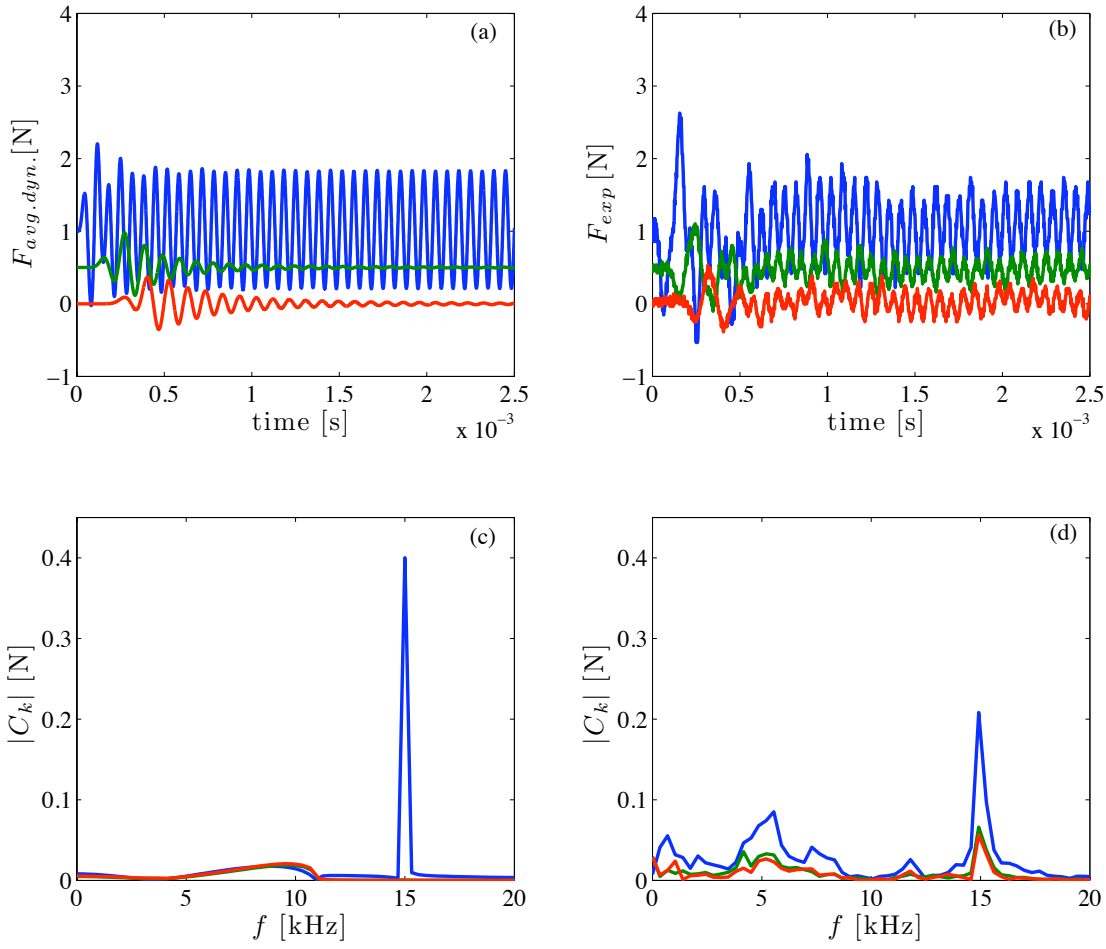

Figure 2.5: The comparison between the numerical calculation of the 15kHz signal propagating through the system and the experimental results. (a) Numerical calculations: dynamic force inside corresponding particles and (c) their Fourier-transforms. (b) Experimental results: dynamic force inside corresponding particles and (d) their Fourier-transforms. In (c) curves corresponding to sensors 2 and 3 are almost identical.

We compared the attenuation of propagating quasiharmonic signals with the increase of frequency for interval of 5 - 20 kHz. Fig. 2.6 presents the relative amplitudes

of the main harmonics detected at the second gauge (A2) and third gauge (A3) with respect to the amplitude of the same harmonic at the gauge 1 (A1). The sudden drop of signal transmission at the frequency of 7kHz was observed. The quasiharmonic signal was able to propagate through the system at only 20% of the input signal strength for the frequencies between 7kHz and 14kHz. At 15kHz the signal amplitude dropped to zero very fast, just at the 5th cell from entrance. We may conclude that at these distances from the entrance in our experiments the system is partially transparent for frequencies above frequency f_1 (Eq.1.5) and non transparent at frequency about 2 f_1. We plan more detailed comparison of numerical and experimental results in our future research.

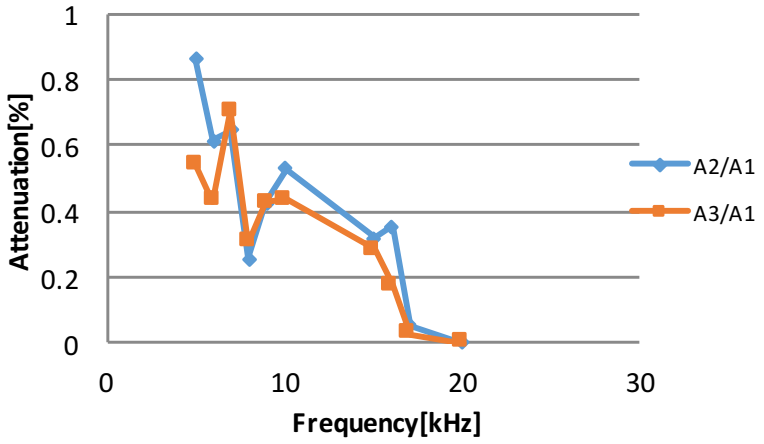

Figure 2.6: The comparison of the attenuation with the increase of frequency in experiments. A1 is the amplitude of the incoming signal measured by sensor 1. A2 is the amplitude of the signal measured by sensor 2. A3 is the amplitude of the signal measured by sensor 3

At higher frequencies of the rod vibrations we were able to generate oscillatory shock waves, presented in Fig. 2.7 (a).

We can see dramatic change of the shape of the pulses. From Fourier transforms (Fig. 2.7(b)) we observe practically complete decay of component at 20kHz and less attenuation at lower frequencies. As a result an initial front was ramped, and oscillations on the shock profile were wiped out while lower frequencies in the propagated signal

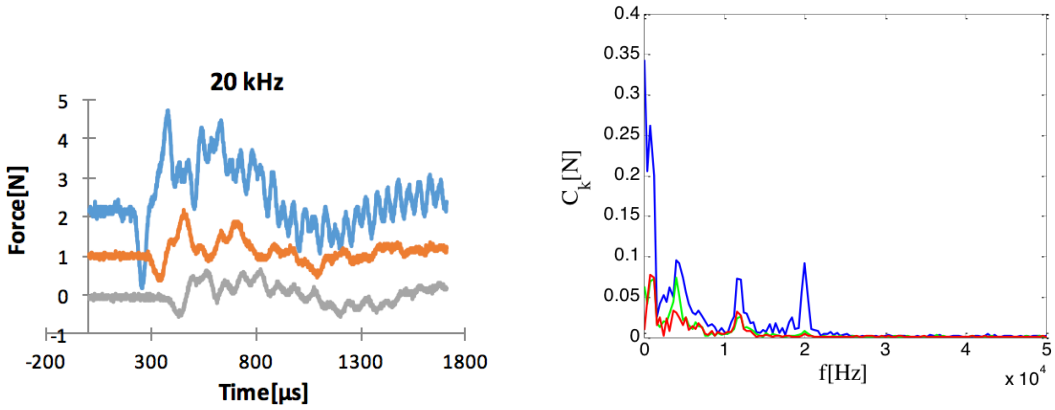

(a) (b)

Figure 2.7: The propagation of oscillatory shock. (a) Experiemntal profiles of forces in three gauges, (b) The fast Fourier transforms of the propagating signals. Nonlinear system, static force $F_0 = 7.8$N. The lower range of the forbidden frequency is $9.2k$Hz.

were detected by sensors 2 and 3. This data are in a qualitative agreement with data in [5] for transformation of oscillatory shocks in PTFE-stainless steel system.

2.2.2 Strongly Nonlinear Case

We consider the system as a strongly nonlinear when the amplitude of the signal (1N) was similar to the initial compression force ($F_0 = 0.82$ N). We investigated first a quasiharmonic signal at the 3 kHz excited at the entrance to the system. The frequency of this signal was lower than the lower bound of band gap for given static compression in linearized system ($f_1 = 6.3k$Hz, $f_2 = 60.6k$Hz). Experimental data are presented in Fig. 2.8. We can see that the signal was transmitted without change of its shape with some attenuation. However, there was no change in fundamental frequency as in case of low frequency for nonlinear system (Fig.2.2).

Numerical calculations presented in Fig. 2.9 shows that the main harmonic with frequency of 3 kHz was carried on during transmission in agreement with the experiments. Numerical data also demonstrate transparency of strongly nonlinear system at frequency

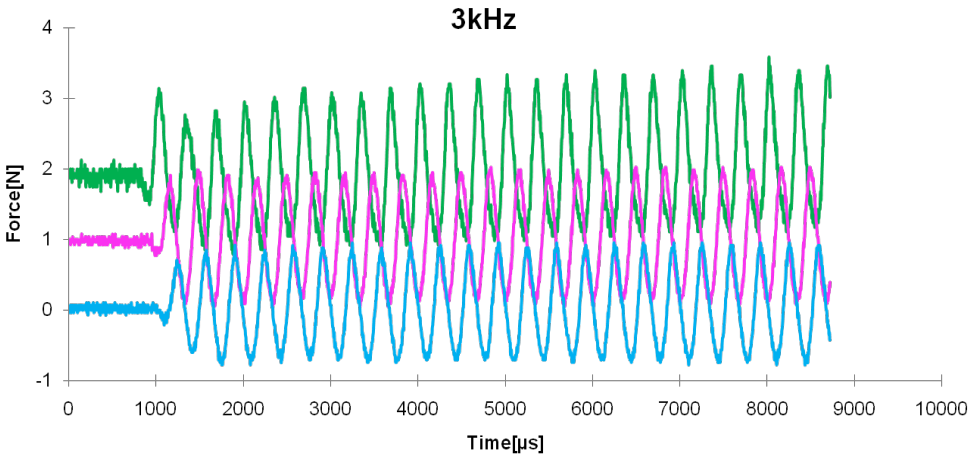

Figure 2.8: Experimental results. The propagation of quasiharmonic nonlinear pulse with frequency of 3kHz in the strongly nonlinear system, static force $F_0 = 0.82$N. The lower range of the forbidden frequency is 6.3 kHz which is higher than the input signal frequency.

about 6 kHz and 9 kHz. The former can be due to a strong nonlinearity of the system.

Experimental results corresponding to the main input frequency 15 kHz are presented in Fig. 2.10. We can observe that high frequency component of strongly nonlinear signal was practically wiped out within short distances from the entrance. This is demonstrated by the Fourier transforms related to numerical calculations and experiments presented in Fig. 2.11. Clearly, there was no transmission of signal in either the numerical calculation or the experimental data at 15 kHz.

We compared the attenuation of propagating quasiharmonic signals with the increase of frequency for interval of 3 -18 kHz for strongly nonlinear system. In the Figure 2.12 the relative amplitudes of the main harmonics detected at the second gauge (A2) and third gauge (A3) with respect to the amplitude of the same harmonic at the gauge 1 (A1) are presented. The cut off of signal transmission at the frequency of 7 kHz was observed with unexpected transparency at higher frequency 9 kHz followed by second drop in transparency at about 10 kHz. The band gap calculated for linear system

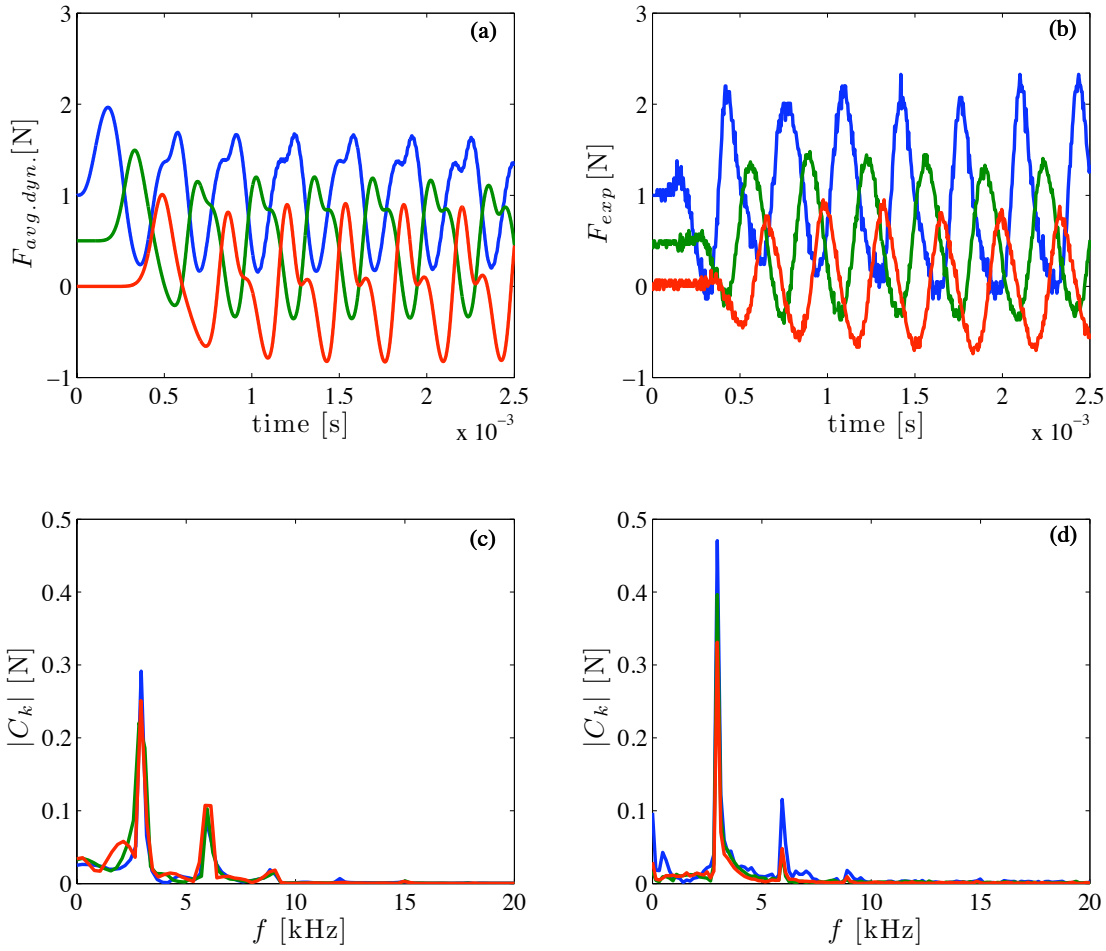

Figure 2.9: The comparison between the numerical calculations and the experimental results for the initial signal with main frequency of 3 kHz. (a) Numerical calculations: dynamic force inside corresponding particles and (c) their Fourier-transforms. (b) Experimental results: dynamic force inside corresponding particles and (d) their Fourier-transforms.

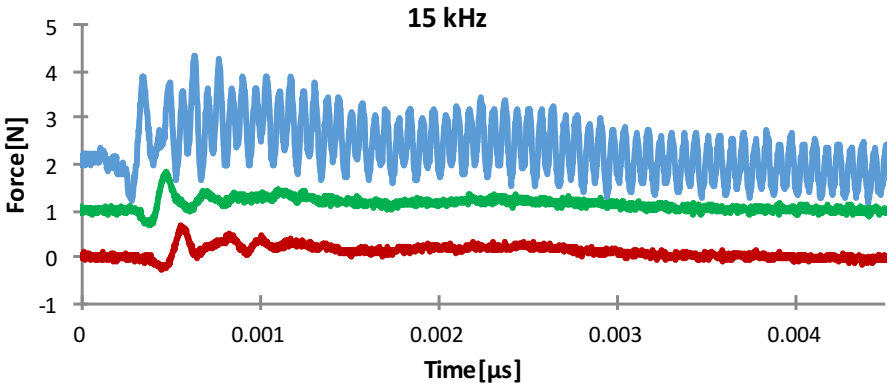

Figure 2.10: The propagation of quasiharmonic nonlinear pulse with the main frequency of 15 kHz in the strongly nonlinear system, with static force F_0 = 0.82N. The lower range of the forbidden frequency is 6.3 kHz which is lower than the main frequency of the input signal.

was 6.3 kHz to 60.6 kHz. It is amazing that strongly nonlinear system also demonstrated transparency inside band gap calculated for the linear system.

At higher frequencies of the rod vibrations we were able to generate oscillatory shock waves for strongly nonlinear system as it was a case for a nonlinear system (Fig. 2.13(a)).

We can observe the transmission of low frequency harmonics and fast decay of high frequency harmonic. As a result the initial front was ramped, and high frequencies were wiped out while the low frequencies remained (Fig. 2.13(b)). This resulted in more monotonous shock profile.

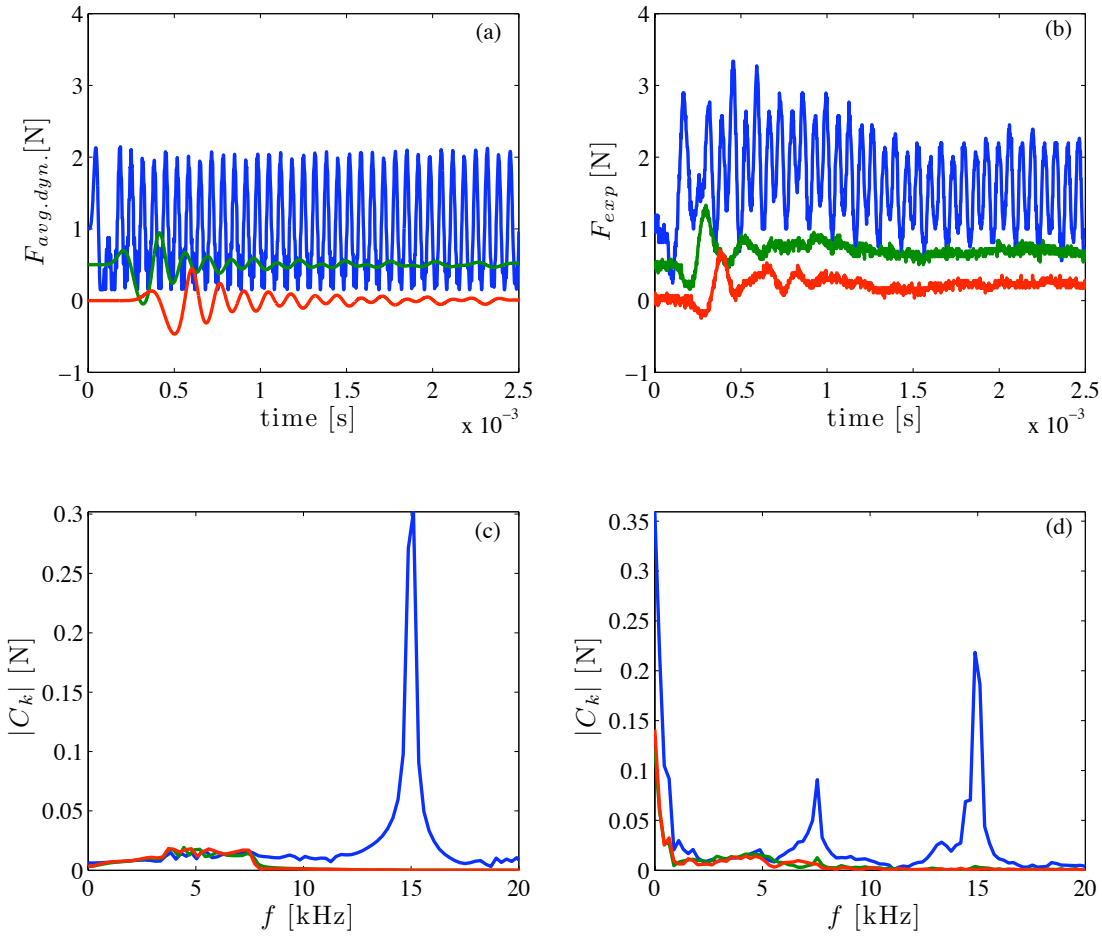

Figure 2.11: The comparison between the numerical calculation of the 15 kHz signal propagating through the system and the experimental results. (a) Numerical calculations: dynamic force inside corresponding particles and (c) their Fourier-transforms. (b) Experimental results: dynamic force inside corresponding particles and (d) their Fourier-transforms.

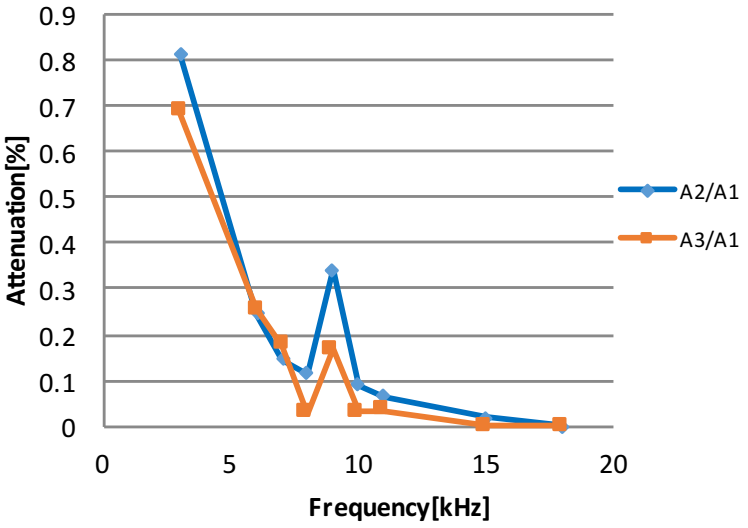

Figure 2.12: The comparison of the attenuation with the increase of frequency. A_1 is the amplitude of the incoming signal measured by sensor 1. A_2 is the amplitude of the signal measured by sensor 2. A_3 is the amplitude of the signal measured by sensor 3.

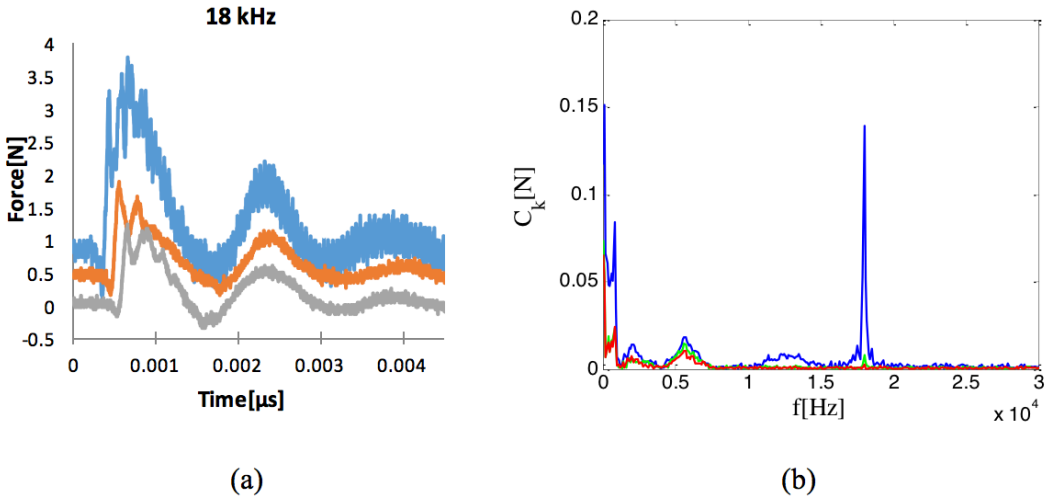

Figure 2.13: The propagation of strongly nonlinear oscillatory shock in the system, static force F_0 = 0.8N. The lower range of the forbidden frequency is 6.3 kHz which is lower than the main input signal frequency. (a) The force dependence on time in gauges 1-3, (b) The fast Fourier transforms of the propagating signals.

2.3 Conclusions

One-dimensional experimental set up was developed to investigate propagation of nonlinear and strongly nonlinear quasiharmonic waves. The quasiperiodic boundary conditions were created by vibrating rod with prescribed frequency contacting with one end of a granular chain. Incoming waves were monitored by gauge inside particle placed near the corresponding end of the chain. This set up allowed control of propagating nonlinear and strongly nonlinear quasiharmonic waves and shock waves. A practically perfect transparency of investigated systems was observed at low frequencies and cut off effects at higher frequencies for nonlinear and strongly nonlinear signals. Numerical calculations of signal transformation by non dissipative granular chains demonstrated transparency of the system at low frequencies and cut off phenomenon at high frequencies in reasonable agreement with experiments. Transition from oscillatory to monotonous shock wave was observed in experiments for nonlinear and strongly nonlinear systems, attributed to mesostructural effects. Strongly nonlinear systems were less transparent than nonlinear systems at the similar amplitude of the exciting signal and at the same distance from the entrance.

The text of Chapter II is, in part, based on the material in the following publications: S. Y. Wang, E. B. Herbold, and V. F. Nesterenko, in "Wave Propagation In Strongly Non- linear Two-Mass Chains", in IUTAM Proceedings on granular materials, J.D. Goddard, J.T. Jenkins, P. Giovine (eds.), AIP Conference Proceedings, IUTAM-ISIMM Symposium on Mathematical Modeling and Physical Instances of Granular Flow, Reggio Calabria, September 14-18, 2009. American Institute of Physics, vol. 1227, Melville, New York, pp. 425-434, (2010). The dissertation author was a primary researcher and an author of the cited material.

Chapter 3

Attenuation of Short Strongly Nonlinear Stress Pulses in Dissipative Granular Chains

Attenuation of short, strongly nonlinear stress pulses in chains of spheres and cylinders was investigated experimentally and numerically for specific two ratios of their masses intentionaly keeping their contacts identical. The chain with mass ratio 0.98 supports solitary waves and another one (with mass ratio 0.55) supports nonstationary pulses which preserve their identity only on relatively short distances, but attenuate on longer distances because of radiation of small amplitude tails generated by oscillating small mass particles. Pulse attenuation in experiments in the chain with mass ratio 0.55 was faster at the same number of the particles from the entrance than in the chain with mass ratio 0.98. It is in quantitative agreement with results of numerical calculations with effective damping coefficient 6 kg/s. This level of damping was critical for eliminating the gap openings between particles in the system with mass ratio 0.55 present at lower or no damping. With increase of dissipation numerical results show that the chain with

mass ratio 0.98 provides faster attenuation than chain with mass ratio 0.55 due to the fact that the former system supports the narrower pulse with the larger difference between velocities of neighboring particles. The investigated chains demonstrated similar behavior at large damping coefficient 100 kg/s.

3.1 Experimental procedures

Experiments were conducted with chains composed from *SS*304 stainless steel cylinders and 440*C* stainless steel balls (Fig. 3.1) arranged alternatively. Stainless steels *SS*304 and 440*C* have a similar elastic properties and density. The chain was placed vertically inside the channel made by four Al alloy rods providing alignment of particles with minimum contacts between them and rods for minimizing friction and dissipation. Two different mass ratios were achieved by keeping the spheres the same, while selecting cylinders with different heights. The larger cylinder has a height $h = 9.6$ mm and a mass (m_c) of 3.77 g and the small cylinder has a height $h = 5.3$ mm and a mass of 2.043 g. In both cases the spheres had a mass (m_s) 2.085 g and diameter $d = 8$ mm, the same as diameter of cylinders. The cell size in this array was equal to $h + d$. The mass ratio of the chain with the smaller cylinder is 0.98 corresponding to the chain which supported solitary wave. For the system with the larger cylinder height, the mass ratio is 0.55, which corresponds to the most efficient attenuation due to dispersion effects in nondissipative chain of spheres [1]. The waves in the systems were generated by impact of 440*C* steel ball with mass 2.085 g (less than the cell mass equal 5.855 g and 4.128 g). Two piezogauges were embedded inside cylinders at different depths, with one gauge embedded in 4th cylinder (used to specify the incoming pulse) and the other one inside the cylinder placed at different depths. The piezogauges, supplied by Piezo Systems Inc. were custom cut and wired, they had the sensitivity in the range 6.8 - 7.1 N/V. The

piezogauges ($RC \sim 537\mu$s), were calibrated using the impact by PTFE sphere (mass 0.12 g) with a recorded velocities ($0.7 - 0.8$ m/s) and based on linear momentum conservation which gives the value of the force integral over time from the start of the impact to the maximum force. The signals from the gauges were recorded using oscilloscope Tektronics TDS 2014.

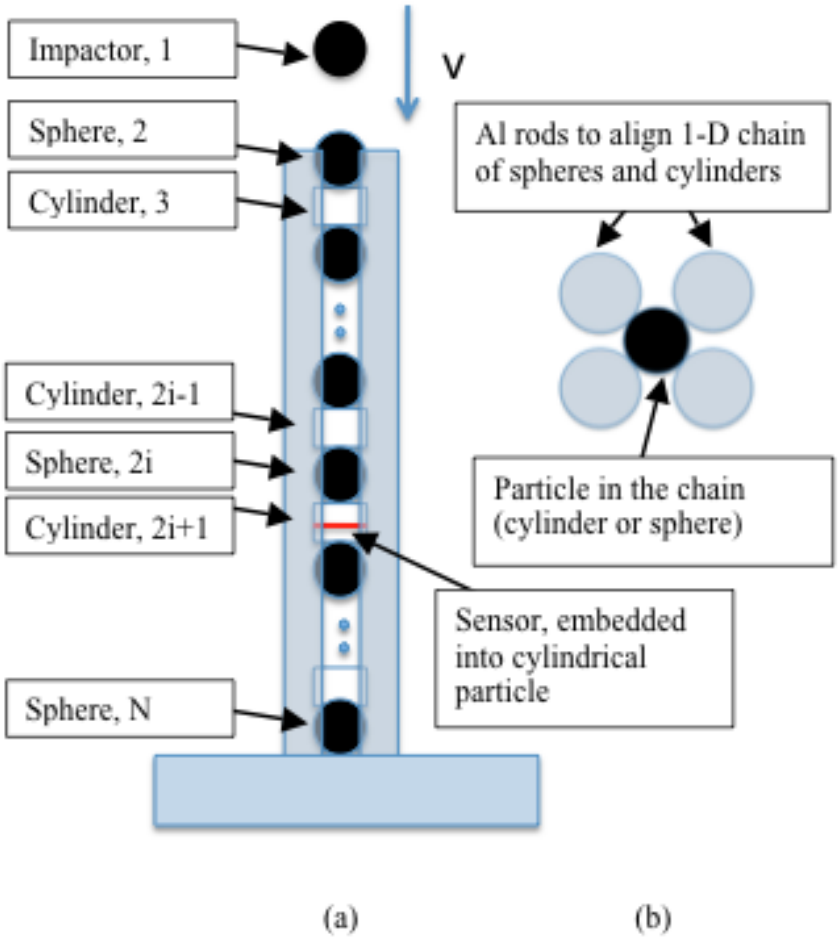

Figure 3.1: Experimental set-up. Cylinders and spheres aligned in 1-D chain inside the holder (a) and cross-sectional view of the assembly (b). Four aluminum rods hold the particles in aligned chain. In the numerical calculations the particles inside the chain with even numbers are spheres and particles with odd numbers are cylinders,$i = 2,3,4,...N/2$. The impactor is a separate particle outside of chain with number 1.

3.2 Numerical Calculations

Numerical calculations of the chain behavior were based on strongly nonlinear contact force between bodies with the radii of contact equal R_1 and R_2 described by a static Hertz law [2] valid for elastic contact deformation,

$$F = \frac{4E_1E_2}{3[E_1(1-\nu_2^2)+E_2(1-\nu_1^2)]}\left(\frac{R_1R_2}{R_1+R_2}\right)^{1/2}\delta^{3/2}, \tag{3.1}$$

where R_1 and R_2 are corresponding radii of the contacting undeformed particles and their Young's moduli (E_1, E_2) and Poisson's ratios (ν_1, ν_2) and δ is the change between centers of interacting bodies due to contact deformation. The curvatures of the surfaces of contacting neighboring particles can be selected independently of their masses. These arrays may have large masses of cylinders with small radii of rounded ends. It allows change of interaction law and the properties of the system, but keeping overall density the same.

To apply static law (Eq. 3.1) for the dynamic contact interaction between particles the pulse duration should be much longer than the characteristic times of sound propagation in the sphere and cylinders equal to their characteristic sizes (diameters, height divided by corresponding sound speeds). The nondissipative equations of motion for particles inside the chain oriented in the vertical direction and thus including gravitational force are the following

$$m_c\ddot{u}_{2i-1} = A[\{(\upsilon_{2i-1,0}+\upsilon_{2i-2})-(u_{2i-1,0}+u_{2i-1})\}_+^{3/2} - \{(u_{2i-1,0}+u_{2i-1})-(\upsilon_{2i,0}+\upsilon_{2i})\}_+^{3/2}] + m_cg, \tag{3.2}$$

$$m_s\ddot{\upsilon}_{2i} = A[\{(u_{2i-1,0}+u_{2i-1})-(\upsilon_{2i,0}+\upsilon_{2i})\}_+^{3/2} - \{(\upsilon_{2i,0}+\upsilon_{2i})-(u_{2i+1,0}+u_{2i+1})\}_+^{3/2}]+m_s g, \quad (3.3)$$

where m_c is the mass of the stainless steel cylinder and m_s is the mass of the stainless steel sphere. Displacements $u_{2i-1,0}$ and $\upsilon_{2i,0}$ represent equilibrium displacements of centers of cylinders and spheres in the gravitationally loaded chain calculated from positions in initially undeformed chain. The other displacements u_{2i-1}, υ_{2i} represent dynamic parts of overall displacements during wave propagation. N is the total number of particles (including the impactor), $i = 2,3,4,...N/2$, and even number N corresponds to the last spherical particle contacting the wall. Even particle numbers correspond to spherical particles in the chain and odd numbers to cylinders, the spherical impactor is particle number 1 (see numbering of particles in Fig. 3.1). Positive subscript corresponds to the force between neighboring particles being in contact, otherwise interaction force is zero.

Coefficient A for contact interaction of flat surfaces of cylinders and spheres with radius R_S is equal

$$A = \frac{4E_C E_S (R_S)^{1/2}}{3[E - S(1-\nu_C^2) + E_C(1-\nu_S^2)]}. \quad (3.4)$$

The constant A depends on the Young's moduli (E_C, E_S) and Poisson's ratios (ν_C, ν_S) of materials of interacting particles and the radius of sphere [2].

The separate equation for the impactor (dynamic displacement υ_1), initially contacting the first sphere in the gravitationally loaded chain (there is no contact deformation

between these two particles prior to the impact) is:

$$m_{imp}\ddot{\upsilon}_1 = -A_1(\upsilon_1-\upsilon_2)_+^{3/2} + m_{imp}g, A_1 = \frac{4E_{imp}E_S(R_{imp})^{1/2}}{3[E-S(1-\nu_{imp}^2)+E_{imp}(1-\nu_S^2)]}, \quad (3.5)$$

where A_1 is corresponding to the contact of the impactor and the first sphere having the same radii and elastic properties.

Equation for the first spherical particle in the chain (dynamic displacement υ_2) is

$$m_s\ddot{\upsilon}_2 = A_1(\upsilon_1-\upsilon_2)_+^{3/2} - A[(\upsilon_{2,0}+\upsilon_2)-(u_{3,0}+u_3)]_+^{3/2} + m_sg. \quad (3.6)$$

Equation for the last spherical particle (dynamic displacement υ_N) contacting the flat wall is

$$m_s\ddot{\upsilon}_N = A[(u_{N-1,0}-u_{N-1})-(\upsilon_{N,0}+\upsilon_N)]_+^{3/2} - A(\upsilon_{N,0}+\upsilon_N)_+^{3/2} + m_sg. \quad (3.7)$$

In all experiments we observed attenuation of the pulse amplitude. To explain this phenomenon we added effective linear viscous term (F_{vis}) to all contact interactions. Introduction of effective viscosity to describe dissipation processes (friction, viscoplastic deformation) on the contacts is similar to the one used in [3-8]. Resulting viscous forces acting on the impactor, first particle, on cylinders and spheres inside the chain and between last particle and the flat wall at the deformed contacts are described by Eqs. 3.8-3.12 with corresponding coefficients of viscous damping $F_{vis,1}$ and $F_{vis,N}$,

$$F_{vis,1} = \mu_1[\dot{\upsilon}_2-\dot{\upsilon}_1)], \quad (3.8)$$

$$F_{vis,2} = \mu_1[\dot{\upsilon}_1-\dot{\upsilon}_2)]+\mu[\dot{u}_3-\dot{\upsilon}_2], \quad (3.9)$$

$$F_{vis,2i-1} = \mu[\dot{\upsilon}_{2i-2}-2\dot{u}_{2i-1}+\dot{\upsilon}_{2i}], \quad (3.10)$$

$$F_{vis,2i} = \mu[\dot{u}_{2i-1} - 2\dot{\upsilon}_{2i} + \dot{u}_{2i+1}], \tag{3.11}$$

$$F_{vis,N} = \mu[\dot{u}_{N-1} - 2\dot{\upsilon}_{N})]. \tag{3.12}$$

When the particles are separated the viscous term is considered to be equal zero as well as elastic part of contact forces. In numerical calculations of dissipative chain a linear momentum were conserved with accuracy $10^{-6}\%$.

In the numerical calculation the pulse was generated by giving an initial velocity to the impactor. Its velocity was adjusted to provide the amplitude of the reference pulse similar to the corresponding experimental values for adequate comparison of its evolution at later times.

3.3 Results and Discussion

3.3.1 Pulse attenuation in the chain with mass ratio 0.98

In experiments short pulse was generated by the impact of a spherical steel particle, the same as the spherical particles in the chain. Impactor mass was close to the half of cell mass ($m_s + m_c$). The drop height of the striker is kept equal to 3 cm resulting in an amplitude of the reference signals (around 110 N) recorded by the gauge embedded into the 4th cylinder.

The impact resulted in a single, solitary like pulse (Fig. 3.2). The pulse speed (618 ± 19 m/s) was calculated using distance between sensors and time interval between maximums of bell shape signals using the data from the sensors embedded into 4th and 5th cylinders.

A reference pulse duration was equal to 55μs based on records from the sensor embedded into the forth cylinder. Based on these data the length of the pulse was equal to 2.5 cell sizes (cell is composed from sphere and cylinder), which is close to the expected

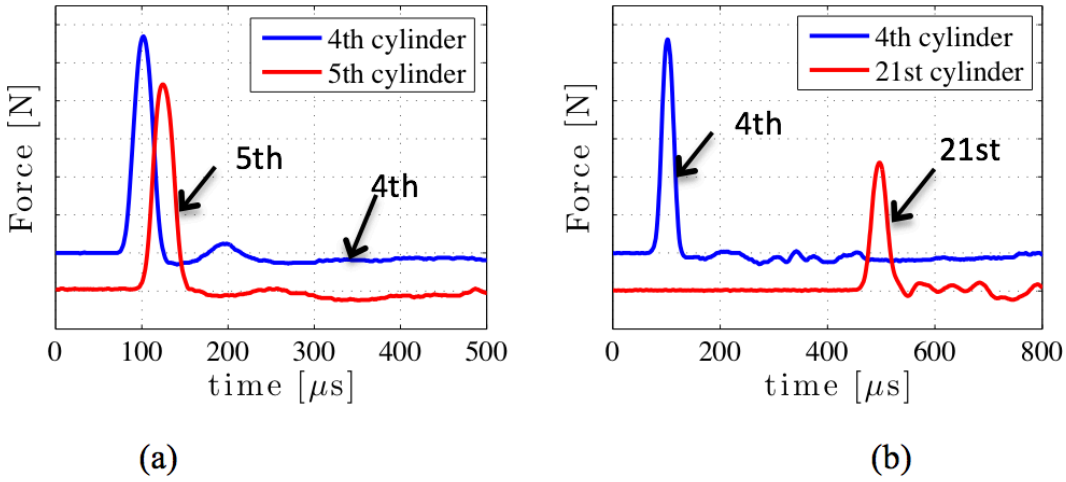

Figure 3.2: Experimental results. Single pulse propagating through a chain with the mass ratio of 0.98. (a) Signals correspond to sensors embedded into the 4th and 5th cylinder. (b) Signals correspond to sensors embedded into the 4th and 21st cylinder. Pulses were excited by the impact of a spherical steel particle. The vertical scale in both figures is 20 N and zero time is arbitrary, the curves are offset for visual clarity.

solitary wave length in the chain with equal masses (5 particles).

As the signal propagates through the system, the amplitude decreases and the time width of the pulse increases which is clearly seen by comparison of signals corresponding to the sensors in 4th and 21st cylinders presented in Fig. 3.2(b). The pulse speed (611 ± 6 m/s) calculated based on records of gauges embedded into 15th and 21st cylinders was slightly lower than a speed measured in the interval between 4th and 5th cylinders, due to the attenuation of the pulse amplitude (Fig. 3.2). The shape of the pulse detected by the gauge in the 21st cylinder was slightly nonsymmetrical probably due to dissipation. The length of this pulse (based on its speed 611 m/s and duration) was equal to 3.5 cell size, being larger than the width of the reference pulse detected by the sensor embedded into the 4th cylinder.

It is interesting to compare the speeds and width of the pulses with exact analytical solution for the nondissipative chain obtained in long wave approximation for the chain without static precompression. This is possible to do because the amplitude of the pulse in

the wave is much larger than gravitational precompression. In numerical calculations we demonstrated that the pulse shape and speed at the investigated distances from entrance were negligibly affected by gravitation.

The separate numerical calculations with mass ratio equal 1 were performed and demonstrated insignificant difference of properties of solitary waves under the same impact at investigated number of particles in comparison with the case when mass ratio was 0.98. In the presence of gravitation a difference in amplitudes at 43th particle was 0.02% in the chains with mass ratios 1 and 0.98. Some differences in the behavior of chains with mass ratio 1 and 0.98 were observed at the impact by larger mass after wave propagation at long distance from the entrance which will be a subject of the separate research.

If we neglect the difference between masses of spheres and cylinders, then the speed of the solitary wave(V_s) can be calculated using the following equation connecting parameters of solitary wave solution in a long wave approximation [9]

$$V_s = \frac{2}{\sqrt{5}} c \xi_m^{1/4} = \left(\frac{16}{25}\right)^{1/5} c^{4/5} \upsilon_m^{1/5}, \tag{3.13}$$

where ξ_m is the maximum strain equal to $2\delta_m/(h+2R)$, δ_m is the maximum change of the distance between centers of neighboring sphere and cylinder, υ_m is a maximum particle velocity in a solitary wave and the constant c corresponds to non-dissipative contact of the sphere and plate

$$c^2 = \frac{E}{6(1-\nu^2)m} \sqrt{\frac{R}{2}} (h+2R)^{5/2}. \tag{3.14}$$

In experiments we measure force acting on the gauge embedded inside the cylinders. The relation between the maximum of this force and speed of solitary wave can be satisfactory described by maximum force acting between neighboring particles

(Eq. 3.15), similar to [9] with constants adjusted for the array of cylinders with flat sides and spheres

$$V_s \approx \frac{h+2R}{\sqrt{5}} \left(\frac{2ER^{1/2}}{3m^{3/2}(1-\nu^2)} \right)^{1/3} F_m^{1/6}. \tag{3.15}$$

This equation demonstrates that the speed of the solitary wave depends on the cell size $(h+2R)$. It can be different for the chains with the same masses of spherical particles and cylinders, if the cylinders have different heights h. It should be mentioned that relation between speed of solitary wave and maximum force acting between particles (Eq. 3.15) uses only the leading approximation in a Taylor series for relative displacements between neighboring particles in the discrete chain and strains in the continuum limit.

The pulse speed calculated using Eq. 3.15 and the value of the maximum force (108 N), recorded by the gauge embedded in the 5th cylinder (Fig. 3.2(a)), is 593 ± 12 m/s, which is close to the pulse speed (618 ± 19 m/s) in the experiments. The speed of the pulse (547 ± 12 m/s), estimated using Eq. 3.15, based on the average force amplitude (68 N) detected by the sensors in the 15th and 21st cylinders was lower than the average speed (611 ± 6 m/s) measured in the interval between 15th and 21st cylinders (based on the distance and corresponding time interval). It should be mentioned that F_m in the Eq. 3.15 is the maximum force acting on the contact between particles, but sensors are embedded inside particles, recording the average force on the corresponding contacts [9, 10]. This average force for the solitary wave stress pulse at low precompression is about 1.4 times smaller than the maximum force [10], contributing to the difference in speeds calculated from the maximum of recorded force and time intervals. We can conclude that despite the wider pulse length and its asymmetric shape its speed was close to the speed of the solitary wave in the uncompressed uniform chain despite dissipation present in the system. Thus this system of cylinder and spheres supports attenuated localized stress pulses close to the solitary like waves predicted in a long wave approximation in

agreement with previous observations in the chains composed from spheres only.

Numerical calculations of the pulse propagating in a discrete chain with mass ratio 0.98 were carried out for the same system parameters. The main focus of our research was on pulse propagation inside the system. To make appropriate comparison with experiments (impact velocity 1.2 m/s), in numerical calculations the velocity of impactor (1.06 m/s) was adjusted to reproduce the same amplitude and shape of the reference pulse in 4th cylinder as in experiments and trace the evolution of this pulse as it propagates inside the chain. Fig. 3.3 shows the comparison between the numerical calculations (with and without dissipation) and the experimental results. It is worth mentioning that gravitational force is considered in our numerical calculations. However, since this is a relatively short chain, calculations without gravitational force show similar results with largest difference in amplitudes of waves about 5% for longest traveling distances investigated in this work.

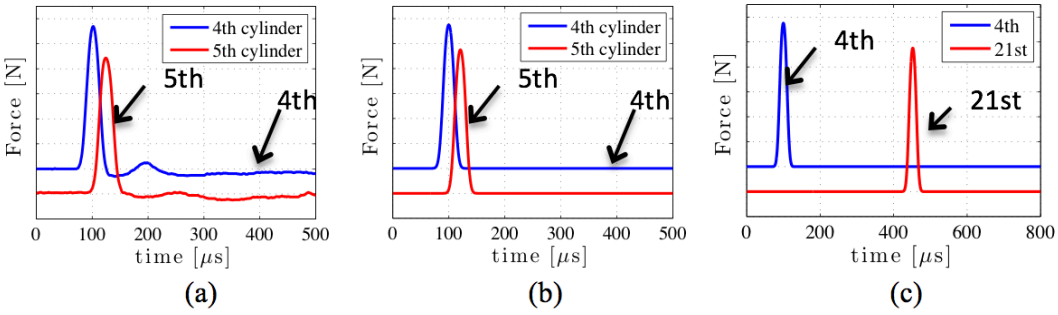

Figure 3.3: Comparison of experimental results and numerical calculations of the pulse propagating through the system which has a mass ratio of 0.98. Sensors are placed in the 4th, 5th and 21st cylinders. (a) Experimental results, (b), (c) numerical calculations (without dissipation) related to the forces in the corresponding cylinders. The vertical scale is 20 N and the curves are offset for visual clarity and zero time is arbitrary.

In numerical calculations without dissipation the solitary wave was quickly formed at the first few particles. It propagated without noticeable changes in its speed (648 m/s) and shape with value of particle velocity in the maximum being equal to 0.74 m/s. Speed of solitary wave with the same amplitude of particle velocity using analytical

solution (Eq. 3.13) was equal to the same value 648 m/s. Their equal values are in the agreement with the comparison of solitary wave speeds in discrete chain and in analytical solution in continuum limit at the same amplitude of particle velocities, the difference being less than 1% [9]. At the same time the value of solitary wave speed in numerical calculations was close to the experimental value of 618 ± 19 m/s, corresponding to the solitary wave with amplitude similar to numerical calculations. Pulse length in numerical calculations was equal to 2.5 cells similar to experimental results.

Detailed comparison between analytical solution in a long wave approximation and results of numerical simulations for a discrete chain were discussed in [11]. Assuming that total displacement in numerical calculations for discrete chain during the passage of the solitary wave is equal to displacement of particles derived from the exact solution for strain the authors found amplitude of displacement in latter solitary wave solution. With this value of strain amplitude in continuum limit the calculated speed of solitary wave was close to the speed in numerical calculations within 2%. At the same amplitude of displacement the calculated maximum of particle velocity was 12% lower than in numerical calculations of discrete chain. A calculated maximum force using two terms in a Taylor series was 13% lower than in numerical calculations of discrete chain [11]. This correspondence of exact solution for long wave approximation with results for a discrete chain explains successful use of the former solution to describe experimental results in 1-D chains made from particles of different materials where the accuracy of force measurements is about 10% [12-14].

It is evident that we have attenuating solitary wave in our experiments. To explain the observed attenuation of the pulse in experiments the dissipation was modeled by introducing a viscous terms into all contact interactions, as described above (Eqs. 3.8-3.12). Fig. 3.4 shows the comparison between the numerical calculations with dissipation ($\mu = 6$ kg/s) and the experimental results.

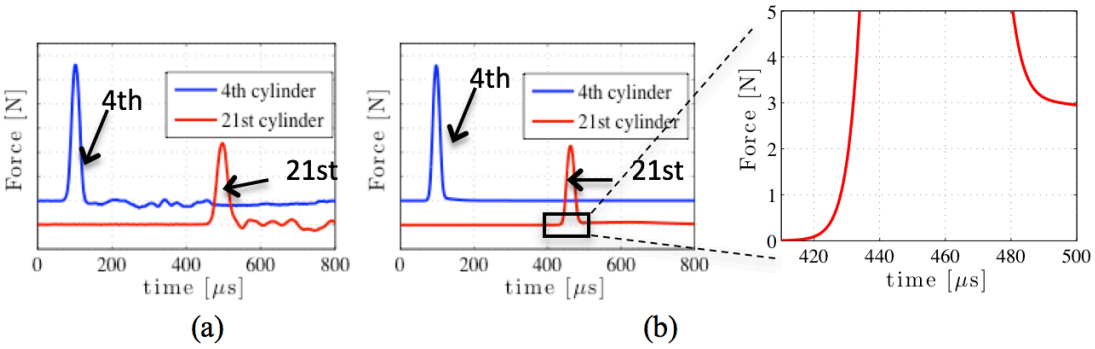

Figure 3.4: Experimental results and numerical calculations of the pulse propagating through the system with mass ratio of 0.98. (a) Experimental results, sensors are placed in the 4th and 21st cylinders, (b) Numerical calculation with damping coefficient 6 kg/s related to the forces in the corresponding cylinders. The vertical scale in (a), (b) is 20 N. The curves are offset for visual clarity and zero time is arbitrary. .

In numerical calculations pulse at 21st cylinder has a tail with small constant positive amplitude equal to 3 N (see insert to Fig. 3.4(b)), which is in qualitative agreement with the modification of corresponding signal shape in experiments (Fig. 3.4a). This is also in agreement with the influence of viscous dissipation on the shape of short pulses which was investigated in [5, 6].

Comparison of attenuation of the relative pulse amplitude (A_i/A_4) in experiments and numerical calculations using damping coefficients 0, 4 and 6 kg/s is shown in the Fig. 3.5. It is clear that introduction of the viscous dissipation correctly explains the signal amplitude decay. Both damping coefficients satisfactory describe the experimental data, and damping coefficient 6 kg/s provides a better fit at largest investigated distances from the impacted end.

The decay of relative pulse amplitude due to damping as it travels through the chain in numerical calculations (damping factor equal 6 kg/s) and in experiments is satisfactory described by exponential function with value of exponent equal to 0.028 (Fig. 3.6). Exponential decay in numerical calculations due to plastic deformation on the contacts was observed in the paper [15].

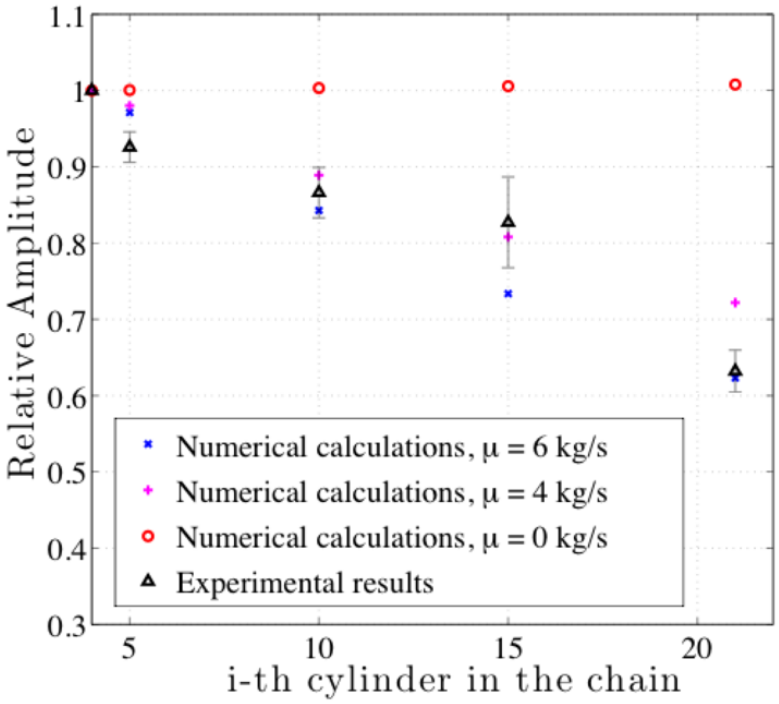

Figure 3.5: Relative amplitude of signal at *i*-th cylinders (corresponding to different depths) with respect to the amplitude of the reference pulse detected by the sensor in the 4th cylinder in the chain with mass ratio 0.98, experimental data and numerical results with different damping coefficients.

The dissipation in one mass chain resulted not only in attenuation of the amplitude of solitary like pulse, but also in the tail wave following this pulse, first introduced in [5, 6]. No such tail was detected in nondissipative chain. This small amplitude tail at relatively close distance from the impacted end is clearly identified in numerical calculations shown in Fig. 3.7. At larger distance from the impacted end the clear separation of the leading solitary wave and shock like pulse are observed in numerical calculations (Fig. 3.7).

The mechanism of this two waves pattern was provided in [5, 6]. The faster attenuation of leading solitary pulse is due to the larger gradients of particle velocity due to small space scale of this pulse (about 5 particles). When its amplitude becomes smaller than amplitude of following shock wave they start a process of convergence

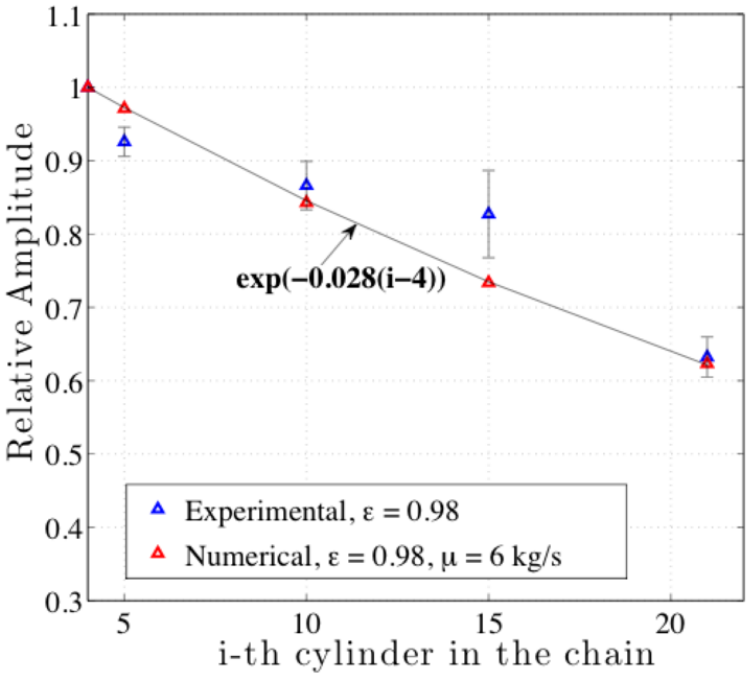

Figure 3.6: Attenuation in experiments (blue) and in numerical calculations with damping coefficient 6 kg/s (red) comparing with exponential decay.

resulting in oscillating shock wave. This unique process of two wave structure generated by dissipation was also observed at a larger damping coefficient 10 kg/s and 15 kg/s. For example, in the latter case two waves were formed at the vicinity of 60th cylinder and they converged approaching the 70th cylinder. Only oscillatory shock wave remained at the depth corresponding to the 80th cylinder. At damping coefficient 100 kg/s two waves pattern was not formed, instead monotonous attenuating shock wave was observed.

3.3.2 Pulse attenuation in the dimer chain with mass ratio 0.55

It is known that the sphere/sphere chain with mass ratio 0.55 does not support stationary solitary waves [1, 3]. Pulse in the dimer chain with mass ratio 0.55 (mass of sphere equal 2.085 g and mass of cylinder was increased to 3.77 g) in experiments was excited by the same impactor (mass 2.085 g) at the same velocity as in the previous chain

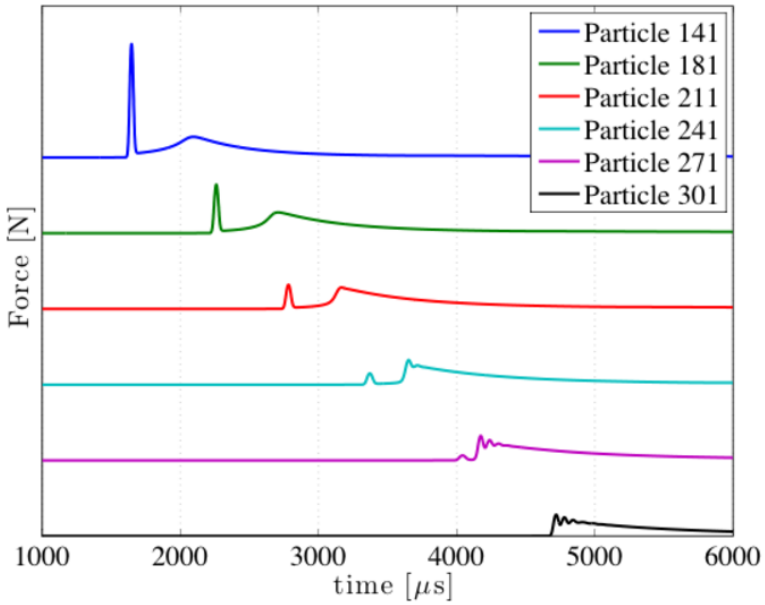

Figure 3.7: The formation of two wave structure (solitary wave followed by shock wave) in one mass chain impacted by sphere with velocity 1.45 m/s, damping coefficient 6 kg/s. The y-axes scale for all curves representing forces in corresponding particles (all of them are cylinders) are offset by 10 N for clarity.

with mass ratio 0.98. This allows comparison of pulse transformation in both chains under identical conditions of impact and contact interaction between particles.

In this work a different cylinder/sphere dimer chain is investigated. The results of numerical calculations for transmission of dynamic force in these chains with fixed contacts depending on mass ratio of particles for a chain composed from 42 particles (21 spheres and 21 cylinders) are shown in Fig 3.8. It is clear that in nondissipative chains the value of mass ratio corresponding to the position of global minimum is close to the values in non-fixed contacts sphere/sphere chains [1,3].

The numerical calculations with damping coefficient 6 kg/s, introduced to explain experimental results with the chain having mass ratio 0.98 and the same contacts as dimer chain are presented in Fig. 3.8 also. It is clear that dissipation shifts the position of the global minimum toward larger values of mass ratio (0.6) in comparison with nondissipative chain. It should be emphasized that the change of transmitted force in

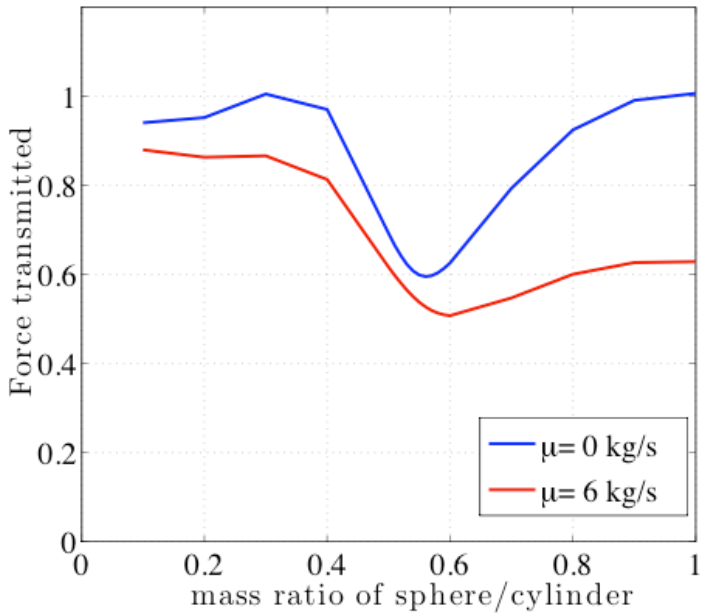

Figure 3.8: Dependence of the force in the 21st cylinder normalized with respect to the force at the entrance (at 4th cylinder) on mass ratio in nondissipative and dissipative chains with fixed contacts. Mass of sphere was kept the same and mass of cylinder changed keeping fixed contacts.

dissipative chains is not symmetric with respect to global minimum - significantly larger reduction of amplitude is observed at mass ratios in the interval 0.6-1 than in the interval 0.1-0.6. We explain this nonsymmetric behavior by larger gradients of particle velocity between neighboring particles in chains with smaller mass differences. This mechanism is qualitatively similar to the difference in attenuation between chains with mass ratios 0.98 and 0.55 explained later.

In agreement with this prediction (Fig. 3.8), impact by stainless steel sphere with velocity 1.4 m/s did not generate a single solitary wave in experiments (Fig. 3.9), unlike in previous case with practically equal masses of sphere and cylinders (Fig. 3.2). Instead a leading pulse was followed by series of smaller amplitude pulses. The leading pulses captured by the gauge imbedded in the heavier particles (cylinders) have double peaks repeatable in all experiments. In numerical calculations of the chain with mass ratio 0.5

leading pulses of particle velocity for light particles also had two peaks, followed by oscillating velocity profiles with negative velocities at some moments (Fig. 1.18(b) in [9]). As the pulse propagates inside the chain it attenuates and the amplitude difference between these two peaks becomes smaller (Fig. 3.9 (b)). The pulses following the leading doable peak transformed into oscillatory tail later (compare signals from sensors embedded in 4th and 5th cylinders with signal from the sensor in 21st cylinder). The decrease in the pulse amplitude is caused by the fact that this chain does not support solitary waves and dissipation.

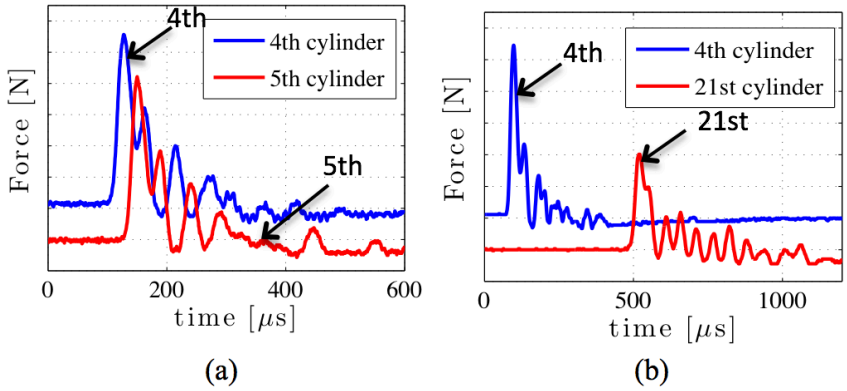

Figure 3.9: Experimental results. Stress pulses propagating through a chain with the mass ratio 0.55, mass of cylinders is larger than mass of spheres. (a) Signals correspond to sensors embedded into the 4th and 5th cylinder. (b) Signals correspond to sensors embedded into the 4th and 21st cylinder. Pulses were excited by the impact of a spherical bead the same as the spherical particles in the chain. The vertical scale in both figures is 20 N and zero time is arbitrary, the curves are offset for visual clarity.

The speed of the leading pulse based on the experimental data recorded by the gauges installed at 4th and 5th cylinder is 771 m/s. The smaller pulse speed of 712 m/s was calculated based on gauges installed in 4th cylinder to 21st cylinder. The 10% decreasing in the pulse speed is due to the attenuating pulse amplitude in the interval between 4th and 21st cylinders.

In numerical calculations the force acting on the gauges imbedded into the corresponding cylinders were found by averaging the forces acting at their contacts

with neighboring spheres similar to [10]. Fig. 3.10 (b),(c) present results of numerical modeling of nondissipative chain related to the experimental data (Fig. 3.10(a)). In numerical calculations reference pulses (corresponding to the force in 4th cylinder) with amplitude similar to experiments were generated using a lower impactor velocity (1.3 m/s) accounting for the dissipation of the signal prior its arrival on 4th cylinder in experiments (impactor velocity 1.4 m/s).

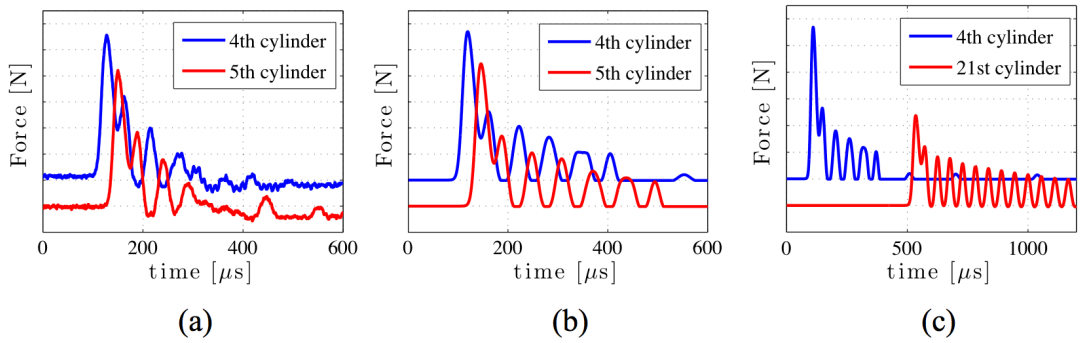

Figure 3.10: Comparison of the experimental results and numerical calculations (without dissipation) of the pulse propagating through the dimer system with mass ratio 0.55, mass of cylinders is larger than mass of spheres. (a) Experimental results; (b), (c) numerical calculations (without dissipation) related to the forces in corresponding cylinders. The vertical scale is 20 N and the curves are offset for visual clarity and zero time is arbitrary.

The pulses in the numerical calculations in nondissipative chain ($\mu = 0$ kg/s) have the double peak feature, and the leading pulse is followed by a similar number of pulses as in experiments. Only small decrease of pulse amplitude (when it propagates from 4th to 5th cylinder) from 111 N to 104 N, and from 111 N to 107 N was observed in experiments and numerical calculations, correspondingly. In numerical calculations pulses, trailing the main double peak pulse, are clearly separated from each other (Fig. 3.10(b) and (c)), unlike in experiments where their separation is less evident (Figs. 3.9 and 3.10(a)). In experiments only second pulse is clearly separated from the leading one in the 4th and 5th cylinders. In numerical calculations, the speed of the leading pulse traveled from 4th to 5th cylinder is 733 m/s. This speed is close to the experimental result

(771 m/s). The pulses frequency spectrums are similar in experiments and numerical calculations.

The number of secondary pulses steadily increases as the wave propagates deeper into the dimer system in experiments and in numerical calculations (Figs. 3.9 and 3.10). This is an important specific feature for a two mass system with investigated mass ratio because it provides a nondissipative mechanism of pulse decay due to energy leak from the leading pulse into increasing number of secondary pulses in oscillatory tails. The mechanism of formation of these secondary pulses without gravitational loading was explained in [1]: for a general value of mass ratio (except some specific values) typically the light bead loses contact with its left neighboring heavy bead retaining a small portion of the energy of the propagating pulse and generating traveling waves in oscillating tails.

It should be mentioned that in numerical calculations the shape of the leading pulses and their amplitudes were negligibly affected by the gravitation in the investigated chains composed from up to 50 cylinders.

At the same time the difference in behavior between gravitationally loaded and free of precompression chains may be very significant for longer chains. For example, in nondissipative, noncompressed chains at relatively short distances from the impacted end the leading double peak, corresponding to force in the heavy particles (cylinder), is followed by a regular sequence of localized pulses. Force in spheres (light particle) has a single leading peak, followed by periodic sequence of double peaks pulses. These regular patterns were transformed correspondingly into two clearly separated triple peaks leading pulses in 499th particle (cylinder) and double peaks in 500th particle (sphere), followed by the chaotically oscillating trails in both cases.

In the same chains under gravitation loading (also with mass ratio 0.55) only one leading double peak was observed up to the distance about 400 particles. At larger distances the sequence of single peak pulses started to form with slowly attenuating

leading pulse (composed from 15 particles) clearly separated from the rest at the 900th particle.

The difference between experiments and results of nondissipative numerical calculations suggests introduction of dissipative damping as with chain with similar masses. By design both chains have identical contacts. Thus the dissipative damping should be similar to previous case of the chain with mass ratio 0.98. It should be mentioned that the dimer systems with different mass ratio, when composed from spherical particles [1, 3], could experience a different damping on the non-fixed sphere/sphere contacts than in our systems with fixed plane/sphere contacts.

Fig. 3.11 shows comparison of numerical results (with different damping coefficients) with the experimental data.

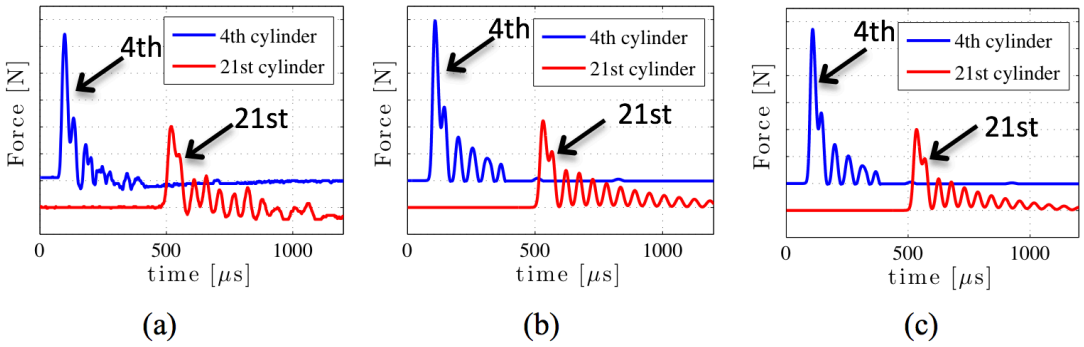

Figure 3.11: Results of experiments and numerical calculations of the pulse propagating through the dimer system, mass of cylinders is larger than mass of spheres. (a) experimental results (sensors are placed in the 4th and 21st cylinders), (b) and (c) results of numerical calculations related to the forces in 4th and 21st cylinders with $\mu = 4$ kg/s and $\mu = 6$ kg/s, correspondingly. The vertical scale is 20 N and the curves are offset for visual clarity, zero time is arbitrary.

The decrease in the first peak amplitudes of the leading pulse at 21st cylinder in the numerical calculation from 109 N to 59 N (with damping coefficient 4kg/s) and from 109 N to 57 N (with damping coefficient 6 kg/s) are similar to the experimental results (109 N to 60 N).

As the signal propagates through the dissipative system, the amplitudes of the

leading double peak pulse decrease, while the number of following pulses increased in numerical calculations in agreement with experiments (Fig. 3.11). Fig. 3.12 presents experimental and numerical results with various damping coefficients related to the amplitude attenuation of leading pulses with cylinder numbers. It is clear that in numerical calculations the leading pulse in the chain with mass ratio 0.55 is attenuating even without dissipation. This is due to the fact that the investigated system with mass ratio 0.55 does not support stationary solitary waves. Without dissipation, decrease of relative amplitude of the force at 21st cylinder is about 40% and this decay is caused solely by dispersion. Dispersion in the pure nonlinear system means dependence of a wave speed on wave length caused by mesostructure, e.g., size of the particles. Like in a weakly nonlinear systems (the equation for corresponding granular chain can be found in [9], see Eq. (1.7) there) the dispersion in strongly nonlinear systems balances strong nonlinearity resulting in a strongly nonlinear solitary wave unique for pure nonlinear systems in one mass chain or in two mass chains at specific values of mass ratio [1]. In two mass chains at arbitrary mass ratio nonlinearity is nor balanced by dispersion. In this case solitary waves are not supported by a system resulting in pulse decay (being maximized at mass ratio 0.59) even in nondissipative chains [1]. The difference with weakly nonlinear system is that in strongly nonlinear case the dispersion term in corresponding wave equation is also nonlinear (Eq. 1.20-1.23 in [9]).

Numerical calculations in dissipative chains (with damping coefficients 4 kg/s and 6 kg/s) demonstrate larger attenuation with decrease of amplitude about 50%. The similar attenuation was observed in experiments. The role of dissipation is significant starting at 15th cylinder, at smaller distances its role is negligible and signal attenuation is mostly due to dispersive effects (Fig.3.12). Based on the attenuation of the amplitudes at different positions (Fig.3.12) inside the chain we conclude that numerical calculations with damping coefficients 6 kg/s satisfactory fit experimental data. This value also

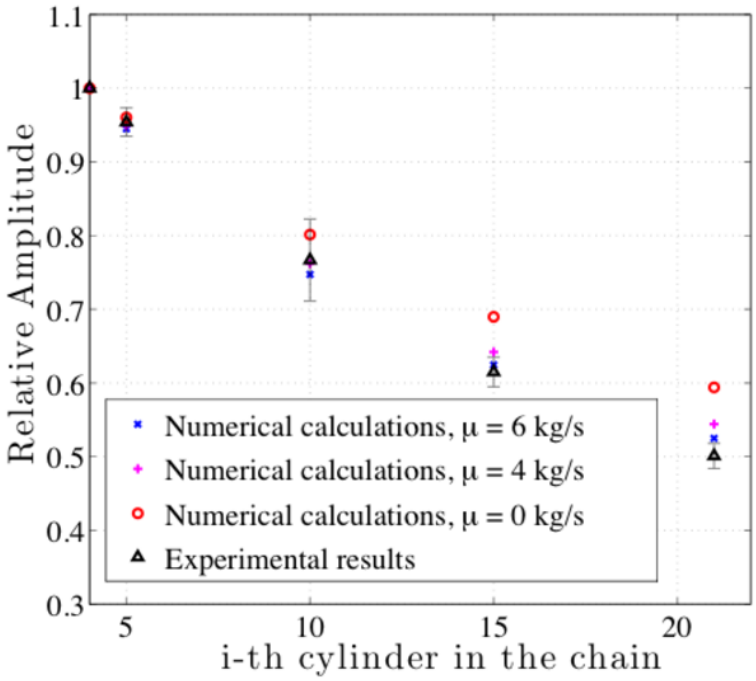

Figure 3.12: The comparison of the experimental results and data from the numerical calculations with different values of damping coefficient in the dimer chain with mass ratio 0.55. Relative amplitude of leading stress pulse at different depths (number of cylinders are shown on the horizontal axes) is calculated with respect to the amplitude of the reference pulse in the 4th cylinder. Mass of cylinders is larger than mass of spheres.

provided the best fit for experimental data in chain with mass ratio 0.98. It is explained by the same nature of contact interaction between surface of the steel cylinder and sphere of the same diameter causing the same mechanism of dissipation.

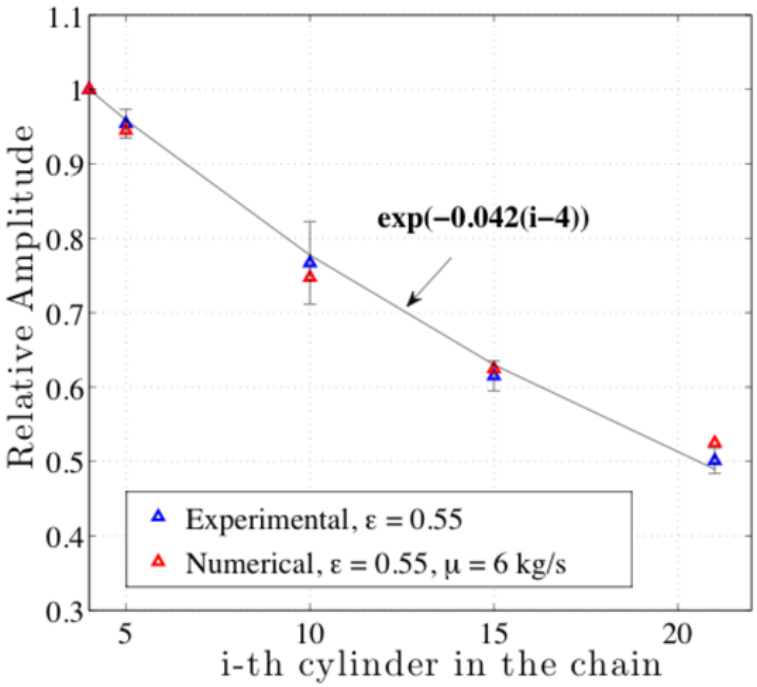

Figure 3.13: Attenuation of relative amplitude in experiments (blue) and in numerical calculations with damping coefficient 6 kg/s (red) comparing with exponential decay. Relative amplitude is calculated with respect to the amplitude of the reference pulse in the 4th cylinder. Mass of cylinders is larger than mass of spheres.

The amplitude of the pulse decays exponentially in experiments and in numerical calculations as it travels through the two mass chain due to the combination of dispersive and dissipative mechanisms (Fig. 3.13). As a result in the two mass chain the exponent (0.042) is larger than in the case of mass ratio equal to 0.98.

The qualitative difference between two mass nondissipative and dissipative chains is the opening of gaps on both sides of 21st cylinder in the former chain as demonstrated in Fig. 3.14(a) by zero forces acting on 21st cylinder corresponding to out of phase displacements of 21st and 22nd spheres.

In dissipative chains at damping coefficient 6 kg/s there are no gaps open (Fig.

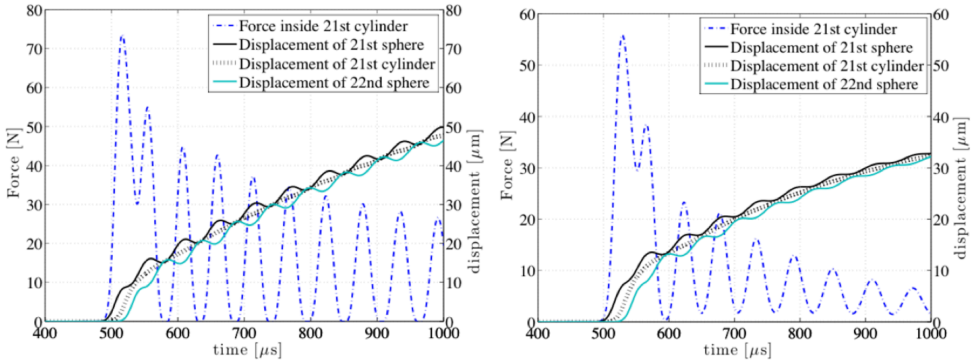

Figure 3.14: Comparison of the forces inside 21st cylinder and out of phase displacements of neighboring spheres in numerical calculations: (a) damping coefficient equal to zero, opening of gaps on both sides of 21st cylinder is evident at moments corresponding to zero forces and (b) no openings of gaps at damping coefficient equal to 6 kg/s. In both cases chain with mass ratio 0.55 impacted by sphere with velocity 1.45 m/s.

3.14(b)) and forces acting on 21st cylinder are not zero though displacements of 21st and 22nd spheres are still out of phase. In both cases the oscillatory force profile in 21st cylinder is observed due to oscillating motion of spheres clearly seen in their displacements curves. Increase of damping coefficient to 10 and 15 kg/s reduces amplitudes of oscillations of spheres also without gaps openings and transforming the sequence of separated pulses into oscillatory tail.

Shape of the wave during the propagation of these pulses into the larger depths (beyond 90th cylinder) changed into attenuating triangular shock like oscillatory pulse with decreasing amplitudes of oscillations with increase of damping coefficient to 10 and 15 kg/s.

The similar impact on dimer chains with damping coefficient 100 kg/s resulted in fast attenuating, smooth nonsymmetric dispersive pulses with increasing duration and ramp time being much shorter than the tail. At this damping coefficient (100 kg/s) shock waves in one mass chain and in two mass chains were practically identical at similar particle numbers with slight differences in speed propagation and amplitudes.

Two wave structure of the attenuating pulse (leading solitary like pulse clearly separated from the following shock like wave) observed at some range of distances from the impacted end in the chain of equal masses at damping coefficient 6 kg/s (Fig.3.7) was not detected in dimer chains. It is interesting to compare relative attenuation in a system with mass ratio 0.55 to the system with mass ratio 0.98 (Fig. 3.15) at the different depths, but corresponding to the same number of cells (dissipative contacts) for chain with different damping coefficients.

Though the damping coefficient 6 kg/s describes experimental data satisfactory for both chains (Figs. 3.5 and 3.12), it is interesting to compare systems with different mass ratio at larger damping coefficients which may correspond to the larger plastic deformation at the contacts or to the chains immersed in liquid. The difference can be expected because solitary wave is not supported in the former case (thus localized pulse is attenuated (Fig. 3.15(a)) even without dissipation losing energy into the oscillatory tail).

At the same time attenuation due to dissipation might mask this difference if widths of pulses are different and contact dissipation is the main source of attenuation. The results are presented in Fig. 3.15 (b), (c), and (d) for damping coefficients 10 kg/s and 15 kg/s, and 100 kg/s, correspondingly. For systems with damping coefficient 6 kg/s (Fig. 3.15 (b)), which gives the results most close to experimental data, the relative amplitude decrease in the system with mass ratio 0.98 (where dissipation is the only mechanism for attenuation) at 21st cylinder contact is about 40%. The amplitude decrease in a system with mass ratio 0.55 at the same contact number is higher being equal close to 50%. The 10% difference is due to the presence of nonlinear dispersion (not balanced by strong nonlinearity) in the latter system.

With the increase of damping coefficient to 10 kg/s the amplitude decrease with increase of contact number in both systems is very close (Fig. 3.15(c)), manifesting that

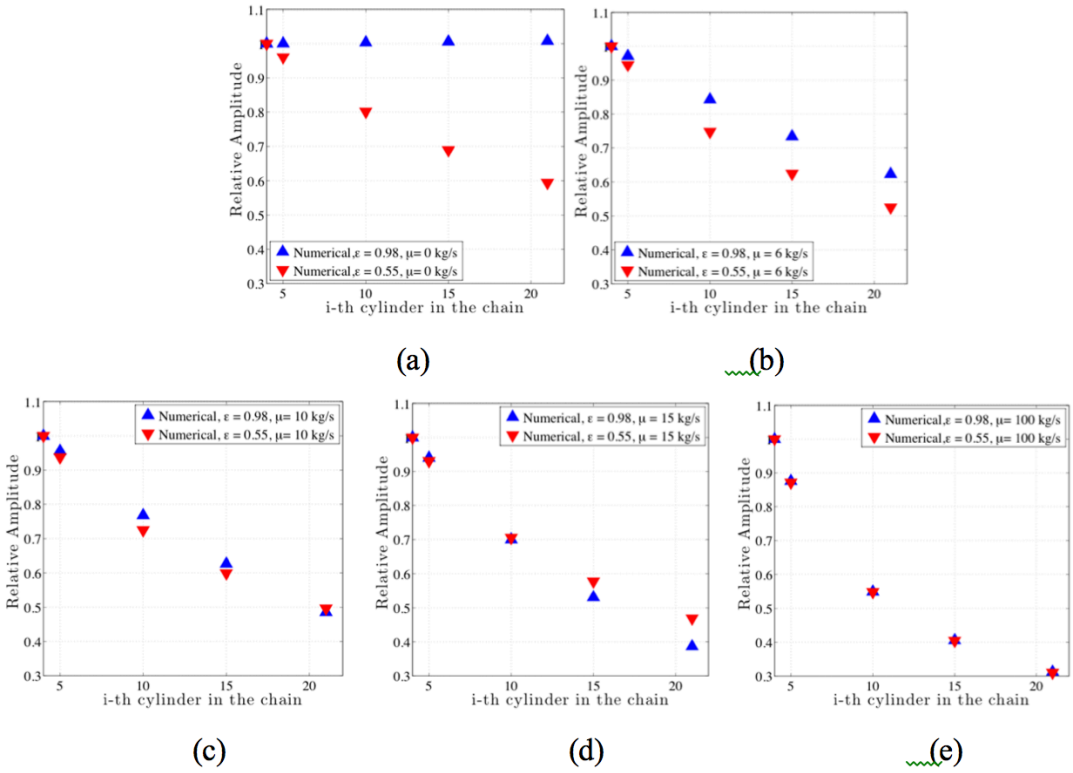

Figure 3.15: The attenuation of the relative pulse amplitude (with respect to the amplitude of the reference pulse in the 4th cylinder, mass ratios 0.98 and 0.55) and change of decay efficiency in two systems with increased damping coefficient at the same contact number in the chains at corresponding values of damping coefficients 0 (a), 6 kg/s (a), 10 kg/s (b), 15 kg/s (c), and 100 kg/s (d). Mass of cylinders is larger than mass of spheres (2.085 g).

nonlinear dispersion is not a major factor in decay in the chain with mass ratio 0.55.

Further increase of the damping coefficient to 15 kg/s demonstrates the surprising result - the attenuation in 0.98 mass ratio system becomes larger than in the two mass system with optimal mass ratio 0.55 (Fig. 3.15(d)), which provides maximum decay in nondissipative dimer chain (Fig. 3.8). We explain this phenomenon by the difference in shapes of particle velocity profiles in investigated systems (Fig. 3.16). From this figure (Fig. 3.16(d)) it is clear that dissipation at the damping coefficient 15 kg/s does not result in significant differences of pulses space scales in comparison with the case without dissipation, only adding tails in particle velocities which amplitude is increasing with increase of damping coefficient. This demonstrates that strong nonlinearity and nonlinear dispersion caused by periodic mesostructure control the shape of the pulses in both systems even in the presence of dissipation.

The important difference between chains with mass ratio 0.98 and 0.55 is that the former chain supports a narrow solitary wave composed from only 5 particles, with major gradients of velocity just between two particles at the front and two particles at the back of this wave [9]. This large differences between velocities of neighboring particles in one mass chain result in larger viscous dissipative losses (Eqs. 3.8-3.12) in comparison with two mass chain were localized pulses (not solitary waves) have a longer dimensions and thus a smaller gradients of velocity between neighboring particles. This difference may explain the reversal in impact mitigation effectiveness of these systems with increased damping coefficients.

Moreover two mass chains in the discussed case (heavy cylinders/light spheres) would be heavier at the same number of particles than one mass chain (light cylinders/light spheres). Thus at this level of dissipation (15 kg/s) one mass chain with the same number of particles has a smaller mass also making it a better protector against impact pulse with a short duration.

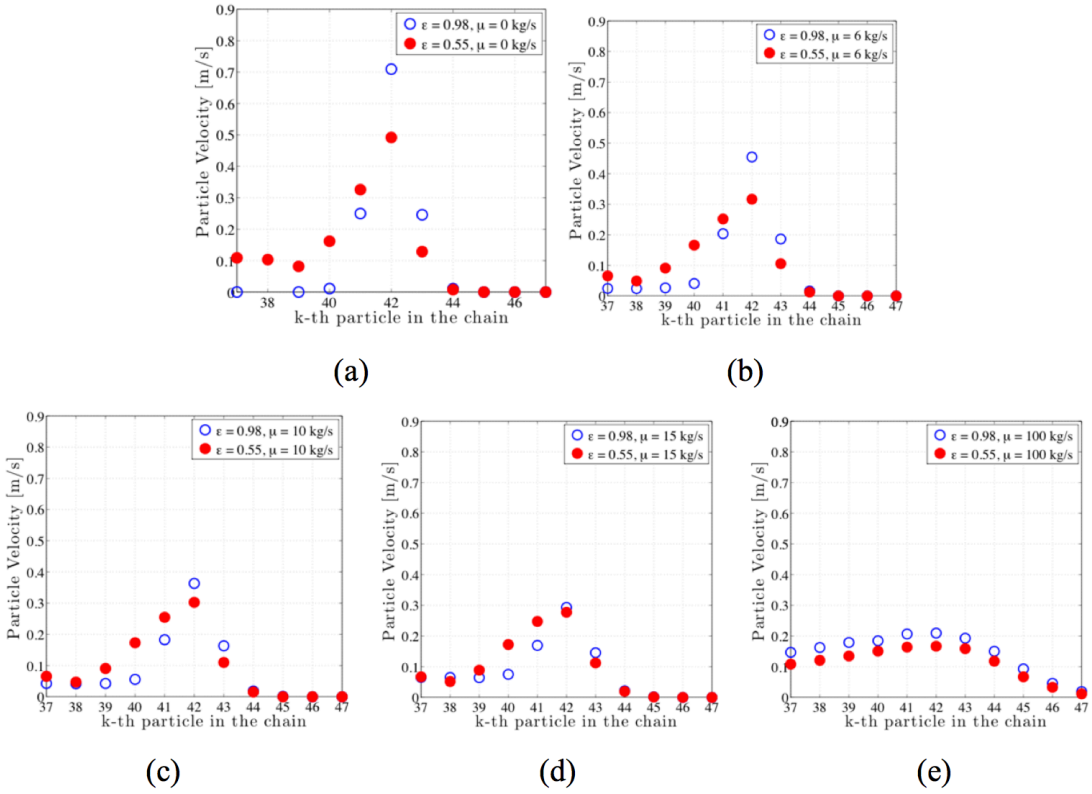

Figure 3.16: The change of particle velocities profiles in both sytems with increase of damping coefficient. The maximum of pulse amplitude corresponds to 42nd particle (21st cylinder), odd numbers are related to spheres and even to cylinders. Numerical calculations with damping coefficients 0 (a), 6 kg/s (b), 10 kg/s (c), 15 kg/s (d) and 100 kg/s (e). Particle velocities in system with mass ratio 0.98 (blue, open circles) and particle velocities in system with mass ratio 0.55 (red, solid circles). Mass of cylinders is larger than mass of spheres (2.085 g).

From comparison of pulse attenuation at damping coefficients 10 kg/s and 15 kg/s we can conclude that the former value is close to critical value corresponding to the reverse of performance of these systems with respect to pulse amplitude decay. This transition corresponds to the prevailing influence of dissipation over decay caused by mesostructure in dimer chain.

The further increase of damping coefficient to 100 kg/s makes the pulse shape in both system very similar (nonsymmetric triangular pulse, Fig. 3.16(e)) resulting in negligible role of nonlinear dispersion and in practically identical attenuation in both systems (Fig. 3.15(e)) after pulse travelling through the same number of particles.

However, the systems with the same numbers of particles, but with different mass ratios have different total masses. For design purpose (for example if mass of the protection layer is the main design parameter, e.g., in helmets), it is interesting to compare the attenuation of the pulses at different values of damping coefficient in the same systems with different mass ratios after propagation not through the same number of particles (as in Fig. 3.15), but through the chains with the same masses. The corresponding data from experiments and numerical calculations are presented in Fig. 3.17, linear approximation was used to approximate the data in Fig. 3.17(a) based on data from Fig. 3.5 and Fig. 3.12.

In experiments the attenuation of signals traveling through the length of chains having the same masses (but with different mass ratios of particles 0.98 and 0.55 composed from the same spheres (2.085 g) and cylinders having masses similar to the sphere mass and heavier, correspondingly) are quite similar (Fig. 3.17(a)). In numerical calculations without dissipation (chain with mass ratio 0.98) no attenuation of the pulse was observed in contrast to significant attenuation in the nondissipative chain with mass ratio 0.55, (Fig. 3.17(b)). The similar attenuation in experiments (Fig. 3.17(a)) in both chains of equal masses, despite the two mechanism of decay existing in two mass chain

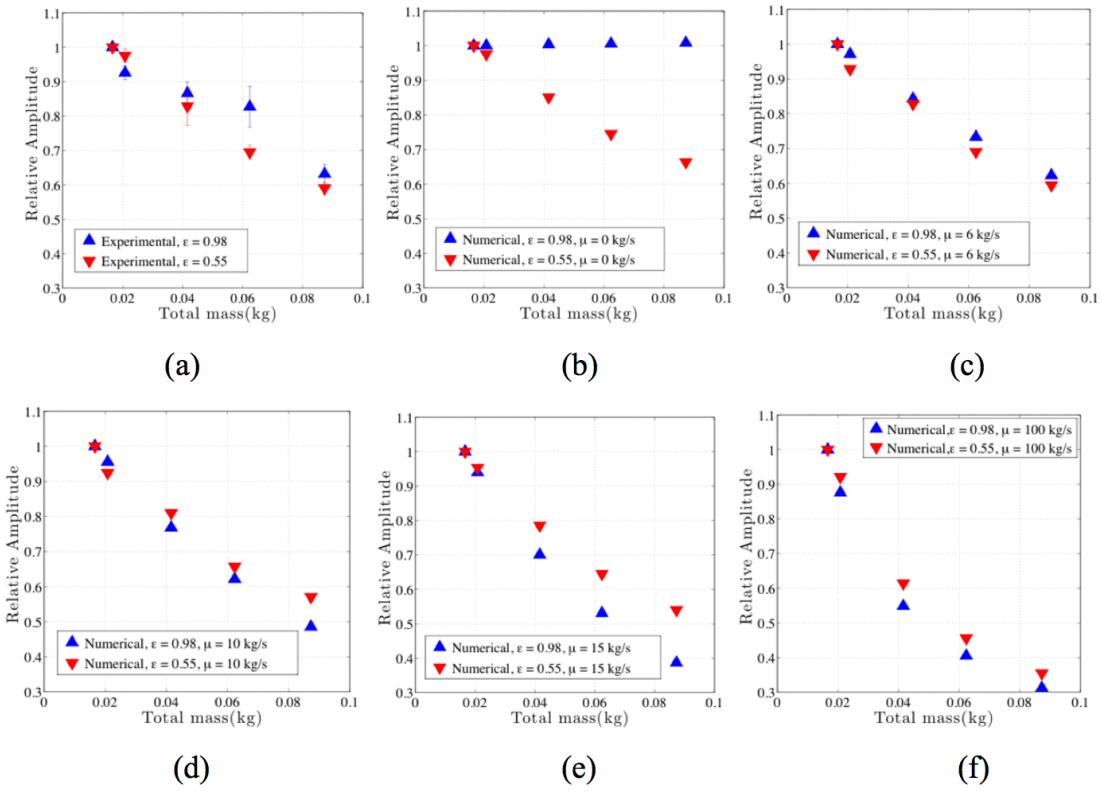

Figure 3.17: Relative amplitude (with respect to the amplitude of the reference pulse at the 4th cylinder) after propagation through the chain with the same mass at different values of damping coefficient in experiments (a) and in numerical calculations with different damping coefficients: 0 (b), 6 kg/s (c), 10 kg/s (d), 15 kg/s (e) and 100 kg/s (f). Mass of cylinders is larger than mass of spheres (2.085 g).

(dispersion and dissipation) versus only one mechanism in one mass chain (dissipation), is apparently due to the stronger effect of dissipation in the latter system.

In numerical calculations with a damping coefficient of 6 kg/s, the respective relative amplitudes are very close to experimental values for both chains (compare Fig. 3.17(a) and (c)). At the increased damping coefficients starting from 10 kg/s, the system with mass ratio 0.98 demonstrates faster pulse attenuation than system with mass ratio 0.55 after the travelling through the chain with the same mass (Figs. 3.17(d) - (f)). This difference in enhanced by a smaller number of contacts in the system with mass ratio 0.55 at the same total mass travelled by the pulse. Though one mass chain is also preferable for pulse mitigation given the same mass of the chain at the damping coefficient 100 kg/s, the difference is smaller than at lower damping coefficients 10 and 15 kg/s. This is explained by the similar gradients of particle velocity between elements in both chains at damping coefficient 100 kg/s (Fig. 3.16(e)) and by a larger number of dissipative contacts in one mass chain (light cylinders/light spheres) versus two mass chains (heavy cylinders/light spheres).

Thus strongly dissipative one mass chains will be again better for the impact protection at the same total mass of particles than two mass chains with larger mass of cylinders relative to the mass of spheres.

It is also interesting to compare behavior of one mass system with two mass system having the mass ratio of particles close to optimal value 0.55 (but with reduced mass of cylinders versus spheres) at the same striker impact. The attenuation of the relative pulse amplitude depending on number of travelled contacts in chains with mass ratios 0.98 and 0.55 is presented in Fig. 3.18. In the latter chain a mass of cylinders is smaller than mass of spheres (2.085 g), unlike in the previous case corresponding to Fig. 3.15.

Numerical calculations (Fig. 3.18) show that with reduced cylinder masses and

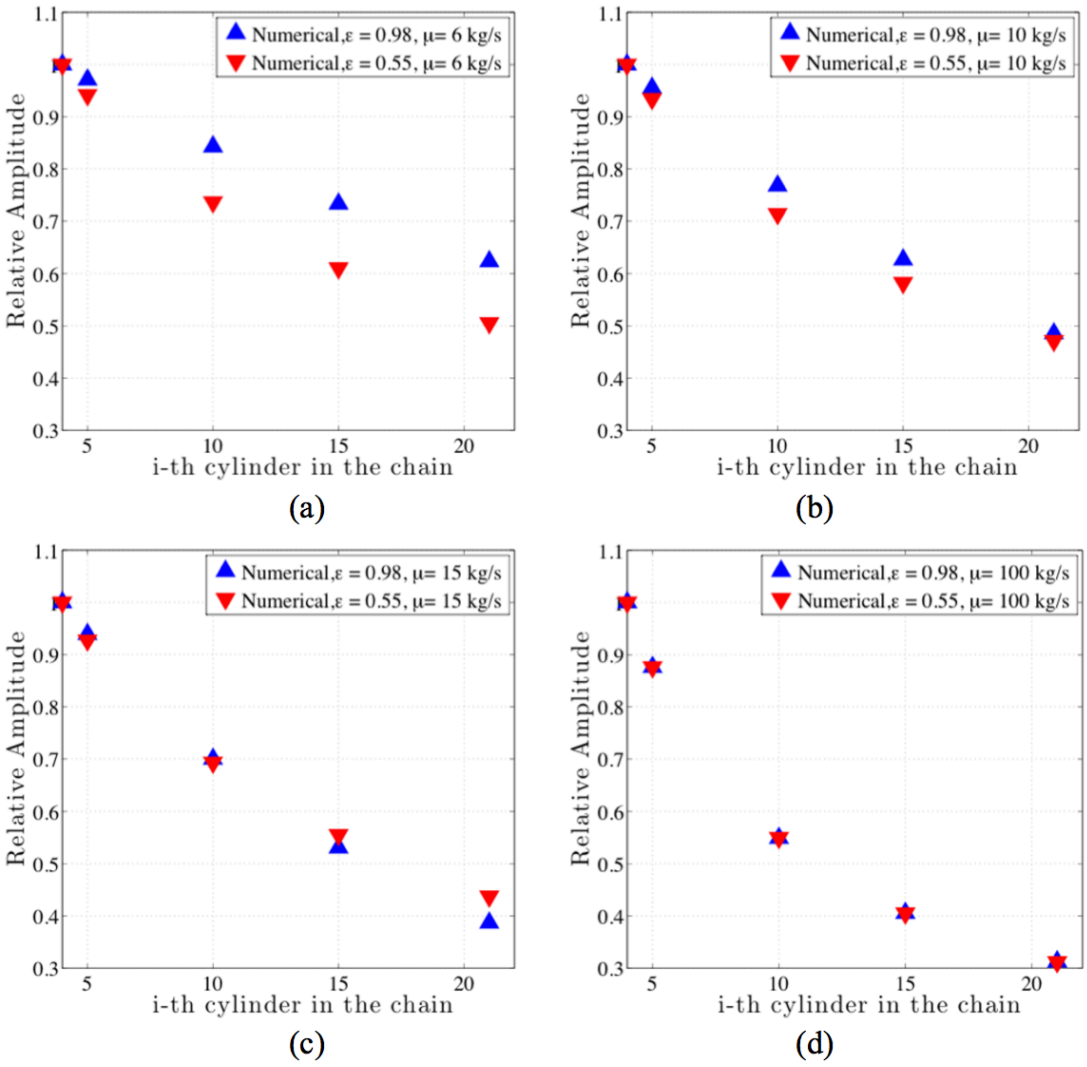

Figure 3.18: The attenuation of the relative pulse amplitude with respect to the amplitude of the reference pulse in the 4th cylinder, mass ratios 0.98 and 0.55, mass of cylinders is smaller than mass of spheres (2.085 g) and change of decay efficiency in two systems with increased damping coefficient. Relative amplitudes in numerical calculations at the same position in the chains at corresponding values of damping coefficients 6 kg/s (a), 10 kg/s (b), 15 kg/s (c), and 100 kg/s (d).

the same masses of spheres, the attenuation of relative amplitude of pulses travelled through the same number of particles in chain (number of contacts) is similar to the previous case of two mass chain with larger cylinder masses (Fig. 3.15). In this case also the one mass system is better in attenuating the pulse amplitude with increased damping coefficient probably for the reason that pulse in two mass system contains a larger number of particles and thus a smaller difference of particle velocities between elements. At the damping coefficient 100 kg/s the difference in attenuation is negligible when pulse travelled the same number of particles.

But in case if the optimal two mass system (mass ratio 0.55) has a smaller cylinder mass it also has a smaller total mass, at the same number of contacts, than one mass system composed from the same spheres and cylinders of equal masses. For the design purpose it is interesting to compare the attenuation of the pulses in these systems having the same mass at different values of damping coefficients. The corresponding results from numerical calculations are presented in Fig. 3.19.

We can see that at damping coefficient 6 kg/s (close to the value in experiments with the identical contacts) the two mass chain with mass of cylinders being smaller than mass of spheres (2.085 g), mass ratio is 0.55 is significantly better at the same chain mass. This is caused by dispersion effects in combination with smaller number of travelled dissipative contacts in one mass chain. With increased damping coefficient the difference in mitigation between thee systems becomes smaller due to the stronger effect of dissipation on signal attenuation in more narrow pulse in one mass chain explained above. Thus this chain is preferable if the mass of the attenuating system is the main design parameter, as in helmets.

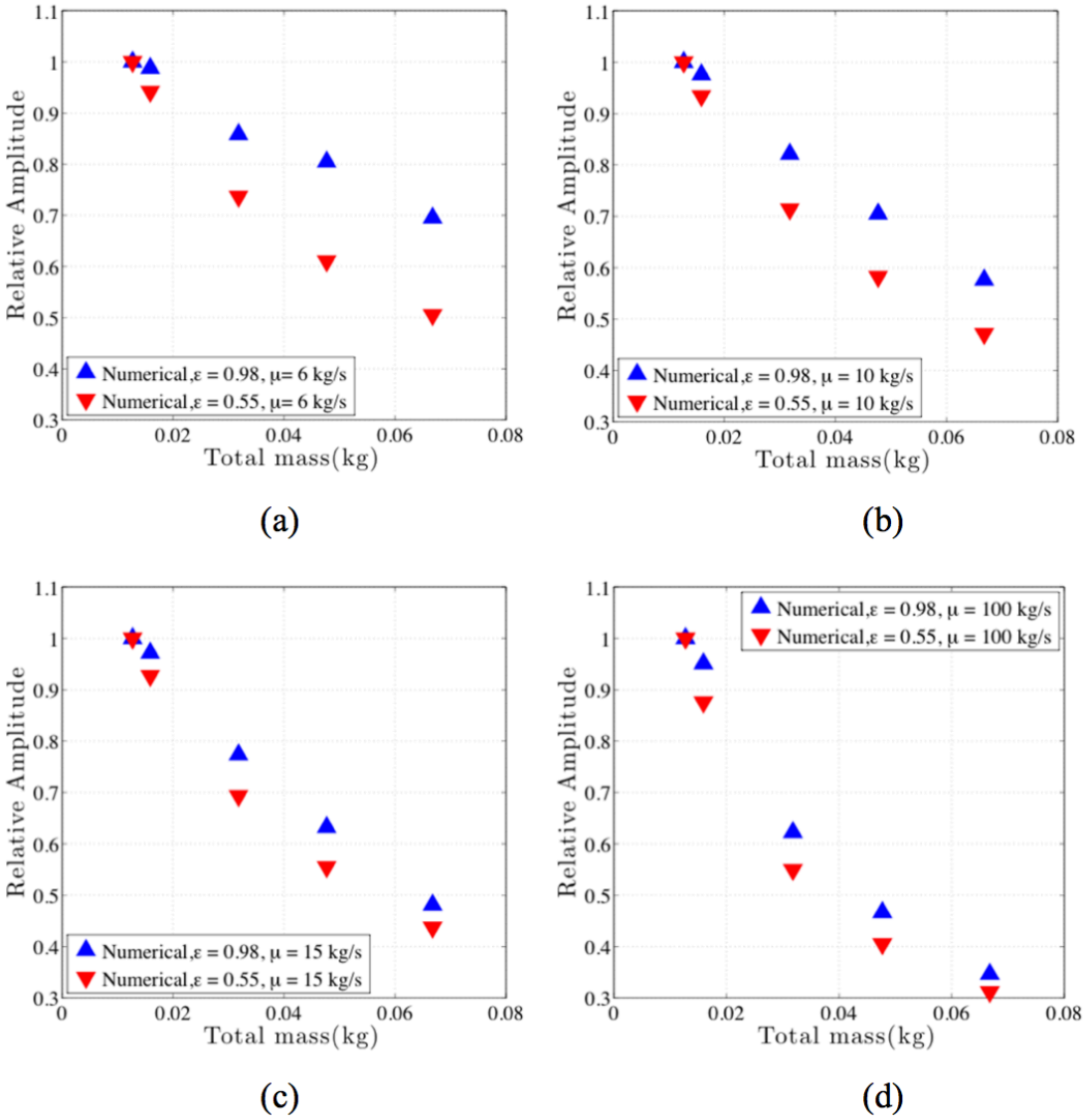

Figure 3.19: Relative amplitude (with respect to the amplitude of the reference pulse at the 4th cylinder) after propagation through the chain with the same mass at different values of damping coefficient in in numerical calculations with different damping coefficients: 6 kg/s (a), 10 kg/s (b), 15 kg/s (c) and 100 kg/s (d). Mass of cylinders is smaller than mass of spheres (2.085 g), mass ratio is 0.55.

3.4 Conclusions

Propagation of short pulse in dimer chains with two different mass ratios (0.98 and 0.55) was investigated in experiments and numerical calculations. The same striker was used to generate short pulses in these systems to compare their effectiveness under the same impact. Both chains had the fixed cylinder-sphere contact, which keeps dissipative properties (damping coefficient) of both systems identical highlighting the role of radiation based attenuation mechanism present in the chain with mass ratio 0.55, unlike in [1, 3]. The cylinder-sphere chains are more convenient with respect to design any mass ratios and keeping diameters of particles the same, which is difficult to accomplish with sphere-sphere chains placed in the channel.

The attenuation of pulse amplitude due to dissipation was modeled using linear viscosity term which qualitatively described the observed rate of attenuation in both systems at the same damping coefficient equal 6 kg/s. In both experiments and corresponding numerical calculations pulses in the system with mass ratio 0.55 attenuates faster.

The change of the dependence of the force on mass ratio in dissipative chains with fixed contacts is not symmetric with respect to global minimum. There is a relatively small change of the transmitted force for small mass ratio up to optimal ratio 0.55, but few times larger change of transmitted force was observed in the chain with small mass difference. We explain this nonsymmetric behavior by larger gradients of particle velocity between neighboring particles in chains with smaller mass differences.

Introduction of viscous damping blocks the gap opening starting at the damping ratio 6 kg/s. Thus damping not only dissipate energy, but also eliminates the process of gap openings and corresponding time scales (gap opening divided by particle velocity) characteristic for nondissipative chains.

The input into pulse decay due to strongly nonlinear dispersion effect in experiments can be illustrated by comparison between chains with the same number of identical dissipative contacts crossed by travelling pulse. In the system with mass ratio 0.98, where the only active mechanism of attenuation is dissipation, 40% amplitude decrease was observed in experiments, unlike larger decrease (50%) in the chain with mass ratio 0.55, being caused by both mechanisms of decay. The influence of the value of damping coefficient on the relative effectiveness of these systems to mitigate identical impact was investigated numerically in the case when mass of cylinders was larger than mass of spheres. If these systems have the same number of particles or the same mass travelled by the pulse, their amplitudes in the dimer system with mass ratio 0.55 attenuate faster than in the system with mass ratio 0.98 only when damping coefficient is below some critical value (below 10 kg/s).

At larger damping coefficients the system with mass ratio 0.98 mitigate the same impact better than the system with mass ratio 0.55. The former chain in this highly dissipative systems has a smaller mass providing the same level of attenuation than the system with mass ratio 0.55. The one mass system is preferable system for the higher level of viscous dissipation (e.g., granular chains in liquid) because it forcefully supports the high gradients in the narrow pulse by strongly nonlinear dispersion. At the highest investigated level of viscous dissipation (damping coefficient 100 kg/s) the pulses in both systems are of the similar width resulting in a similar viscous dissipation of pulses travelling the same number of contacts.

A different behavior of two and one mass chains with increase of damping ratio was observed with respect of shape of the propagating pulses. One mass chain excited by impact of sphere demonstrates a two wave structure (solitary wave plus oscillatory shock wave), this phenomena was not observed in two mass chain. At the largest damping ratio 100 kg/s both chains behave in a similar way.

Numerical calculations for a different system where a cylinder masses are smaller than masses of spheres show similar results to the system with larger mass of cylinders for the same number of contacts crossed by travelling pulse. But in this case dimer system with the same total mass has larger number of dissipative contacts enhancing pulse attenuation at all values of investigated damping coefficients.

These results help to select appropriate mesostructure and dissipative properties of the strongly nonlinear discrete systems for protection barriers.

3.5 References

1 K.R. Jayaprakash, Y. Starosvetsky, A. F. Vakakis, "New family of solitary waves in granular dimer chains with no precompression", in *Phys. Rev. E* **83**, 036606 (2011).

2 H. Hertz, "On the contact of elastic solids", in *J. Reine Angew. Math.* **92**, 156 (1881).

3 R.Potekin, K.R. Jayaprakash, D.M. McFarland, K. Remick, L.A. Bergman, A.F. Vakakis, "Experimental Study of Strongly Nonlinear Resonances and Anti- Resonances in Granular Dimer Chains", in *Exper. Mech.* **53**, 861 (2013).

4 A. Rosas and K. Lindenberg, "Pulse dynamics in a chain of granules with friction", in*Phys. Rev. E* **68**, 041304 (2003).

5 A. Rosas, A. H. Romero, V. F. Nesterenko, and K. Lindenberg, "Observation of Two-Wave Structure in Strongly Nonlinear Dissipative Granular Chains", in *Phys. Rev. Lett.* **98**, 164301 (2007).

6 A. Rosas, A. H. Romero, V. F. Nesterenko, and K. Lindenberg, "Short-pulse dynamics in strongly nonlinear dissipative granular chains", in *Phys. Rev. E* **78**, 051303 (2008).

7 E. B. Herbold and V. F. Nesterenko, "Shock wave structure in a strongly nonlinear lattice with viscous dissipation", in *Phys. Rev E* **75**, 021304 (2007).

8 E.B. Herbold, V.F. Nesterenko, "Periodic waves in a Hertzian chain", in *Physics Procedia 3*, 465(2010).

9 V. F. Nesterenko, *Dynamics of Heterogeneous Materials*. New York: Springer, 2001.

10 C. Daraio, V.F. Nesterenko, E.B. Herbold, S. Jin,"Strongly nonlinear waves in a chain of Teflon beads", in *Phys. Rev. E* **72**, 016603 (2005).

11 E.J. Hinch and S. Saint-Jean, "The Fragmentation of a Line of Balls by an Impact", in *Proc. R. Soc. London A* **455**, 3201 (1999).

12 C. Coste, E. Falcon, and S. Fauve, "Solitary waves in a chain of beads under Hertz contact", in *Phys. Rev. E* **56**, 6104 (1997).

13 S. Job, F. Melo, A. Sokolow, and S. Sen, "How Hertzian solitary waves interact with boundaries in a 1D granular medium", in *Phys. Rev. Lett.* **94**, 178002 (2005).

14 J. Yang, M. Gonzalez, E. Kim, C. Agbasi, M. Sutton, "Attenuation and localization of solitary waves in 1D granular crystals visualized via high speed photography", in *Experimental Mechanics* **54**, 1043 (2014).

15 R.K. Pal, A.P. Awasthi, and P.H. Geubelle, "Characterization of wave propagation in elastic and elastoplastic granular chains", in *Phys. Rev. E* **89**, 012204, (2014).

Chapter 4

Solitary Waves In "Sonic Vacuum" Generated By the Striker Impact

The striker impact generates a single solitary wave or train of solitary waves in discrete strongly nonlinear systems depending on the relation between impactor mass and mass of the particle in the system. The striker did not rebound from the chain with infinite mass if its mass is larger than the effective mass of solitary wave, its linear momentum and energy are completely transferred into the discrete system. The resulting train of solitary waves emerges from the collective behavior of many particles and thus in general it can't be predicted based on two conservation laws. This chapter presents an approach based on imaginary collision of impactor with quasiparticle with some effective mass. This approach is based on two conservation laws and it satisfactory predicts the linear momenta, energies and amplitudes in the train of solitary wave in far field depending on the relative mass of the striker and particles in the chain.

4.1 Experimental procedure

Chains were composed from steel spheres (440*C*) and steel cylinders (304), arranged alternatively with the diameter d and height h correspondingly, the cell size was equal to $a = h + d$. They were placed inside the space formed by four aluminum rods arranged vertically (Fig. 4.1). The mass ratio was changed by using cylinders with different heights, but keeping the nature of contacts the same.

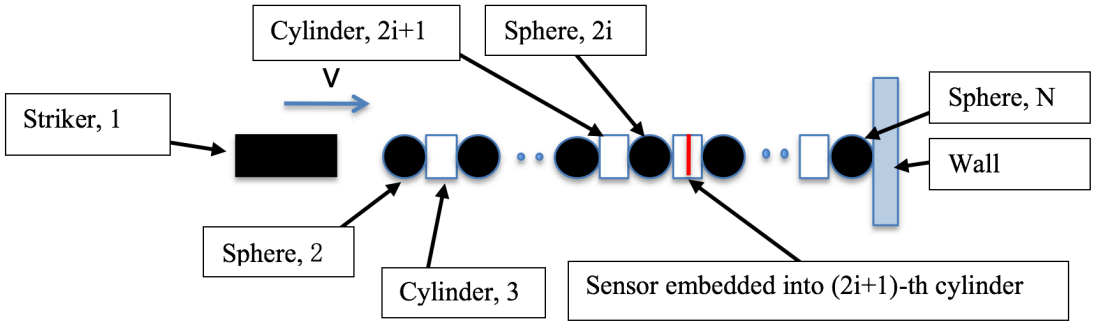

Figure 4.1: Cylinders and spheres aligned in 1-D chain. The numeration of particles in the chain ($i = 1,2,3,...N/2$) corresponds to the numerical calculations, striker is particle 1.

The chain was assembled from 45 steel spheres (440*C*) with a mass $m = 2.085$ g and 44 steel cylinders (304) with a height $h = 5.3$ mm and a mass of 2.043 g. This chain with the mass ratio equal to 0.98 supports solitary like waves very close to the expected solitary wave in the chain with equal masses of particles [1].

Wave in experiments were generated by of impact the stainless steel rods with a flat end having masses 39.14 g and 10 g on the first spherical particle. The velocity of impact measured using high speed camera Phantom V12 was equal to 0.25 m/s. The impactors did not recoil at least during the time of optical observation equal 31.654 ms, it is about 15 times longer than expected time of the arrival of the reflected wave from the bottom of the nondissipative chain. The wave reflected from the supporting wall would result in the recoil of the striker. We assume that the negligible velocity of the striker's

recoil is caused by the attenuation of reflected wave.

The forces acting inside cylinders were measured by piezogauges embedded in the 4th cylinder (used to specify the incoming pulse) and inside the cylinders placed deeper in the chain (10th, 15th and 21st) similar to [2,3,4]. The piezogauges supplied by Piezo Systems Inc. were custom cut and wired, their sensitivity was in the range 6.8 - 7.1 N/V, (time constant of the RC circuit $RC \sim 537\mu$s, where R is the resistance of the oscilloscope entrance and C is capacity of the piezogauge). The signals from the gauges were recorded using oscilloscope Tektronics TDS 2014.

Piezogauges were calibrated using impact by the PTFE sphere (mass 0.12 g) with a recorded impact velocities (0.7 - 0.8 m/s) based on linear momentum conservation of impactor and measured force-time history up to the maximum force similar to [3].

4.2 Numerical Calculations

Static Hertzian law was used to describe elastic dynamic contact interaction of cylinders with flat ends and spheres depending on their relative displacements. This approach is valid under some assumptions [2,5] proven in experiments by different groups of researchers [6-10]. We neglect very small difference in masses of spheres and cylinders. The equations of motion of the cylinders and spheres with equal masses in the nondissipative chain are presented below

$$\begin{aligned} m\ddot{u}_i &= A[\{(u_{i-1,0}+u_{i-1}-(u_{i,0}+u_i)\}_+^{3/2} - \{(u_{i,0}+u_i-(u_{i+1,0}+u_{i+1})\}_+^{3/2}] + mg, \\ A &= \frac{4E_C E_S (R_S)^{1/2}}{3[E - S(1-\nu_C^2) + E_C(1-\nu_S^2)]}, \end{aligned} \tag{4.1}$$

where m is the mass of the particles (cylinder or sphere), $u_{i-1,0}, u_{i,0}$, and $u_{i+1,0}$ represent equilibrium displacement of centers of corresponding particles in the gravitationally

loaded chain calculated from initially undeformed positions. Variables u_{i-1}, u_i, and u_{i+1} represent dynamic parts of overall displacements during wave propagation,$i = 3,4,...N-1$, where N is the total even number of particles including the impactor (particle 1) and the last spherical particle contacting the wall. Positive subscript corresponds to forces acting between neighboring particles being in contact (otherwise interaction force is zero). The constant A depends on the Young moduli (E_C, E_S) and Poisson's ratios (ν_C, ν_S) of materials of interacting particles and the curvature of contacting areas [4]. In our experiments we had the radii R_S of spherical particles equal 4 mm and constant A corresponds to interaction of spherical particles and cylinders with a flat faces. Density and elastic properties of contacting particles were selected as follows $\rho = 8000 kg/m^3$, Young's modulus $E = 193G$Pa, and the Poisson ratio $\nu = 0.3$.

The separate equation for the impactor (dynamic displacement u_1), initially contacting the first sphere in the gravitationally loaded chain (there is no contact deformation between these two particles prior to the impact) is

$$m_{imp}\ddot{u}_1 = -A_1(u_1 - u_2)_+^{3/2} + m_{imp}g, A_1 = \frac{4E_{imp}E_S(R_{imp})^{1/2}}{3[E - S(1-\nu_{imp}^2) + E_{imp}(1-\nu_S^2)]}, \quad (4.2)$$

where A_1 is corresponding to the contact of the impactor (end radius of impactor R_{imp}, Young's modulus E_{imp} and Poisson's ratios v_{imp}) and the first sphere.

Equation for the first spherical particle (dynamic displacement u_2) is

$$m_s\ddot{u}_2 = A_1(u_1 - u_2)_+^{3/2} - A[(u_{2,0} + u_2) - (u_{3,0} + u_3)]_+^{3/2} + mg. \quad (4.3)$$

Equation for the last spherical particle (dynamic displacement u_N) contacting the flat wall is

$$m_s\ddot{u}_N = A[(u_{N-1,0} - u_{N-1}) - (u_{N,0} + u_N)]_+^{3/2} - A(u_{N,0} + u_N)_+^{3/2} + mg. \quad (4.4)$$

We include gravitational precompression in our numerical modeling (Eq. 4.1) because it reflects vertical position of our chain in experiments. But influence of this initial precompression on the wave propagation in experiments and in calculations was negligible at the length of our chain and at relatively high amplitude of dynamic force.

In numerical calculations a total energy was conserved with accuracy $10^{-4}\%$ in nondissipative chain and linear momentum was conserved with accuracy $10^{-6}\%$ (ratio of energy/linear momentum deviations from their average values in percentages). Numerical calculations were conducted without dissipation to clarify role of dispersion and strong nonlinearity on the wave transformation.

4.3 Results and Discussion

The pulses in the numerical calculations were generated by the striker with mass 39.136 g (being equal about $18.7m$). Its velocity was adjusted to create the amplitude of the force in the 4th cylinder similar to experimental data. This pulse was considered as a reference input. The generated shock like oscillating triangle wave profile (Fig. 4.2 (a)) demonstrated its clear tendency to the start of separation into train of solitary waves. Similar behavior was observed in experiments Fig. 4.2 (b)), except that the amplitude of the leading peak was practically constant in numerical calculations unlike its weak decay in experiments (115N to 105N).

As the pulse propagated deeper into the chain a tendency to clear separation of oscillating pulses into train of solitary waves can be observed in numerical calculations of (Fig. 4.3(a), (c), and (d)). The leading part of the pulse is transformed into solitary wave around fiftieth cylinder (Fig. 4.3(c)). It is a typical feature of strongly nonlinear discrete systems, especially evident in nondissipative granular chains where finite duration propagated pulses are split into train of solitary waves [2,6,11]. In case

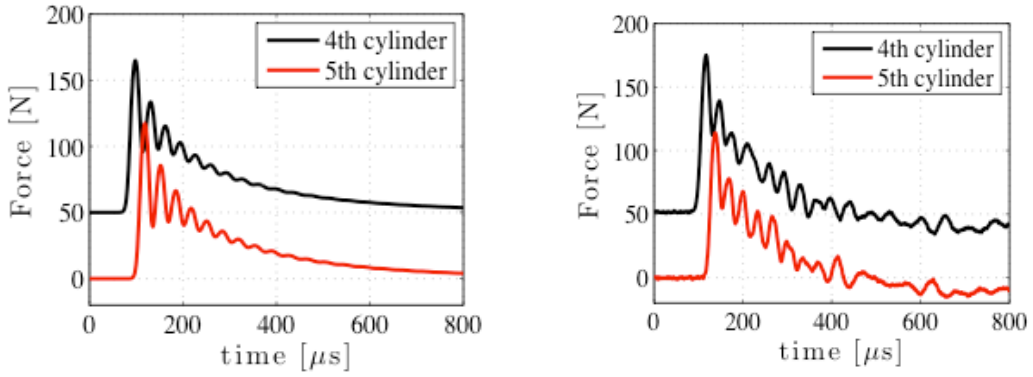

(a) (b)

Figure 4.2: Comparison of experimental results and numerical calculations of the pulse propagating through the system. Pulses were excited by the impact of rod with mass of 39.136 g. Sensors are placed in the 4th and 5th cylinders. (a) Numerical calculations, (b) experimental results. The vertical scale is 20 N and the curves are offset for visual clarity and zero time is arbitrary.

of the negligible or small dissipation we could expect that the incoming pulse would be eventually transformed into train of solitary waves, their number with significant amplitude being determined by the mass ratio of impactor to the mass of particles in the chain [2].

It is important to emphasize that amplitude of this leading solitary wave is very close to the amplitude of the leading peak in the oscillating shock like wave on the very early stages of wave propagation (compare Fig. 4.3(a) and Fig. 4.3 (c) and (d)). Thus the leading amplitude of oscillatory shock wave can be estimated based on the amplitude of leading solitary wave in far field.

The same phenomenon was not observed in the experiment (Fig 4.3 (b)) though the tendency to the separation of the leading peak is present. This difference in behavior is caused by dissipation in experiments which was not considered in the calculations. It is clear that with wave propagation the leading peak in experiments is more separated from the rest of the force profile similar to numerical calculations. It is interesting that in experiments impact by striker with smaller mass equal to five mass of spherical steel

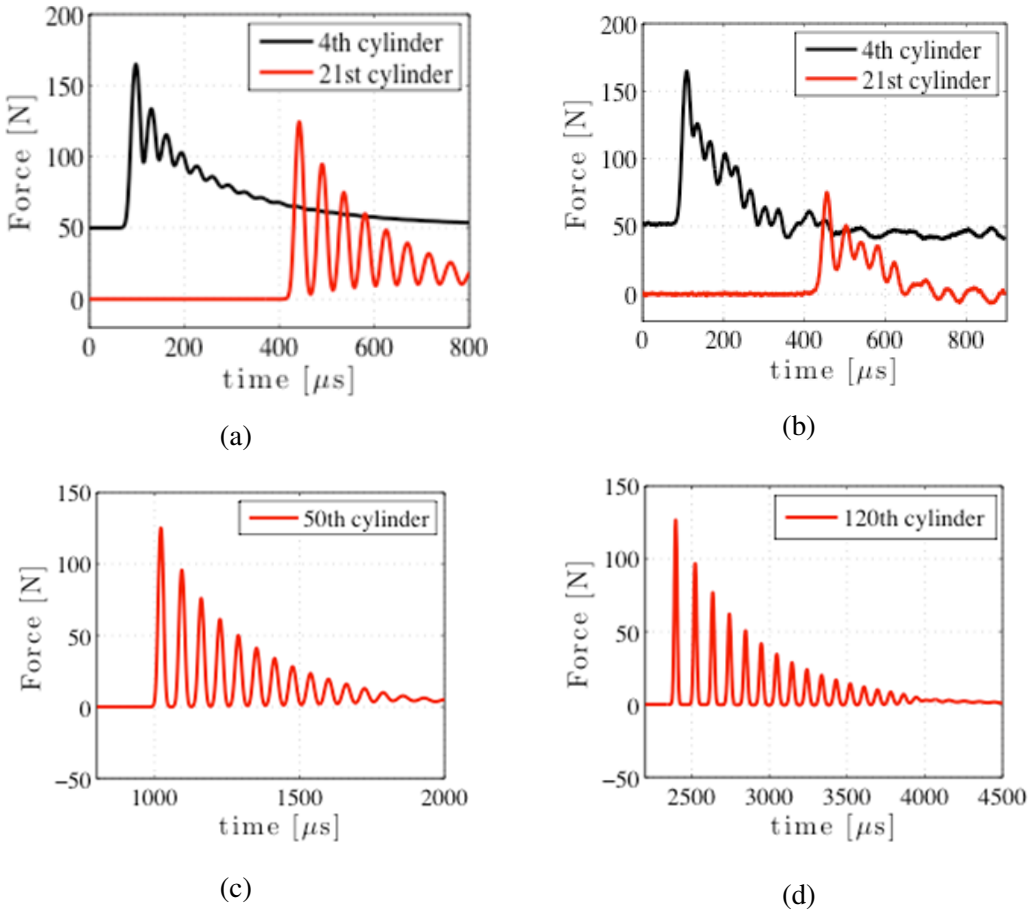

Figure 4.3: Numerical calculations of the compression pulse propagating through the system which has a mass ratio of 0.98 and experimental results. Pulses were excited by the impact of rod with mass of 39.136 g equal about 18.7m. (a), (c) and (d) numerical calculations related to the forces in the 4th and 21st (a), 50th (c), and 120th (d) cylinders; (b) experimental results, sensors are placed in the 4th and 21st cylinders. The curves are offset for visual clarity and zero time is arbitrary.

particles forming the chain resulted in a faster separation into train of solitary waves (compare Fig. 4.3(b) and Fig. 3 in [6] or Fig. 1.23(a) in [2]), a complete separation of the pulse into train of solitary waves was observed at 40th particle [2, 6]. This comparison illustrates that splitting of incoming pulse into train of solitary waves is faster at smaller striker mass.

In numerical calculations the speed of the leading pulse propagating in the interval between 4th and 5th cylinder was 659 m/s and between 4th and 21st cylinders was 657.8

m/s. Numerical calculations demonstrated that gravitational precompression increases the speed of leading pulses within investigated intervals by less than two percent. The difference between numerical calculations and experimental results presented above (665 m/s and 656 m/s, correspondingly) is less than one percent being within error margins. The close values of the pulse speeds in experiments despite attenuation are due to the weak dependence of solitary wave speed on amplitude in the chain with Hertzian interaction [2].

We can see that initial pulse excited by striker in nondissipative chain is split into train of multiple solitary waves in far field from the entrance if the striker mass is significantly larger than mass of particles in the chain (Fig. 4.3(c) and (d)). Parameters of these solitary waves can be found based on different approaches which introduce additional hypothesis which are complimentary to energy and momentum conservation laws [7, 12, 13].

In this chapter we consider hypothetical scenario of generating the train of solitary waves in far field considering the multiple sequential striker impacts with imaginary mass being in rest such that each collision generates corresponding solitary wave in the train with linear momentum being close to the calculated values in exact numerical approach. This scenario preserves linear momentum and energy of the system and it does not require any additional hypothesis. This is similar to the approach used to calculate the parameters of solitary wave train generated at the interface of two sonic vacua (granular chains) proposed in [14] where the movement of the last heavy particle adjacent to the interface was generating solitary train.

This scenario oversimplifies the process of striker interaction with the particles in a granular chain considering only interaction of striker with imaginary effective mass. In fact it interacts with collective of particles at the vicinity of impact point and these particles are not yet self-organized themselves into particular motion for example,

representative for solitary wave. Second simplification in the proposed scenario is the neglect of recoil of end particles and the striker from the chain [2,6,15]. These recoiled masses carry linear momentum and energy, which is not accounted in the proposed scenario. This assumption is feasible because recoiled particles do not carry significant portion of energy and linear momentum. For example, recoiled particles take only 2% percent of the linear momentum and even less kinetic energy (0.04%) [2] after impact of striker with mass equal to the mass of two particles. This approach is intended to provide simple estimation of the amplitude of the leading solitary wave and neglects possibility to create small amplitude solitary waves when mass of striker is larger than mass of the particles in the chain.

In this chapter we investigate the accuracy of this scenario, which considers only interaction of striker with imaginary effective mass to predict parameters of solitary wave in the train in far field for different striker masses for nondissipative chains.

To apply the proposed scenario to the generation of the train of solitary waves we first introduce effective mass of solitary wave considered as quasiparticle. The velocity of particles in the solitary wave, determining their linear momenta and kinetic energy, are proportional to the maximum particle velocity υ_m in the solitary wave [2]. Thus linear momentum of solitary wave is also proportional to υ_m and its kinetic energy E_k is proportional to υ_m^2. The ratio of kinetic to potential energy (E_p) of the solitary wave in sonic vacuum, corresponding to particles interaction according to the Hertz law, is close to 1.25. This ratio does not depend on solitary wave amplitude [2]. Thus total energy of the solitary wave is close to $1.8E_k$. These properties allow consideration of a solitary wave as a quasiparticle with the effective mass m_s and with effective kinetic energy equal to sum of kinetic and potential energies of particles in it. This effective mass does not depend on the amplitude of solitary wave and it can be calculated from the following equation:

$$\frac{P^2}{2m_s} = E_k + E_p, \tag{4.5}$$

where P is the total linear momentum of particles (each with mass m) in the solitary wave. The left part is the effective kinetic energy of the solitary wave (quasiparticle) represented by a sum of E_k and E_p, which are a total kinetic and potential energies of real particles in the chain. Using this equation and results from numerical simulations, it was found that the effective mass of the solitary wave ms is close to 1.3m, which is slightly lower than presented in [2, 14].

The following relation between maximum particle velocity in the strongly nonlinear solitary wave υ_m and its linear momentum P was found in numerical calculations (Eq.4.6).

$$P \approx 1.67\upsilon_m m. \tag{4.6}$$

This equation is useful for calculation of linear momentum of solitary waves based on the value of maximum particle velocity. It should be emphasized that sum of the linear momenta of particles in the solitary wave P is not equal to $m_s V_s$ (V_s is a phase speed of solitary wave). This phase speed is much larger than velocity of particles and it depends nonlinearly on the maximum particle velocity υ_m. The effective mass of solitary wave and relation between maximum particle velocity and linear momentum do not depend on elastic properties of particles, but they do depend on the type of interaction force between grains, e.g., for power law interaction force they depend on the value of exponent [2].

The chain impacted by striker undergoes a complex behavior due to strongly nonlinear interaction between multiple particles and their self organization into train of solitary waves in far field. This complex behavior is simplified in the proposed scenario

of the sequential impacts of the striker with the imaginary particle in rest with effective mass m_{eff} (the striker mass $m_{st} > m_{eff}$). This approach allows using conservation of linear momentum and energy resulting in the following equation for linear momentum P_n of the n-th solitary wave generated by the n-th impact of the striker [14]:

$$P_n = \frac{2P_0(B-1)^{n-1}}{(B+1)^n}, \tag{4.7}$$

where P_0 is the initial linear momentum of the striker, $B = m_{st}/m_{eff} > 1$, and number n corresponds to the n-th solitary wave.

Linear momentum of striker after impact, resulted in the generation of n-th solitary wave, is equal to

$$P_{st,n} = \frac{P_0(B-1)^n}{(B+1)^n}. \tag{4.8}$$

The multiple impacts of striker and the imaginary mass equal to m_{eff} transfer all initial linear momentum and energy of striker into the chain generating infinite number of solitary waves with decreasing amplitude without recoil of the striker. The proposed scenario is different than considered in [7] where only parameters of the leading solitary wave were determined based on the collision of the striker with effective mass in rest being equal to effective mass of solitary wave and the amplitudes of the other solitary waves were assumed to follow exponential dependence on their number.

The values of imaginary effective mass in rest can be chosen based on different approaches. It is natural to select this mass being equal to the effective mass of solitary wave because these waves are eventually emerged at the far range [2, 7,14].

Another approach to choose m_{eff} can be based on the observed phenomena in numerical calculations that maximum particle velocity in the leading solitary wave is equal exactly to twice of the velocity of the piston moving with constant mass or striker

with very large mass, $B \gg 1$ [2]. This is demonstrated in Fig. 4.4. For example, the maximum particle velocity in the leading solitary wave reaches $1.976\upsilon_{st}$ when the mass of the striker is 1000 times greater than the mass of the particles, and it increases to $1.9980\upsilon_{st}$ when this mass ratio become 10000.

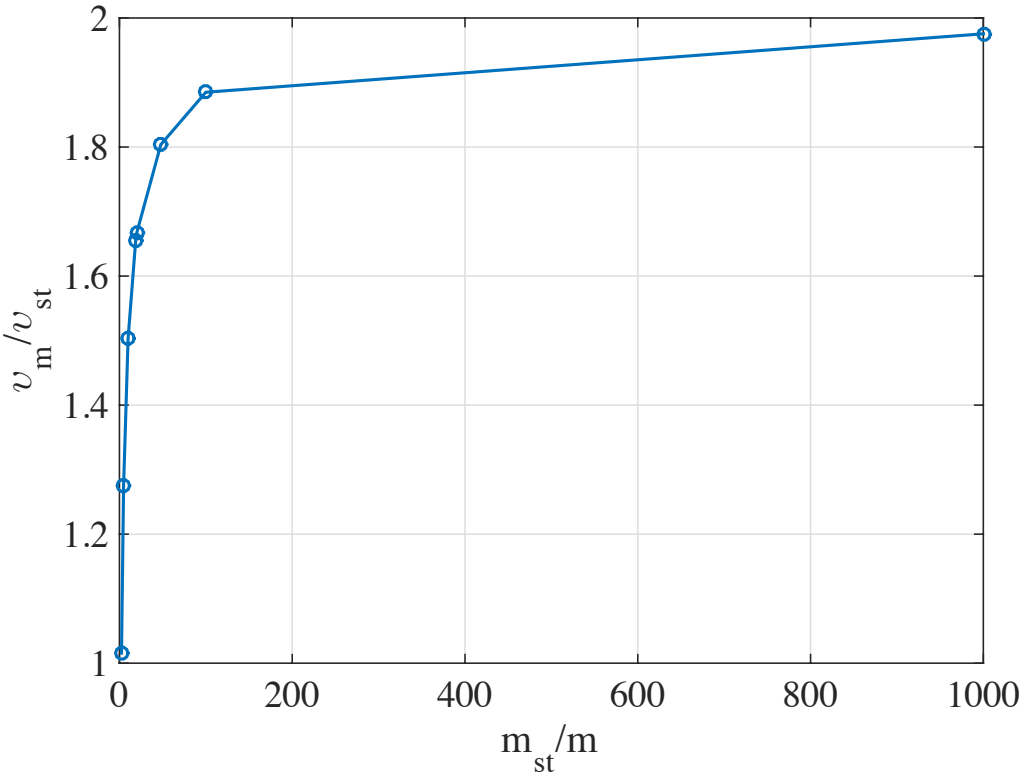

Figure 4.4: Ratio of maximum particle velocity to striker initial velocity depending on the ratio ratio of striker mass to mass of spheres in the chain.

It should be mentioned that equation for the relation between linear momentum of the striker and leading solitary wave in [7] does not predict the value of the maximum particle velocity in the leading solitary wave being twice the velocity of impactor when its mass much larger than mass of particles. The predicted maximum velocity in the leading solitary wave at very large mass of striker using Eq. 19 in [7] and Eq. 4.6 is equal to $1.61\upsilon_{st}$.

The linear momentum of the leading solitary wave at $B \gg 1$ ($n = 1$, $P_0 = m_{st}\upsilon st$),

using imaginary scenario where striker interacts with m_{eff}, is equal $P_1 = 2\upsilon_{st} m_{eff}$. (Eq. (4.7)). Combining this result with Eq. (4.6) and taking into account that $\upsilon_m = 2\upsilon_{st}$ obtain $m_{eff} \approx 1.67$m.

Striker interaction with the different effective masses m_{eff} might reflect different pictures of the self-organized motion of the end particles in the chain generating a leading solitary wave in a far field.

In case if striker mass in the proposed scenario is smaller than imaginary effective mass in rest ($B = m_{st}/m_{eff} < 1$) then only one interaction happened with the chain and linear momentum of generated single solitary wave P is

$$P = \frac{2P_0}{(B+1)}. \tag{4.9}$$

The linear momentum of recoiled striker P_{st} is equal

$$P_{st} = \frac{P_0(B-1)}{(B+1)}. \tag{4.10}$$

The proposed scenario predicts linear momentum of the solitary waves in the far field where initial disturbance is transformed into the train of solitary waves in case $B > 1$. If $B < 1$ then completely different behavior is described by Eqs. (4.9) and (4.10).

To investigate if the proposed simplified scenario provides the reasonable estimation of the parameters of solitary waves in the train (or single solitary wave) we compare the numerical and the analytical results using Eqs.4.7-4.10. The momenta of solitary waves and strikers with different masses in numerical calculations performed without gravitational precompression and using Eqs. 4.7-4.10 are presented in Tables 4.1-4.8 for different values of imaginary effective mass. Numerical (P_{num}) and analytical (P_a, P'_a, P''_a) results for linear momentum of single solitary wave ($B < 1$) and striker ($P_{st,num}, P_{st}, P'_{st}, P''_{st}$) are presented. Values of P'_a, and P_{st} were found using the mass of

particles in the chain as ($m_{eff} = m$); P_a and P_{st} were calculated using coefficient B based on the $m_{eff} = m_s \approx 1.3m$; P_a'', and P_{st}'' were found assuming collisions of striker with imaginary effective mass m_{eff}= $1.67m$.

Table 4.1 presents results of the impact by striker with velocity 0.457 m/s and the mass $0.1m$ (smaller than mass of particles in the chain) on the chain of particles with mass $m = 2.086$ g. The initial momentum of the striker $P_0 = 9.533 \times 10^{-5}$ kgm/s.

In numerical calculations a single solitary wave was excited in the chain (maximum velocity 0.05641 m/s, on its back 0.0176 m/s, on the back at the bottom, 0.0004457 m/s; ahead of maximum 0.01924 m/s, next to it 0.000543 m/s) with linear momentum $P_{num} = 19.658 \cdot 10^{-5}$ kgm/s. The numerical calculations demonstrate conservation of linear momentum in the system with accuracy $10^{-8}\%$. The striker rebounds with the velocity -0.3746 m/s corresponding to its linear momentum $-7.814 \cdot 10^{-5}$ kgm/s. But the sum of these linear momenta is equal to $11.844 \cdot 10^{-5}$ kgm/s and it is larger than initial linear momentum of the striker $P_0 = 9.533 \cdot 10^{-5}$ kg m/s.

The difference between sum of the linear momentum of recoiled striker and solitary wave and the initial linear momentum of striker is $-2.333 \cdot 10^{-5}$ kg m/s. Its magnitude corresponds to the magnitude of the linear momentum of recoiled end particles (24.47% of initial linear momentum). In numerical calculations the recoiled eight end particles have fast decreasing velocities starting with the first particle: -0.005671 m/s, -0.002429 m/s, -0.001275 m/s, -0.0007163 m/s, -0.0004135 m/s, -0.0002409 m/s, -0.0001404 m/s, and -0.00008153 m/s, velocities of other particles are presented in Fig. 4.5. These particles have the linear momentum $-2.288 \cdot 10^{-5}$ kgm/s. Sum of linear momenta of recoiled striker, solitary wave and eight end particles is smaller than initial value only by 0.4%. Inclusion of linear momenta of additional recoiled end particles increases the accuracy of momentum conservation. It is interesting that dependence of the recoiled velocities of particles on their position in the chain follows exponential law

Table 4.1: Linear momenta (kg m/s) of the single solitary wave (P_{num}, P_a, P'_a, P''_a) in numerical calculations and in analytical approach with corresponding values of $B = m_{st}/m_s, B' = m_{st}/m$, and $B'' = m_{st}/m_{eff}$. Striker mass $m_{st} = 0.1m$, $m_{eff} = 1.67m$.

P_{num}	P_a	P'_a	P''_a	$\frac{P_a - P_{num}}{P_{num}}$	$\frac{P'_a - P_{num}}{P_{num}}$	$\frac{P''_a - P_{num}}{P_{num}}$
$19.658 \cdot 10^{-5}$	$17.71 \cdot 10^{-5}$	$17.33 \cdot 10^{-5}$	$17.99 \cdot 10^{-5}$	-0.0997	-0.118	-0.0894

Table 4.2: Linear momenta (kg m/s) of the recoiled striker ($P_{st,num}$, P_{st}, P'_{st}, P''_{st}) in numerical calculations and in analytical approach with corresponding values of $B = m_{st}/m_s, B' = m_{st}/m$, and $B'' = m_{st}/m_{eff}$. Striker mass $m_{st} = 0.1m$, $m_{eff} = 1.67m$.

$P_{st,num}$	P_{st}	P'_{st}	P''_{st}	$\frac{P_{st} - P_{st,num}}{P_{st,num}}$	$\frac{P'_{st} - P_{st,num}}{P_{st,num}}$	$\frac{P''_{st} - P_{st,num}}{P_{st,num}}$
$7.814 \cdot 10^{-5}$	$8.171 \cdot 10^{-5}$	$7.780 \cdot 10^{-5}$	$8.457 \cdot 10^{-5}$	0.0457	-0.0044	0.0823

first introduced in [15] for the striker mass equal mass of particle with similar exponents ($-0.56n$ and $-0.55n$, correspondingly).

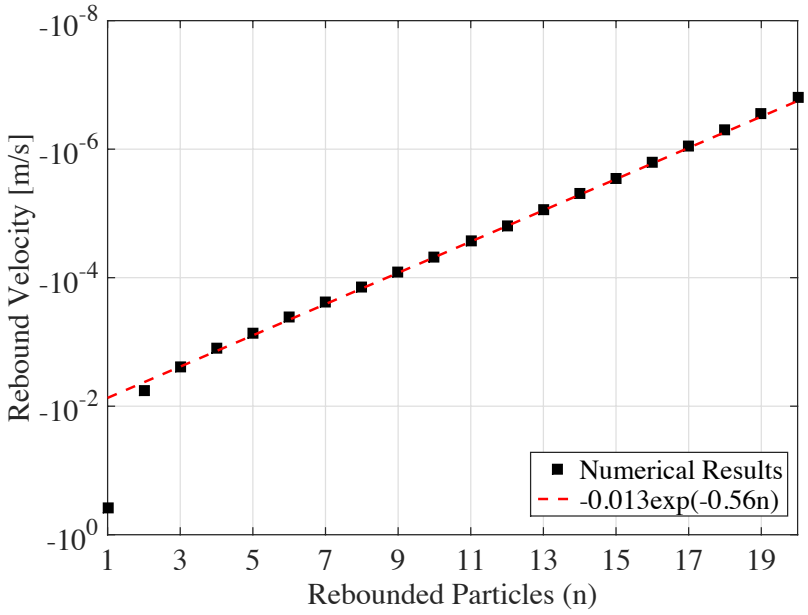

Figure 4.5: Velocity of rebounded striker and particles as function of their initial position in the chain ($n = 2$ corresponds to the first particle in the chain and $n > 2$ correspond to subsequent particles) after impact by striker ($n = 1$) with mass $0.1m$.

Fig. 4.6 illustrates that at the moment of striker's recoil in numerical calculations the velocity of the second particle is very small. In other words, at very small mass of striker its interaction time with top particles is very small and disturbance does not propagate in into significant depth in the particle chain.

It is also clear from particles velocities in Fig. 4.6 that at the moment of striker's recoil the contact between the first and second particles is under compression. In later moments it also results in the recoil of the first particle with velocity equal -0.005671 m/s (other particle contacts are less compressed resulting in particles recoil later with smaller velocities (Fig. 4.6), see below). This recoil of the particles near impacted end contributes to the linear momentum of formed solitary wave in numerical calculations.

This self-organization of particles movement near the impacted end of the chain

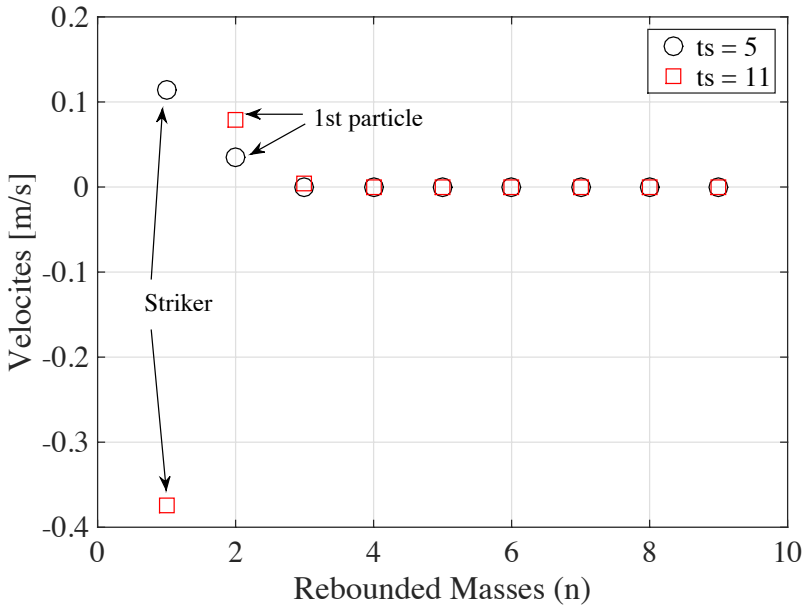

Figure 4.6: Velocities of the striker ($n = 1$) and particles in the chain at different time (before (5th time step) and right after striker's recoil (11th time step), each time step is equal 1.4 microseconds)) in numerical calculations. Striker mass $0.1m$, its initial velocity 0.457 m/s. .

and their recoil is not included into proposed imaginary scenario of the strike impact with some effective mass. It is assumed that resulting amplitude of the emerging solitary wave can be estimated by adjusting values of effective mass. Estimation of the solitary wave linear momentum in analytical approach assuming striker impact with effective mass m_{eff} equal mass of solitary wave ms provides a better agreement with numerical calculations than impact of striker with effective mass $m_{eff} = m$. Selecting $m_{eff} = 1.67m$ provides slightly better agreement of linear momentum of solitary wave still being smaller by less than 10% with respect to values obtained in numerical calculations (Table 4.1)

The recoil velocity of striker assumed to be interacting with particle mass (m) in analytical approach ($P'_{st} = 7.780 \cdot 10^{-5}$) is closer to the results of numerical calculations ($P_{st,num} = 7.814 \cdot 10^{-5}$).

Increase of striker mass to the value $0.5m$ (velocity 0.457 m/s, linear momentum

$P_0 = 4.7665 \cdot 10^{-4}$ kgm/s) results in the following parameters of the recoiled striker and single solitary wave (Table 4.3, 4.4).

In numerical calculations a single solitary wave was excited in the chain with linear momentum $P_{num} = 7.519 \cdot 10^{-4}$ kgm/s. The striker rebounds with the velocity -0.1661 m/s corresponding to its linear momentum $-1.732 \cdot 10^{-4}$ kgm/s. The sum of these linear momenta is equal to $5.787 \cdot 10^{-4}$ kgm/s and it is larger than initial linear momentum of the striker $P_0 = 4.7665 \cdot 10^{-4}$ kg m/s and the difference is $-2.333 \cdot 10^{-5}$ kg m/s. Its magnitude corresponds to the magnitude of the linear momentum of recoiled end particles (14% of initial linear momentum). In numerical calculations the recoiled eight end particles have fast decreasing velocities starting with the first particle: -0.0156 m/s, -0.0071 m/s, -0.0038 m/s, -0.0022 m/s, -0.0012 m/s, -0.00073 m/s, -0.00042m/s, and -0.00025 m/s. These particles have a total linear momentum of $-6.56 \cdot 10^{-5}$ kgm/s corresponding to 14% of initial linear momentum. Sum of linear momenta of recoiled striker, solitary wave and accounted eight end particles is smaller than initial value only by 0.2%.

Again the recoiled velocity of striker is better predicted in analytical calculations assuming that it interacted only with mass of particles in the chain (m) and solitary wave linear momentum is better predicted using the effective masses for the similar reasons outlined above for the case of striker impact with mass $0.1m$. As in the previous case the initial linear momentum of striker is distributed mainly between recoiled striker and first particle, but significant part of its energy is stored in the particles contacts near impacted end which later is partially transformed into kinetic energy of solitary wave.

We can see that increase of the striker mass from $0.1m$ to $0.5m$ resulted in the decrease of its recoil velocity. Impact by both strikers generates solitary wave due to self-organization of a few particles near impacted end. It is interesting to use broader variation of striker mass to probe what is the effective mass, which can describe interaction of

Table 4.3: Linear momenta (kg m/s) of the single solitary wave (P_{num}, P_a, P'_a, P''_a) in numerical calculations and in analytical approach with corresponding values of $B = m_{st}/m_s, B' = m_{st}/m$, and $B'' = m_{st}/m_{eff}$. Striker mass $m_{st} = 0.5m$, $m_{eff} = 1.67m$.

P_{num}	P_a	P'_a	P''_a	$\frac{P_a - P_{num}}{P_{num}}$	$\frac{P'_a - P_{num}}{P_{num}}$	$\frac{P''_a - P_{num}}{P_{num}}$
$7.159 \cdot 10^{-4}$	$6.885 \cdot 10^{-4}$	$6.355 \cdot 10^{-4}$	$7.337 \cdot 10^{-4}$	-0.0383	-0.077	0.0248

Table 4.4: Linear momenta (kg m/s) of the recoiled striker ($P_{st,num}$, P_{st}, P'_{st}, P''_{st}) in numerical calculations and in analytical approach with corresponding values of $B = m_{st}/m_s, B' = m_{st}/m$, and $B'' = m_{st}/m_{eff}$. Striker mass $m_{st} = 0.5m$, $m_{eff} = 1.67m$.

$P_{st,num}$	P_{st}	P'_{st}	P''_{st}	$\frac{P_{st} - P_{st,num}}{P_{st,num}}$	$\frac{P'_{st} - P_{st,num}}{P_{st,num}}$	$\frac{P''_{st} - P_{st,num}}{P_{st,num}}$
$1.732 \cdot 10^{-4}$	$2.118 \cdot 10^{-4}$	$1.589 \cdot 10^{-4}$	$2.57 \cdot 10^{-4}$	0.2229	-0.0826	0.4838

the striker with the chain, and compare it with the effective mass of solitary wave. The history of striker velocities for its different mass are presented in Fig. 4.7.

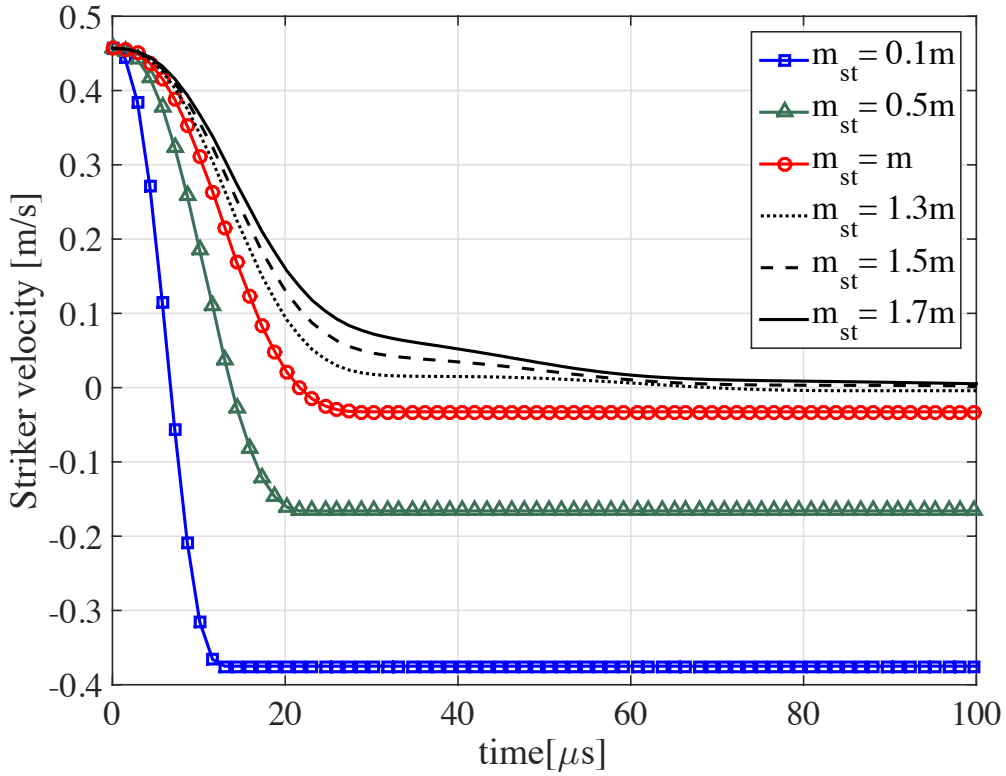

Figure 4.7: The history of striker velocities with different masses $0.1m - 1.7m$. Note the negligible recoil of striker with mass equal to the effective mass of solitary wave ($m_{st} = m_{eff} = 1.3m$).

It is clear that increase of striker mass results in the increase of its interaction time with the top particle (which effectively increases the number of particles in the interaction process). The fact that striker recoils when its mass equal to the particle mass clearly demonstrates that striker interacts with some effective mass larger than particle mass (Fig. 4.7). At striker mass equal to the effective mass of solitary wave ($1.3m$) it recoils with very small velocity being less than 1% of the initial velocity. At larger striker mass it practically stopped by the interaction with the chain, for example at striker mass equal $1.7m$ its recoil velocity is 0.02% of the initial velocity and at striker mass 1.8m

(not shown in Fig. 4.7) no recoil was detected.

It should be mentioned that when striker's mass is equal $1.3m$ impact generates a secondary solitary waves with very small amplitudes in numerical calculations (their amplitude is less than 2%).These solitary waves are not captured by analytical approach if B is calculated based on $m_{eff}= 1.3m$. But selecting B based on $m_{eff} = m$ results in less accurate prediction of the parameters of the leading solitary wave which is the main goal of our approach.

As striker mass become $1.8m$ it does not recoil and the chain of the solitary waves is formed with rapidly decreasing amplitude, e.g., the amplitude of the forth wave is about 40 times smaller than the first one (Table 4.5). This striker behavior is in agreement with analytical approach and if $m_{eff} = 1.3m$ gives better predictions of the amplitude of the leading solitary wave (and other waves in the train) then other two values of the affective mass (m and $1.67m$).

The parameters of the first 10 fully developed leading solitary waves at far field at relatively large striker's masses ($m_{st} = 2.4m \sim 48m$) are presented in Fig. 4.8 (these strikers do not recoil).

Selecting effective mass $m_{eff} = 1.3m$ in the analytical approach predicts amplitude of the first and second solitary waves with accuracy better than 10% when striker masses are equal 5g and 10g. The analytical approach fails to predict amplitudes of subsequent smaller amplitude solitary waves with this accuracy (Fig. 4.8(a) and (b)).

The analytical approach at striker mass close to 19m (selecting effective mass $m_{eff} = 1.3m$) predicts amplitude of the first solitary wave with slightly less accuracy than selecting effective mass $m_{eff} = 1.67m$ (Fig. 4.8(c)). The analytical approach fails to predict amplitudes of subsequent smaller amplitude solitary waves. It is interesting that amplitudes of the subsequent solitary waves are better predicted using effective mass interacting with the striker equal to the effective mass of the solitary wave.

Table 4.5: Linear momentum(kg m/s) of the first five solitary waves created by an striker with $m_{st} = 5g \approx 2m$.

	P_{num}	P_a	P'_a	P''_a	$\frac{P_a - P_{num}}{P_{num}}$	$\frac{P'_a - P_{num}}{P_{num}}$	$\frac{P''_a - P_{num}}{P_{num}}$
P_1	$1.622 \cdot 10^{-3}$	$1.620 \cdot 10^{-3}$	$1.3 \cdot 10^{-3}$	$1.880 \cdot 10^{-3}$	-0.0159	-0.1875	0.1875
P_2	$4.346 \cdot 10^{-4}$	$4.790 \cdot 10^{-4}$	$5.531 \cdot 10^{-4}$	$3.363 \cdot 10^{-4}$	0.102	0.2723	-0.2262
P_3	$1.257 \cdot 10^{-4}$	$1.420 \cdot 10^{-4}$	$2.283 \cdot 10^{-4}$	$5.982 \cdot 10^{-5}$	0.13	0.8146	-0.5239
P_4	$3.944 \cdot 10^{-5}$	$4.232 \cdot 10^{-5}$	$9.361 \cdot 10^{-5}$	$1.064 \cdot 10^{-5}$	0.0736	1.3756	0.7299

Table 4.6: Linear momentum(kg m/s) of the first five solitary waves created by an striker with $m_{st} = 10g \approx 5m$.

	P_{num}	P_a	P'_a	P''_a	$\frac{P_a - P_{num}}{P_{num}}$	$\frac{P'_a - P_{num}}{P_{num}}$	$\frac{P''_a - P_{num}}{P_{num}}$
P_1	$2.024 \cdot 10^{-3}$	$1.949 \cdot 10^{-3}$	$1.6 \cdot 10^{-3}$	$2.4 \cdot 10^{-3}$	-0.0367	-0.2095	-0.2095
P_2	$1.038 \cdot 10^{-4}$	$1.120 \cdot 10^{-4}$	$1.0 \cdot 10^{-4}$	$1.1 \cdot 10^{-4}$	0.0790	-0.0366	0.0597
P_3	$5.590 \cdot 10^{-4}$	$6.410 \cdot 10^{-4}$	$6.76 \cdot 10^{-4}$	$5.507 \cdot 10^{-4}$	0.147	0.2129	-0.0148
P_4	$3.130 \cdot 10^{-4}$	$3.670 \cdot 10^{-4}$	$4.43 \cdot 10^{-4}$	$2.658 \cdot 10^{-4}$	0.173	0.4153	-0.1508
P_5	$1.779 \cdot 10^{-4}$	$2.107 \cdot 10^{-4}$	$2.90 \cdot 10^{-4}$	$1.283 \cdot 10^{-4}$	0.183	0.6301	-0.2788
P_6	$1.033 \cdot 10^{-4}$	$1.208 \cdot 10^{-4}$	$1.90 \cdot 10^{-4}$	$6.189 \cdot 10^{-5}$	0.169	0.8393	-0.4009
P_7	$6.174 \cdot 10^{-5}$	$6.926 \cdot 10^{-5}$	$1.24 \cdot 10^{-4}$	$2.987 \cdot 10^{-5}$	0.122	1.0084	-0.5162
P_8	$5.163 \cdot 10^{-5}$	$3.971 \cdot 10^{-5}$	$8.14 \cdot 10^{-5}$	$1.441 \cdot 10^{-5}$	-0.23	0.5771	-0.7209
P_9	$3.732 \cdot 10^{-5}$	$2.277 \cdot 10^{-5}$	$5.33 \cdot 10^{-5}$	$6.956 \cdot 10^{-6}$	-0.39	0.4290	-0.8136
P_{10}	$2.721 \cdot 10^{-5}$	$1.305 \cdot 10^{-5}$	$3.49 \cdot 10^{-5}$	$3.357 \cdot 10^{-6}$	-0.52	0.2826	-0.8766

Table 4.7: Linear momentum(kg m/s) of the first five solitary waves created by an striker with $m_{st} = 39.136g \approx 19m$.

	P_{num}	P_a	P'_a	P''_a	$\frac{P_a - P_{num}}{P_{num}}$	$\frac{P'_a - P_{num}}{P_{num}}$	$\frac{P''_a - P_{num}}{P_{num}}$
P_1	$2.634 \cdot 10^{-3}$	$2.318 \cdot 10^{-3}$	$4.0 \cdot 10^{-3}$	$2.9 \cdot 10^{-3}$	0.1199	0.5186	0.1010
P_2	$2.110 \cdot 10^{-3}$	$2.018 \cdot 10^{-3}$	$3.6 \cdot 10^{-3}$	$2.5 \cdot 10^{-3}$	-0.0436	0.7062	0.1848
P_3	$1.738 \cdot 10^{-3}$	$1.756 \cdot 10^{-3}$	$3.2 \cdot 10^{-3}$	$2.0 \cdot 10^{-3}$	0.0104	0.8412	0.1507
P_4	$1.454 \cdot 10^{-3}$	$1.528 \cdot 10^{-3}$	$2.9 \cdot 10^{-3}$	$1.7 \cdot 10^{-3}$	0.0509	0.9945	0.1692
P_5	$1.230 \cdot 10^{-3}$	$1.330 \cdot 10^{-3}$	$2.6 \cdot 10^{-3}$	$1.4 \cdot 10^{-3}$	0.0813	1.1138	0.1382
P_6	$1.000 \cdot 10^{-3}$	$1.200 \cdot 10^{-3}$	$2.3 \cdot 10^{-3}$	$1.2 \cdot 10^{-3}$	0.2	1.3	0.2
P_7	$0.890 \cdot 10^{-3}$	$1.000 \cdot 10^{-3}$	$2.1 \cdot 10^{-3}$	$1.0 \cdot 10^{-3}$	0.123	1.3596	0.1236
P_8	$0.760 \cdot 10^{-3}$	$0.878 \cdot 10^{-3}$	$1.9 \cdot 10^{-3}$	$0.838 \cdot 10^{-3}$	0.155	1.5	0.1026
P_9	$0.655 \cdot 10^{-3}$	$0.764 \cdot 10^{-3}$	$1.7 \cdot 10^{-3}$	$0.701 \cdot 10^{-3}$	0.166	1.5954	0.0702
P_{10}	$0.564 \cdot 10^{-3}$	$0.665 \cdot 10^{-3}$	$1.5 \cdot 10^{-3}$	$0.586 \cdot 10^{-3}$	0.179	1.6596	0.039

Table 4.8: Linear momentum(kg m/s) of the first five solitary waves created by an striker with $m_{st} = 100g \approx 50m$.

	P_{num}	P_a	P'_a	P''_a	$\frac{P_a - P_{num}}{P_{num}}$	$\frac{P'_a - P_{num}}{P_{num}}$	$\frac{P''_a - P_{num}}{P_{num}}$
P_1	$2.885 \cdot 10^{-3}$	$2.413 \cdot 10^{-3}$	$4.1 \cdot 10^{-3}$	$3.1 \cdot 10^{-3}$	-0.164	0.4211	0.0745
P_2	$2.572 \cdot 10^{-3}$	$2.186 \cdot 10^{-3}$	$3.9 \cdot 10^{-3}$	$2.9 \cdot 10^{-3}$	-0.111	0.5163	0.1275
P_3	$2.347 \cdot 10^{-3}$	$2.217 \cdot 10^{-3}$	$3.8 \cdot 10^{-3}$	$2.7 \cdot 10^{-3}$	-0.055	0.6191	0.1504
P_4	$2.153 \cdot 10^{-3}$	$2.050 \cdot 10^{-3}$	$3.6 \cdot 10^{-3}$	$2.5 \cdot 10^{-3}$	-0.0478	0.6721	0.1612
P_5	$1.984 \cdot 10^{-3}$	$1.942 \cdot 10^{-3}$	$3.5 \cdot 10^{-3}$	$2.3 \cdot 10^{-3}$	-0.0212	0.7641	0.1593
P_6	$1.843 \cdot 10^{-3}$	$1.840 \cdot 10^{-3}$	$3.3 \cdot 10^{-3}$	$2.2 \cdot 10^{-3}$	-0.0163	0.7906	0.1931
P_7	$1.713 \cdot 10^{-3}$	$1.742 \cdot 10^{-3}$	$3.2 \cdot 10^{-3}$	$2.0 \cdot 10^{-3}$	0.0169	0.8681	0.1657
P_8	$1.594 \cdot 10^{-3}$	$1.650 \cdot 10^{-3}$	$3.1 \cdot 10^{-3}$	$1.9 \cdot 10^{-3}$	0.0351	0.9448	0.1920
P_9	$1.486 \cdot 10^{-3}$	$1.563 \cdot 10^{-3}$	$2.9 \cdot 10^{-3}$	$1.8 \cdot 10^{-3}$	0.0518	0.9515	0.2113
P_{10}	$1.386 \cdot 10^{-3}$	$1.481 \cdot 10^{-3}$	$2.8 \cdot 10^{-3}$	$1.6 \cdot 10^{-3}$	0.0685	1.0202	0.1544

The tendency to predict amplitude of the leading solitary wave with better accuracy (at $m_{eff} = 1.67m$ than at $m_{eff} = 1.3m$) is clear at larger striker mass $m_{st} = 100$ g$\approx 50m$ (Fig. 4.8(d)). This is a natural behavior because effective mass $m_{eff} = 1.67m$ was selected based on the requirement that amplitude of particle velocity of the leading solitary wave is equal to twice of the velocity of striker when its mass is much larger than mass of particles in the chain.

Presented data in Fig. 4.8 demonstrate that better estimates of the amplitude of the leading solitary wave in the analytical approach are obtained at different values of effective mass at small and relatively large striker mass. At striker mass less than 18m the effective mass $1.3m$ results in the prediction of the leading amplitude with accuracy better than 10%. As striker mass becomes much larger than particle mass, the prediction with effective mass $1.67m$ works better and always provide an upper boundary of linear momentum for all solitary waves in the train. It should be emphasized that proposed simple scenario does not require additional assumption of the exponential decay of the solitary wave in the chain with its number as in [7].

Numerical calculations with larger striker mass demonstrated that the proposed approach with $m_{eff} = 1.67m$ gives a better estimate of the amplitude of the leading solitary waves and provides an upper estimates of the amplitudes of 20 leading solitary waves.

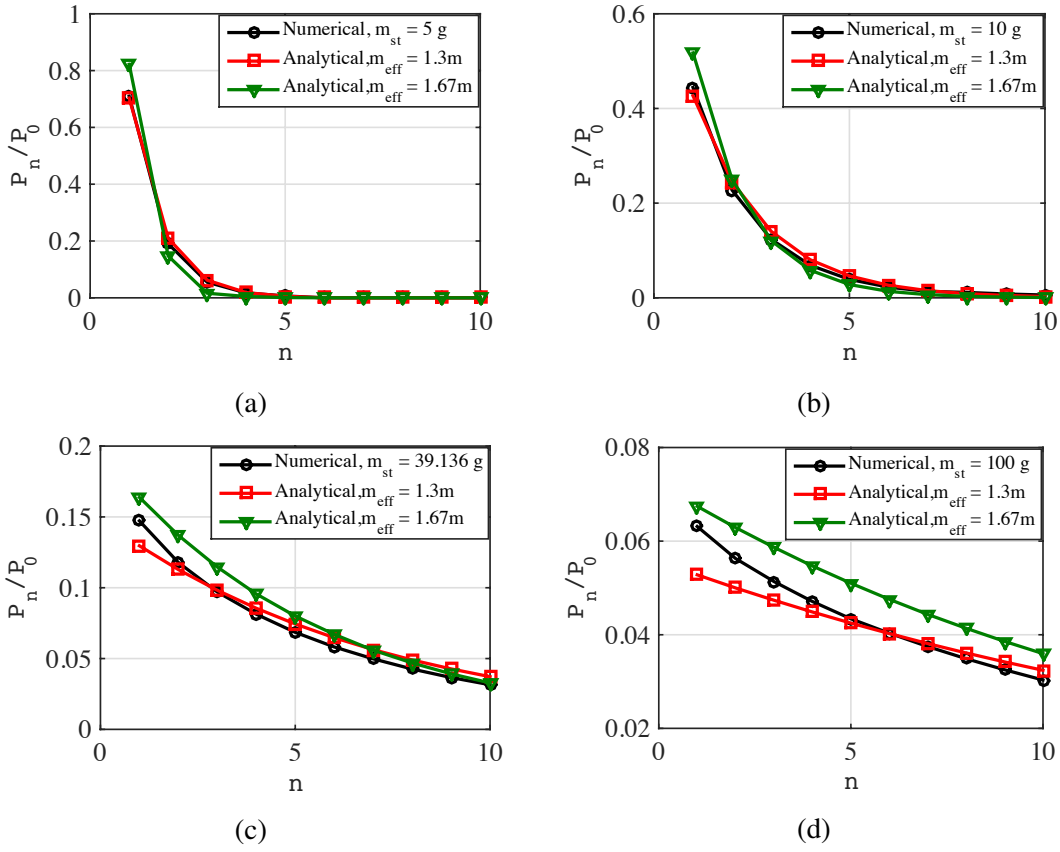

Figure 4.8: Comparison of numerical and analytical results for the ratio P_n/P_0 of the first ten solitary wave created by striker mass 5 g (2.4m) (a), 10 g (4.7m) (b), 39.136 g (19m) (c) and 100 g (48m) (d). The linear momentum is normalized with respect to the initial linear momentum of the striker. Velocity of striker 0.457 m/s.

4.4 Conclusions

The amplitudes of the leading solitary waves in far field generated by the striker impact can't be exactly predicted based on conservation of linear momentum and energy. Nevertheless the simple approach based on two conservation laws provides reasonable approximation for the amplitudes of the leading solitary waves in the train though it was not possible to describe the amplitudes of the subsequent solitary waves in the chain with the same accuracy using only one value of the effective mass interacting with the striker. It is based on the imaginary multiple independent collisions of striker with effective mass in rest, increasing with striker mass.

At striker mass below $18m$ the effective mass equal effective mass of solitary wave gives predictions of the linear momentum of the leading solitary wave better than 10%, at larger striker mass the similar accuracy of prediction is achieved at effective mass equal $1.67m$. It is important that this effective mass results in a maximum particle velocity in the leading solitary wave approaching a value being two times larger than the velocity of the striker with very large mass ($m_{st}/m = 2 \cdot 10^4$). This result matches the results of numerical calculations. The estimate of the amplitude of the leading solitary wave is also a reasonable estimate of the leading amplitude of the oscillating profile close to the impacted end where the pulse still did not split into train of separate solitary waves.This approach can be used to obtain upper estimates for the parameters of leading solitary waves in experiments with weak dissipation.

It is interesting that amplitudes of the subsequent solitary waves are better predicted using effective mass interacting with the striker equal to the effective mass of the solitary wave practically at all investigated ratios of striker mass to the mass of particles.

The striker does not rebound when with its mass is equal or larger than $1.8m$. This behavior is important for practical applications where preventing rebound of strikers

is important additionally to the attenuation of generated shock waves due to impact. It explains why large mass initially resting on the granular bed does not recoil under contact explosive loading.

4.5 References

1 S. Y. Wang, and V. F. Nesterenko, "Attenuation of short strongly nonlinear stress pulses in dissipative granular chains", in *Physical Review E*, **91**, 062211 (2015).

2 V. F. Nesterenko, *Dynamics of Heterogeneous Materials*, Springer-Verlag, New York, (2001), Chap. 1.

3 C. Daraio, V.F. Nesterenko, E. Herbold, and S. Jin "Strongly Nonlinear Waves in a Chain of Teflon Beads", in *Phys. Rev E*, **72**, 016603, (2005).

4 V.F. Nesterenko, C. Daraio, E. Herbold, and S. Jin "Anomalous wave reflection at the interface of two strongly nonlinear granular media", in *Physical Review Letters*, **95**, 158702-1, (2005).

5 V. F. Nesterenko, "Propagation of nonlinear compression pulses in granular media", in *Prikl. Mekh. Tekh. Fiz.* **24**, 136 (1983) [*J. Appl. Mech. Tech. Phys.* **24**, 733 (1984)].

6 A. N. Lazaridi and V. F. Nesterenko, "Observation of a new type of solitary waves in a one-dimensional granular medium", *Prikl. Mekh. Tekh. Fiz.* **26**, 115 (1985); [*J. Appl. Mech. Tech. Phys.* **26**, 405 (1985)].

7 S. Job, F. Melo, A. Sokolow, and S. Sen, "Solitary wave trains in granular chains: experiments, theory and simulations", in *Granular Matter*, **10**, 13-20, (2007).

8 C. Coste, E. Falcon, and S. Fauve, "Solitary waves in a chain of beads under Hertz contact", in *Phys. Rev. E* **56**, 6104 (1997).

9 S. Job, F. Melo, A. Sokolow, and S. Sen, "How Hertzian solitary waves interact with boundaries in a 1D granular medium", in *Phys. Rev. Lett.* **94**, 178002 (2005).

10 V.F. Nesterenko, C. Daraio, E. Herbold, and S. Jin, "Anomalous wave reflection at the interface of two strongly nonlinear granular media", in textitPhysical Review Letters, **95**, 158702 (2005).

11 V. F. Nesterenko, “Solitary waves in discrete media with anomalous compressibility and similar to “sonic vacuum””, in *JOURNAL DE PHYSIQUE IV, Colloque C8, supplement au Journal de Physique III*, **4**, C8-729 - C8-734 (1994).

12 A. Sokolow, E.G. Bittle, S. Sen, “Solitary wave train formation in Hertzian chains”, in *Europhys. Lett*. **77**, 24002 (2007).

13 X. M. Arif Hasa and Sia Nemat-Nasser “Universal relations for solity waves in granular crystals under shocks with finite rise and decay times”, in *Phys. Rev E*, **93**, 042905, (2016).

14 A. M. Tichler, L. R. Gomez, N. Upadhyaya, X. Campman, V. F. Nesterenko, and V. Vitelli, “Transmission and reflection of strongly nonlinear solitary waves at granular interfaces”, in *Physical Review Letters*, **111**, 048001 (2013).

15 E. J. Hinch and S. Saint-Jean, “The Fragmentation of a Line of Balls by an Impact”, in *Proc. R. Soc. A* **455**, 3201 (1999).

Chapter 5

Role of dissipation on the striker behavior and shape of propagating pulses

5.1 Introduction

One dimensional chains of elastic particles interacting according to Hertz contact law exhibit trongly nonlinear wave dynamics. Without precompression, this system is called "sonic vacuum" [4]. Sound waves cannot propagate in "sonic vacuum", but it supports strongly nonlinear solitary waves (Nesterenko solitary waves) with unique properties [1-5]. These solitary waves were observed experimentally by many researchers, though they may significantly attenuate due to dissipation in experimental settings.

Different studies have introduced dissipations into numerical calculations and analytical models for discrete systems [6-10]. Impact by striker with different masses larger than mass of the particles in the chain, may result in solitary wave trains, in oscillating or monotonous shock like profiles in experiments and in numerical calculation

[1,2,4,11-15]. There exists a critical value of viscosity the stationary stress pulse excited by boundary movement with constant velocity is monotonous [15, 16]. The critical value of viscosity was developed for weakly nonlinear systems described by Korteweg de Vries (KdV) equations [17] and for strongly nonlinear systems corresponding to long-wave approximation [18]. But the critical values of the viscosity (separating weakly dissipative from strongly dissipative behavior) causing the transition from train of decaying solitary waves to oscillatory or to monotonous wave profiles excited by a striker with finite mass were not identified. Using numerical calculations, we found that the critical value of viscosity for stress waves with finite duration is of the similar order of magnitude to the value derived for transition from oscillatory to smooth stationary stress wave [15].

5.2 Experimental Setup

The experimental set up is similar to the settings in Chapter 4 except that small mass striker with the shape shown below was used to verify damping coefficient for the contact interaction of sphere and cylinder. Chains were composed from steel spheres (440*C*) with diameter d and steel cylinders (304) with height h arranged alternatively. The cell size was $a = h + d$. Particles are hold in chain geometry by four aluminum rods arranged vertically (Fig. 5.1). The mass ratio was changed by using cylinders with different heights, but keeping the nature of contacts the same.

High speed camera was used to measure the recoil velocity of the small mass striker to verify value of damping coefficient for the sphere/cylinder contact interaction.

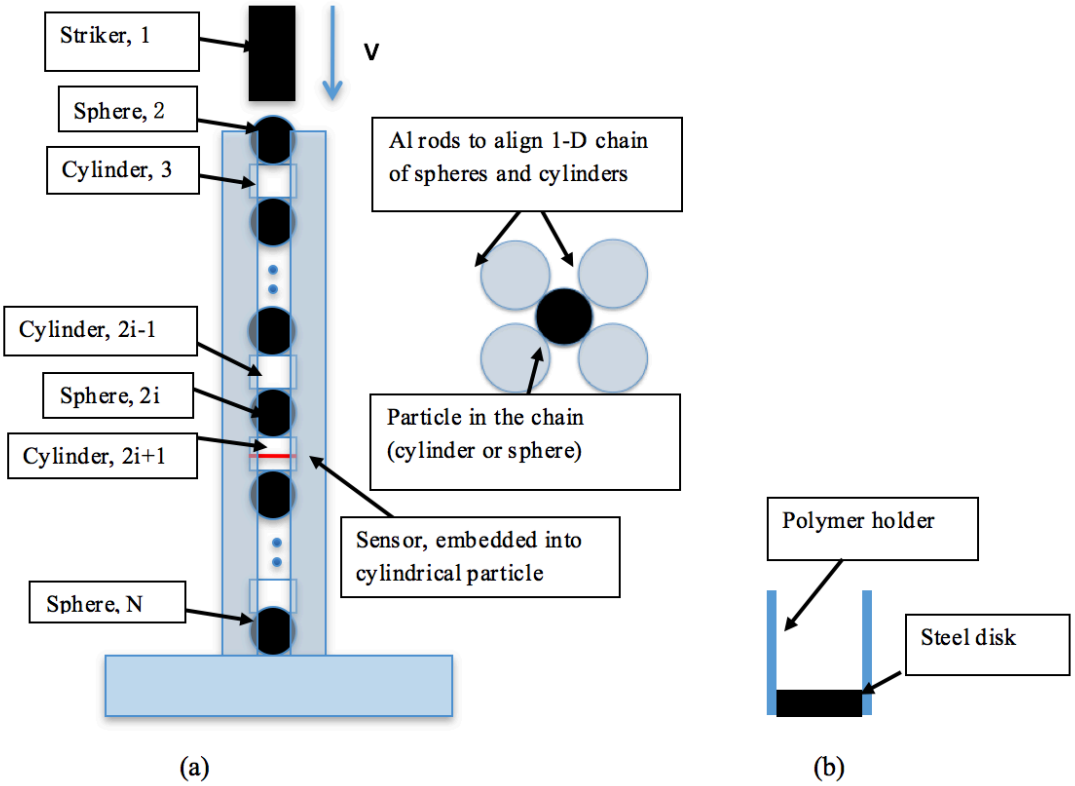

Figure 5.1: Experimental set-up. (a) Cylinders and spheres aligned in 1-D chain inside the holder (left) and cross-sectional view of the assembly (right). Four aluminum rods hold the particles in aligned chain. The numeration of particles in the chain ($i = 1, 2, 3?N/2$) corresponds to the numerical calculations. (b) Small striker with mass of bottom steel disc 3.9 g and light polymer holder with mass 0.4 g.

5.3 Numerical Calculations

The chain with mass ratio of elements close to $1(0.98)$ was assembled from 45 steel spheres ($440C$) with a mass (m) 2.085 g and 44 steel cylinders (304) with a height $h = 5.3$ mm and a mass of 2.043 g was investigated in numerical calculations. This chain with the mass ratio equal to 0.98 supports solitary like waves almost identical to the expected solitary wave in the chain with equal masses of particles [19].

Hertzian contacts were assumed between the spherical particles and the cylinders with flat surfaces similar to Chapter 4 (Eqn 4.1-4.4). Additionally forces representing a linear viscous dissipation (F_{vis}) were added to all contact interactions (striker and the first

particle, last particle and the supporting wall and between particles in the chain):

$$\begin{aligned} F_{vis,1} &= \mu_1(\dot{u}_2 - \dot{u}_1), \\ F_{vis} &= \mu(\dot{u}_{i-1} - 2\dot{u}_i + \dot{u}_{i+1}), \\ F_{vis,N} &= \mu(\dot{u}_{N-1} - 2\dot{u}_N), \end{aligned} \tag{5.1}$$

where μ_1 and μ are the effective coefficients of viscous damping corresponding to interaction between striker and first particle, between last particle and the supporting wall and particles in the chain. This simple dissipative model with effective viscous damping coefficient was able to describe successfully the transformation of stress wave in granular chains with similar contacts (decreasing of amplitude and change of wave shape) at similar conditions of loading [13]. In numerical calculations a total energy was conserved with accuracy $10^{-4}\%$ in nondissipative chain and linear momentum was conserved with accuracy $10^{-6}\%$ (ratio of energy/linear momentum deviations from their average values in percentages) in nondissipative and dissipative chains.

5.4 Behavior of strikers

In Chapter 3 the effective viscous dissipation (damping coefficient 6 kg/s) was introduced to explain experimentally observed attenuation of stress pulse amplitudes. This effective dashpot was attributed to the contact deformation of steel sphere/steel cylinder in the frame of Kelvin-Voigt model. In this chapter we performed additional experiments with measurements of recoil velocity of low mass striker ($m_{st} = 0.43$ g) impacting the top steel sphere. The recoil velocity of this striker is sensitive to the viscous dissipation on its contact with top sphere, this contact is the same as between cylinders and spheres in the chain. The results of numerical calculations are presented in 5.2. Damping coefficient equal 6 kg/s resulted in recoil velocity of striker in numerical

calculations 0.83 m/s, which is in agreement with experimental value 0.84 ± 0.04 m/s (initial velocity of striker $\upsilon_{st} = 1.457$ m/s).

This result gives additional justification to use Kelvin-Voigt model for contact interaction between flat steel cylinder surface and steel spherical particles with damping coefficient 6 kg/s.

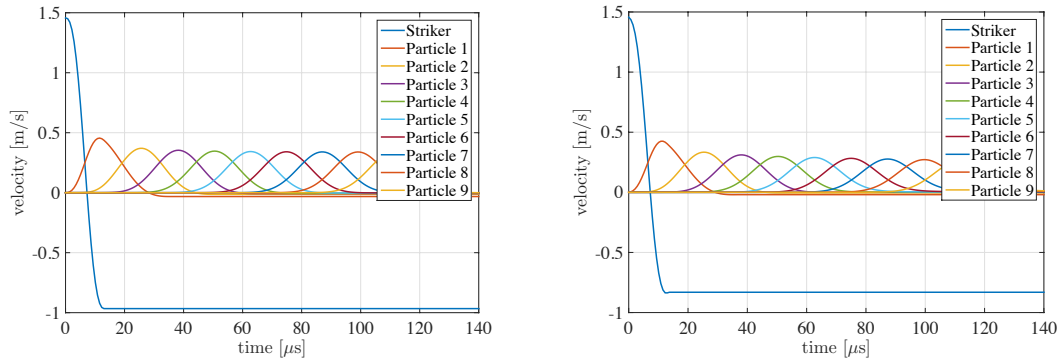

Figure 5.2: The recoil of striker with small mass ($m_{st} = 0.43$ g) impacting steel sphere at the chain top with velocity $\upsilon_{st} = 1.457$ m/s, (a) $\mu = 0$ kg/s, (b) $\mu = 6$ kg/s. Velocities of particles 1-9 are also shown to demonstrate the establishment of fast quasistationary solitary wave with very slow rate of amplitude decay.

For a system with a heavier striker of 39.13 g and impact velocity of 0.457 m/s, the velocity history of the striker is presented in Fig. 5.3 for nondissipative chain.

The striker was practically stopped by the chain at about 1742μ s after impact. In numerical calculations without dissipation the striker bounced back at about 1742μs from the moment of impact due to the arrival of reflection wave from the bottom where the chain was in contact with a rigid wall. The second recoil is detected at about 1871μs from the moment of impact due to arrival of the second reflected wave from the bottom. The striker was subject to sequential reflections until fully separated from the chain and remains a constant recoil velocity -0.3859 m/s at 13450μs.

The introduction of the damping coefficient of 6 kg/s, which satisfactory explained the attenuation of signal amplitude and recoil velocity of small mass striker, did not

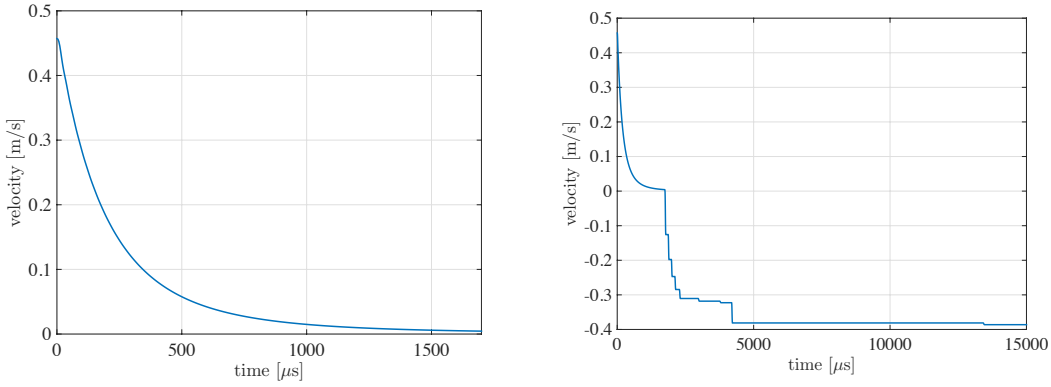

Figure 5.3: The dependence of the striker velocity on time, striker mass 39.13 g, at different time scales. The chain is nondissipative ($\mu = 0$ kg/s). Gravitation is not included.

change the first stage of the striker velocity decrease (compare Figs. 5.3 and 5.4), but recoil velocity was reduced from -0.3 m/s to -0.22 m/s and the striker was separated from the chain at this moment due to the arrival of the reflected wave from the bottom support.

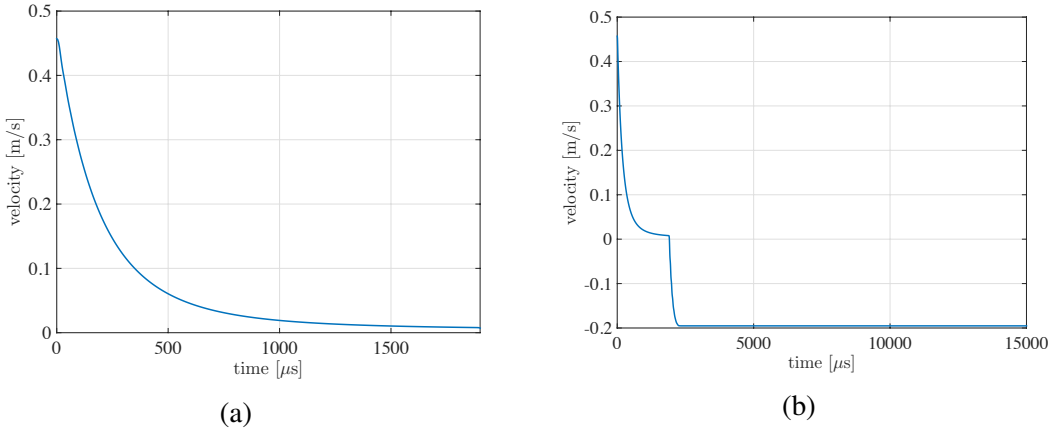

Figure 5.4: The dependence of the striker velocity on time, striker mass 39.13 g, at different time scales.The chain is dissipative with $\mu = 0$ kg/s. Gravitation is not included.

In experiments, we did not see the bouncing back of the striker up to the time 31654μs after impact. Based on the minimal distance recognizable in the high speed camera records and duration of the record we can conclude that the recoil velocity was less than a few hundredth mm/s. Thus this system softly catches striker preventing its

recoil in experiments unlike in numerical calculations with viscosity 6 kg/s. It should be emphasized that the recoil of the striker is exclusively due to the reflected wave from the supporting wall even in case of nondissipative chain. If elastic striker impact a solid elastic wall it always recoils if penetration is prevented.

The discrepancy between experiments and calculations may be related to more significant attenuation at larger propagation distances, for example due to interaction of cylinders with holder. Because of the relative rigidity of the chain the displacements of the striker during interaction with the top particle was very difficult to detect using high speed Phantom *v*12 camera.

This is very interesting behavior of the striker characteristic for its masses being larger than masses of particles in the chain. It is analogous to the impact of striker with the object which has the similar mass where striker will be stop and the object will assume the velocity of the striker. It is probably one of the major reasons why granular beds are used to support items undergoing explosive loading [4]. The behavior of granular bed allows these items stay practically at the same place despite experienced contact explosive loading.

5.5 Stress pulses generated by striker impact

Shapes of the stress pulses generated by impact of striker with mass 39.13g at different depth in the chain in the numerical calculations with different viscosities and in experiments are shown in Fig. 5.5. They are fundamentally different from the pulse excited by a small striker mass (Fig. 5.2). The numerical calculation with viscosity matches well with experimental results. The amplitude of the peak pulse in the 21st cylinder decreases to about 70% of the signal amplitude in 4th cylinder.

The system with higher damping coefficient demonstrated faster attenuation in

signal strength and slower transformation of oscillatory shock like pulse into stationary pulses. At the same depth, when dissipation is absent, the first stationary pulse is already forming, while with $\mu = 6$ kg/s no stationary pulse is visible. The later case is a better representation of the experimental results.

From the frequency spectrum (Fig. 5.5 (d) (e) (f)), all frequencies are shifted to the lower end. It is interesting to see that some of the higher frequencies are wiped out as it propagated through the system. Increasing damping coefficient from 4 to 6 kg/s results in rather significant changes in spectrum in numerical calculations with higher attenuation of higher frequency harmonics. In both cases the range of frequency spectrum is the same as in experiments. It is interesting that the similar increase of harmonic amplitude with frequency close to $20k$Hz was observed in experiments.

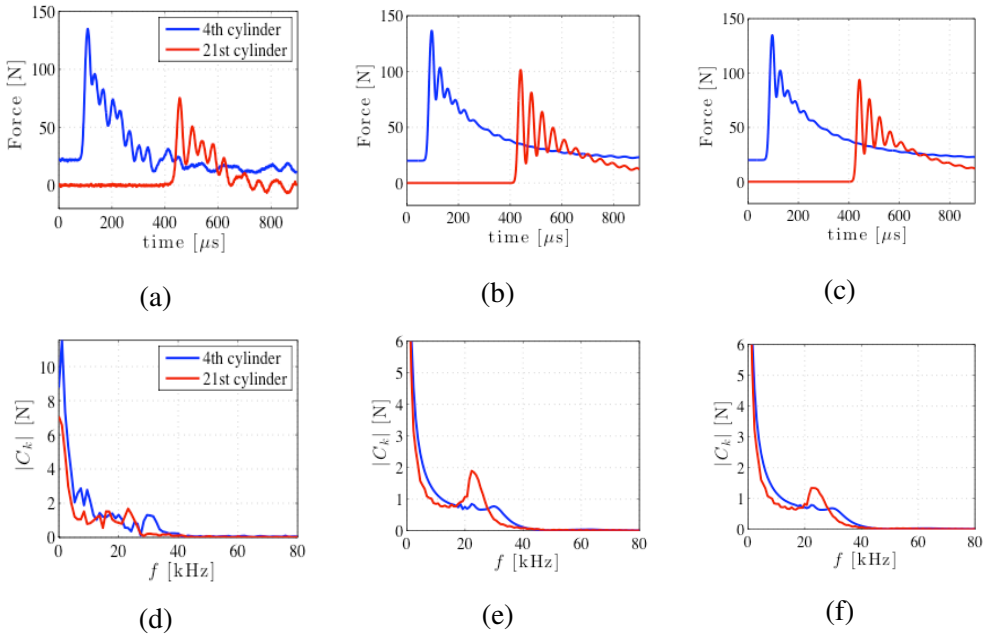

Figure 5.5: Results of experiments and numerical calculations of the pulse excited by the impact of rod with mass of 39.136 g: (a) experimental results (sensors are placed in the 4th and 21st cylinders), (b) and (c) results of numerical calculations (gravitationally loaded chain) related to the forces in 4th and 21st cylinders with $\mu = 4$ kg/s and $\mu = 6$ kg/s, correspondingly. The vertical scale is 20 N and the curves are offset for visual clarity, zero time is arbitrary. (d) (e) (f) Frequency spectrum corresponding to (a) (b) (c).

It need to be mentioned that in oscillatory shock profile the loading path is very different than in a single solitary wave. There are multiple cycles of loading/unloading unlike in solitary wave, but still constant viscosity provide attenuation in reasonable agreement with experiments.

5.6 Critical damping for the transition from oscillatory to monotonous shock profiles

5.6.1 Quasistationary shock wave with long duration generated by large mass striker

It is well known that the shape of the stationary shock front is transformed from the oscillatory to monotonous at some critical value of damping coefficient for weakly and strongly nonlinear discrete systems [17,18]. For the strongly nonlinear uncompressed chain ("sonic vacuum") with power law interaction between masses this damping coefficient μ can be calculated using the corresponding equation for p_{cr} in [18]:

$$\mu_{cr} = \frac{mV_{sh}}{a}\sqrt{\frac{n(n-1)}{3}}, \tag{5.2}$$

where m is the mass of particles, V_{sh} is the shock wave speed, n is exponent in power law interaction and a is the distance between mass centers of particles. More complex equation for the precompressed chain can be found in [17,18].

The shock profile in dissipative one mass chain close to stationary can be excited if mass of striker is much larger than the mass of the particles (2.08 g)). The shock wave profiles generated by the striker with mass 4 kg and velocity 0.457 m/s corresponding to different values of damping coefficients are presented in Fig. 5.6.

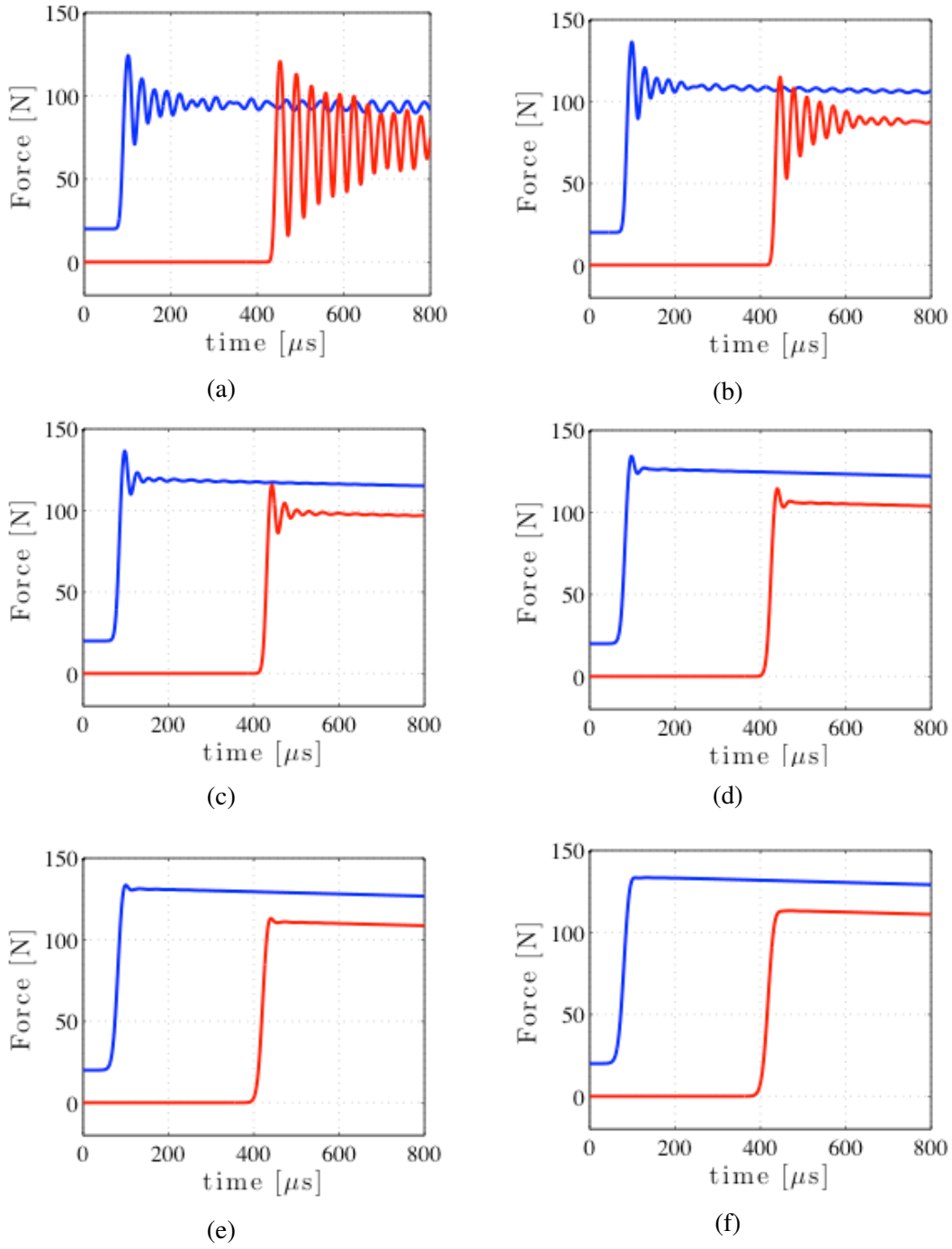

Figure 5.6: Comparison of shock profiles excited by striker with mass 4 kg in numerical calculations in the one mass spheres/cylinders chain without gravitational load and different damping coefficients: (a)$\mu = 0$ kg/s, (b) $\mu = 6$ kg/s. (c) $\mu = 20$ kg/s, (d) $\mu = 40$ kg/s. (e) $\mu = 60$ kg/s, (f) $\mu = 80$ kg/s. The signals are recorded in the 4th and 21st cylinders.

The initial pulse generated by impact is dramatically changing during propagation disintegrating into train of solitary waves in nondissipative chain (Fig. 5.6(a)). The same impact results in quasistationary oscillatory or monotonous shock waves depending on damping. The shock wave was considered a monotonous when amplitude of the kink on the leading front was less than 2% of the amplitude (Fig. 5.6(e)). The speed of the shock wave in initially noncompressed chain in the numerical calculations was equal to 631 m/s ($\mu = 60$ kg/s) and was not significantly influenced by the level of dissipation (Fig. 5.6(b)-(f)). Using this value of the shock speed V_{sh} and Eq. 5.2 ($n = 3/2$, $m = 2.08$ g, $a = 6.65$ mm) obtain a theoretical critical value of damping coefficient corresponding to the transition of a stationary oscillatory shock wave to a monotonic shock profile $\mu = 99$ kg/s. This theoretical value of critical damping coefficient is about 1.6 times larger than observed in numerical calculations (about 60 kg/s) for uncompressed chain (Fig. 5.6(e)). Thus theoretical estimate of critical viscosity gives upper estimate for the transition from oscillatory to monotonous shock profiles.

5.6.2 Finite duration shock wave generated by relatively small mass striker

Eqn. 5.2 was derived for a stationary shock profile, but in most experiments we do not have a flat shock profiles, but triangular pulses. There is no theoretical result related to the transition from oscillatory to monotonous shock profile for finite duration pulses. It is interesting to investigate if the critical value of damping coefficient related to the transition from oscillatory to monotonous shock profiles is also relevant for triangular pulses. Results of the numerical calculations for triangular pulses in free chain are shown in Fig. 5.7 corresponding to the impact by striker with mass 39.13 g as in our experiments.

From comparison of the critical damping coefficient for flat shock and for a finite

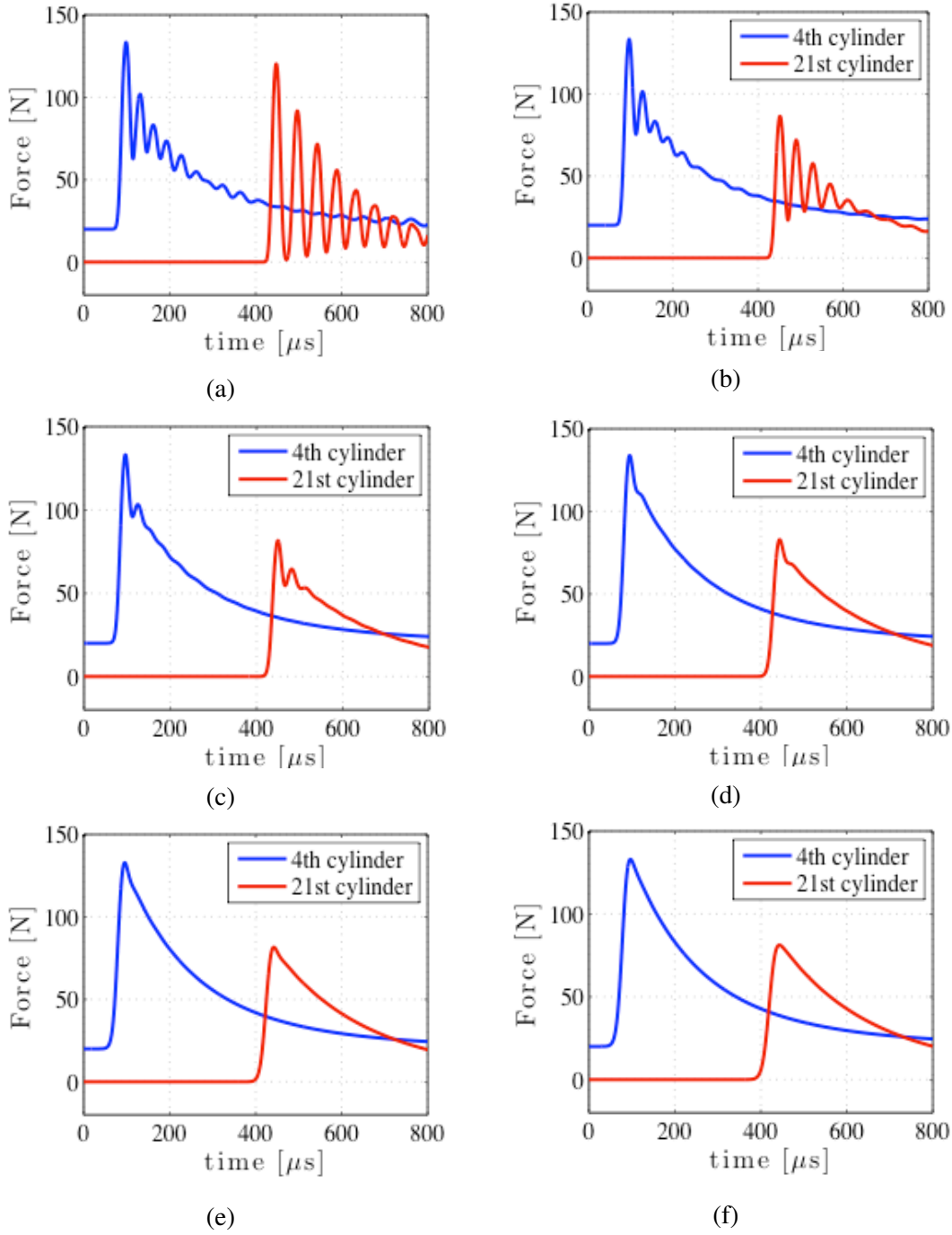

Figure 5.7: Numerical calculations of the pulse propagating through the noncompressed system excited by a striker with mass 39.136 g at different values of damping coefficient: (a)$\mu = 0$ kg/s, (b) $\mu = 6$ kg/s. (c) $\mu = 20$ kg/s, (d) $\mu = 40$ kg/s. (e) $\mu = 60$ kg/s, (f) $\mu = 80$ kg/s. At damping coefficient 60 kg/s we see a monotonous triangular profile of the shock.

duration triangular profile we can conclude that critical damping coefficients (60 kg/s) are similar for these two cases. Thus theoretical value for the critical damping coefficient ensuring transition to monotonous shock profile for stationary shock (Eq. 5.2) can be also considered as upper estimate of critical damping coefficient for the finite durations shocks.

5.7 Conclusions

The dissipation not only results in the attenuation of the pulse amplitudes but also reduces the propensity of the system to the generation of solitary wave train. At small values of viscosities the initial pulse is split into attenuating train of solitary waves. The critical value of viscosity preventing splitting of the initial pulse into train of solitary waves or into oscillatory shock wave is about 1.5 of critical viscosity obtained analytically for stationary shock wave.

5.8 References

1 V.F. Nesterenko, “Propagation of nonlinear compression pulses in granular media”,in *Prikl. Mekh. Tekh. Fiz*. **24**, 136 (1983) [*J. Appl. Mech. Tech. Phys*. **24**, 733 (1984)].

2 A.N. Lazaridi and V.F. Nesterenko, “Observation of a new type of solitary waves in a one-dimensional granular medium”, in *Prikl. Mekh. Tekh. Fiz.* **26**, 115 (1985) [*J. Appl. Mech. Tech. Phys.* **26**, 405 (1985)].

3 V. F. Nesterenko, “Solitary waves in discrete media with anomalous compressibility and similar to ‘sonic vacuum’ , *JOURNAL DE PHYSIQUE IV, Colloque C8, supplement au Journal de Physique III*, **4**, C8-729 - C8-734 (1994).

4 V. F. Nesterenko, *Dynamics of Heterogeneous Materials*. New York: Springer, 2001.

5 K.R. Jayaprakash, Y. Starosvetsky, A. F. Vakakis,"New family of solitary waves in granular dimer chains with no precompression", in *Phys. Rev. E* **83**, 036606 (2011).

6 R. Ramrez, T. Pschel, N. V. Brilliantov, and T. Schwager, "Coefficient of restitution of colliding viscoelastic spheres", in *Phys. Rev. E* **60**, 4465 (1999).

7 N. V. Brilliantov, F. Spahn, J.-M. Hertzsch, and T. Pschel, "The collisions of particles in granular systems", in *Phys. Rev. E* **53**, 5382 (1995).

8 A. Rosas and K. Lindenberg, "Pulse dynamics in a chain of granules with friction", in*Phys. Rev. E* **68**, 041304 (2003).

9 M. Manciu, S. Sen, A.J. Hurd, "Impulse propagation in dissipative and disordered chains with power-law repulsive potentials", in *Physica D* **157**, 226 (2001).

10 G. E. Duvall, R. Manvi, and S. C. Lowell, *J. Appl. Phys.* **40**, 3771 (1969)

11 E.J. Hinch and S. Saint-Jean, "The Fragmentation of a Line of Balls by an Impact", in *Proc. R. Soc. London A* **455**, 3201 (1999).

12 S. Job, F. Melo, A. Sokolow, S. Sen, "Solitary wave trains in granular chains: experiments, theory and simulations", in *Granular Matter* **10**,13 (2007).

13 A. Sokolow, E.G. Bittle, S. Sen, "Solitary wave train formation in Hertzian chains", in*Europhys. Let.* **77**, 24002 (2007).

14 A. Shukla, M. H. Sadd, Y. Xu, and Q.M. Tai, "Influence of loading pulse duration on dynamic load transfer in a simulated granular medium", in *J. Mech. Phys. Solids* **41**, 1795 (1993).

15 C. Daraio, V. F. Nesterenko, and S. Jin, "Strongly Nonlinear Waves in 3D Phononic Crystals", in *Proceedings of the Conference of the American Physical Society Topical Group on Shock Compression of Condensed Matter*, AIP, New York, **706**, 197 (2004).

16 S. Y. Wang, and V. F. Nesterenko, "Attenuation of short strongly nonlinear stress pulses in dissipative granular chains", *Physical Review E*, **91**, 062211 (2015).

17 V. Karpman, *Nonlinear Waves in Dispersive Media*, Pergamon Press, New York, 1975.

18 E. B. Herbold and V. F. Nesterenko, "Shock Wave Structure in a Strongly Nonlinear Lattice with Viscous Dissipation", *Phys. Rev E*, **75**, 021304 (2007).

19 C. Daraio, V.F. Nesterenko, E. Herbold, and S. Jin, “Strongly Nonlinear Waves in a Chain of Teflon Beads”, in *Phys. Rev E*, **72**, 016603 (2005).